①

COMPUTATIONAL ANALYSIS OF A TWO-SLOT CIRCULATION CONTROL AIRFOIL

THESIS

Donald Joseph Ferguson
Captain, USAF

AFIT/GAE/ENY/89D-8

DEPARTMENT OF THE AIR FORCE
AIR UNIVERSITY
AIR FORCE INSTITUTE OF TECHNOLOGY

Wright-Patterson Air Force Base, Ohio

DISTRIBUTION STATEMENT A
Approved for public release;
Distribution Unlimited

①

AFIT/GAE/ENY/89D-8

COMPUTATIONAL ANALYSIS OF A TWO-SLOT CIRCULATION CONTROL AIRFOIL

THESIS

Donald Joseph Ferguson
Captain, USAF

AFIT/GAE/ENY/89D-8

Approved for public release; distribution unlimited

AFIT/GAE/ENY/89D-8

COMPUTATIONAL ANALYSIS OF A TWO-SLOT CIRCULATION CONTROL AIRFOIL

THESIS

Presented to the Faculty of the School of Engineering
of the Air Force Institute of Technology
Air University
In Partial Fulfillment of the
Requirements for the Degree of
Master of Science in Aeronautical Engineering

Donald Joseph Ferguson, B.S.
Captain, USAF

December, 1989

Acknowledgments

Without a lot of support, this project would not have been possible. I want to thank my faculty advisor, Dr. Franke for his support and patience. I also want to thank my other committee members, Capt. Phil Beran and Capt. Dan Fant for their assistance and patience. I owe a great deal to Steven Williams for retracing his steps with me, for documenting is programming steps, and for his technical assistance. Thanks goes to Dr. Shang, Dr. Mach, Dr. Visbal, and others of WRDC/FIMM for their computer support and assistance.

I also wish to acknowledge the outstanding support from the computer systems personnel involved. This includes Jack Cornelli of Aeronautical Systems Division as well as those at AFIT: Dan Zambon, Kris Larsen, Doug Burkholder, Anthony Schooler, Joe Hamlin, Capt. Ronald Eddy, Lt. David Daniel, and the computer operators. I'm sure their jobs will be a little easier now that this project is finished.

Most of all I want to thank my family. I thank Vikki for her neverending support. Without her support this project and degree would not have been possible. Now I can begin repaying her and our children. And finally, I thank God for helping us through all this.

Donald Joseph Ferguson

Table of Contents

List of Figures

Figure Page

List of Tables

List of Symbols

Symbol	Definition
A	- Jacobian matrix for implicit algorithm
B	- Jacobian matrix for implicit algorithm
b_i	- Viscous coefficients
C_d	- Section drag coefficient
C_{d_f}	- Section friction drag coefficient
C_{d_p}	- Section pressure drag coefficient
C_l	- Section lift coefficient
$C_{m_{c/2}}, C_m$	- Section pitching moment coefficient about 50% chord
C_p	- Pressure coefficient
C_μ	- Blowing momentum coefficient
C_{μ_i}	- Blowing momentum coefficient for i^{th} slot
C_{μ_T}	- Total blowing momentum coefficient
c	- Airfoil chord length
c_i	- Viscous coefficients
c_p	- Specific heat at constant pressure
d_i	- Viscous coefficients
e	- Internal energy per unit mass
$F, \hat{F}$	- Flux vectors
F_B	- Bradshaw curvature correction factor
$G, \hat{G}$	- Flux vectors
J	- Transformation Jacobian
k	- Clauser's constant
l	- Turbulence model mixing length
M	- Local Mach number
M_∞	- Free-stream Mach number

$\mathcal{M}$ - Jacobian matrix for implicit algorithm

$\dot{m}$ - Jet mass flow rate

$\mathcal{N}$ - Jacobian matrix for implicit algorithm

p - Static pressure

p_t - Jet total pressure

p_∞ - Free-stream static pressure

$q, \hat{q}$ - Vectors of dependent variables

r - Local free-stream radius of curvature

P_r - Molecular Prandtl number

P_{r_t} - Turbulent Prandtl number

R - Perfect gas constant

Re - Reynolds number

S - Turbulence model curvature term

t - Time

T - Static temperature

T_t - Jet total temperature

U - Local velocity

U_∞ - Free-stream velocity

V_j - Jet velocity

u, v - Velocity components in Cartesian coordinate axes

$\mathcal{U}, \mathcal{V}$ - Contravariant velocity components

x, y - Cartesian coordinate axes

Greek Symbols

α - Airfoil angle of attack

α_{eff} - Airfoil effective angle of attack

β - Jet detachment angle

γ - Specific heat ratio

ε	- Turbulent eddy viscosity
Θ	- Bradshaw empirical curvature constant
λ_T	- Second coefficient of viscosity
μ	- Molecular dynamic viscosity
ξ, η	- Transformed coordinates
ρ	- Static density
ρ_∞	- Free-stream static density
$\tau_{xx}, \tau_{xy}, \tau_{yy}$	- Viscous stress components
ϕ	- Slot angle relative to the x-coordinate direction
ω	- Vorticity

Subscripts

inner	- Inner layer of Baldwin-Lomax turbulence model
T	- Total condition

AFIT/GAE/ENY/89D-3

Abstract

A two-slot circulation control airfoil was analyzed using the two-dimensional, compressible, mass-averaged, Navier-Stokes equations. The implicit Beam-Warming approximate factorization technique was used to calculate airfoil characteristics for a flight Mach number of 0.3 and a Reynolds number near 3 million. The results were then compared to a previous one-slot solution.

An existing circulation control airfoil was modified to include a second slot. Different blowing rates were then applied to each slot in various combinations. The lift generated for a given total blowing momentum for the two-slot airfoil was nearly identical to that for a single-slot airfoil when the lowest blowing rate was applied to the first slot. Although the lift per unit blowing momentum did not increase over the single-slot case, the maximum lift coefficient was increased due to the increased momentum available from the additional slot. Separation angle increased when a small amount of blowing was applied to the first slot, and additional blowing applied to the second slot. The airfoil moment followed the same trend as the single slot, and was less dependent on which slot the flow was applied. Due to the lack of experimental data, and the difficulty in modeling drag for the circulation control airfoil, it is difficult to compare drag.

COMPUTATIONAL ANALYSIS OF A TWO-SLOT CIRCULATION CONTROL AIRFOIL

I. Introduction

Aircraft designers are interested in high-lift devices for short takeoff and landing (STOL) aircraft as well as rotorcraft. One technique for creating high lift is through airfoil circulation control.

Circulation control incorporates a rounded trailing-edge airfoil with a slot (or slots) near the trailing edge. High-pressure air is blown from the slot tangential to the airfoil surface, creating a wall jet which wraps around the airfoil. The jet entrains the airflow from the upper surface around the trailing edge until it finally separates. This is known as the Coanda effect. The increase in lift is roughly proportional to the product of mass flow and jet velocity (10:1). The stagnation points near the front and rear of the airfoil shift toward the center of the lower airfoil surface. By delaying airflow separation, circulation and lift are increased. Figure 1 shows the configuration of a circulation control airfoil. Two advantages that the circulation control airfoil has over a conventional airloil is that a higher lift coeffient, C_l, can be attained at the same flight conditions, and the maximum lift coefficient, $C_{l_{max}}$, is also increased. This reduces takeoff and landing speeds for STOL aircraft, and increases payload for cargo aircraft. Lift can be varied without changing the angle of attack by varying the blowing rate. Rotorcraft and X-wing aircraft can benefit by using blowing to vary lift and eliminate the need for blade pitching (20:1). Because varying lift is not restricted to angle of attack changes, several flight controls can be changed by the blowing rates, such as climb, pitch, and roll.

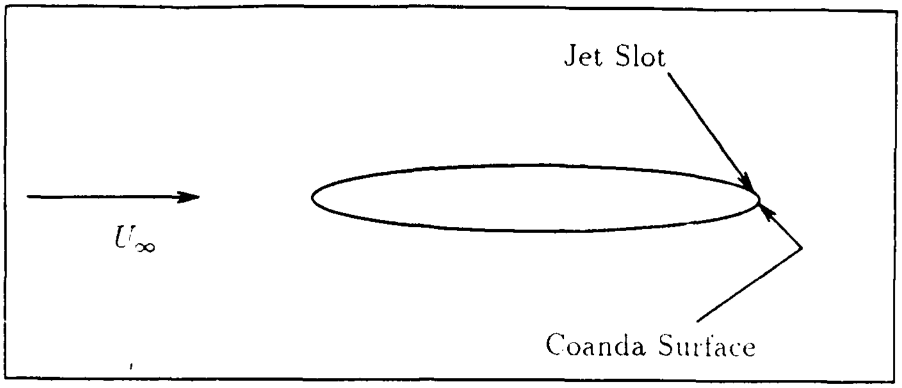

Figure 1. Typical Circulation Control Airfoil

The circulation contol airfoil could replace mechanical flaps but would require additional weight and complexity in the aircraft wing interior. Aircraft performance would also be affected by energy requirements to provide airfoil blowing and by the negative pitching moments generated by the circulation control airfoil exhibits.

1.1 Background

Many factors contribute to the difficulty in the flow-field analysis. The airfoil lift performance is very sensitive to stagnation point locations, therefore the flow separation point must be accurately determined. The boundary layers of the flow after the wall-jets have different length scales, and a free-shear layer forms between airfoil surface flow and the wall-jet flow. Compressibility is a factor even at low free-stream Mach numbers due to high wall-jet velocities.

Several researchers have applied various techniques to model the nonlinear flow behavior numerically using the Navier-Stokes equations. Shrewsbury (13, 15, 14) and Pulliam (11) have had good results using the Baldwin-Lomax turbulence model (3), with a curvature correction factor suggested by Bradshaw (5). The empirical correction factored was adjusted to best match expermintal data. Williams (19) used the same type of modeling to predict airfoil performance for various turbulance factors.

Harvell and Franke (8, 9) found experimentally that if two slots were used near the trailing edge instead of one, greater lift can be obtained using the same blowing momentum.

1.2 *Objective*

The purpose of this study is to numerically investigate the effect of blowing through two wall-jet slots compared to a one wall-jet slot circulation control airfoil. The objective is to evaluate the airfoil performance at different blowing rates to determine the effect on lift, drag, moment, and separation. This is an extension of the work begun by Williams, and similar to Shrewsbury's work. The Beam-Warming implicit approximate factorization algorithm is used to solve the two-dimensional, compressible, mass-averaged, Navier-Stokes equations. The Baldwin-Lomax turbulance model is used, with the curvature correction factor by Bradshaw applied.

II. Analysis

The mass-averaged, Navier-Stokes equations have been a very successful tool in numerically analyzing the flow-field. The governing equations for two-dimensional, compressible flow are described below, followed by a description of the technique used to solve them. The boundary conditions, turbulence model, and the grid generation are then discussed.

2.1 Governing Equations

The equations of motion for the fluid flow-field are based on the conservation of mass, momentum, and energy. The variable formulation reflects the those used in the solution technique developed by Dr. M.R. Visbal (16). In 2-D Cartesian coordinates, these equations appear as follows:

Conservation of mass (continuity)

$$\frac{\partial \rho}{\partial t} + \frac{\partial(\rho u)}{\partial x} + \frac{\partial(\rho v)}{\partial y} = 0 \tag{1}$$

Conservation of momentum

(x-direction)

$$\frac{\partial(\rho u)}{\partial t} + \frac{\partial(\rho u^2)}{\partial x} + \frac{\partial(\rho uv)}{\partial y} + \frac{\partial p}{\partial x} = \frac{\partial \tau_{xx}}{\partial x} + \frac{\partial \tau_{yx}}{\partial y} \tag{2}$$

(y-direction)

$$\frac{\partial(\rho v)}{\partial t} + \frac{\partial(\rho uv)}{\partial x} + \frac{\partial(\rho v^2)}{\partial y} + \frac{\partial p}{\partial y} = \frac{\partial \tau_{xy}}{\partial x} + \frac{\partial \tau_{yy}}{\partial y} \tag{3}$$

Conservation of energy

$$\frac{\partial e}{\partial t}+\frac{\partial(eu)}{\partial x}+\frac{\partial(ev)}{\partial y}-\frac{\partial(kT_x)}{\partial x}-\frac{\partial(kT_y)}{\partial y}=$$

$$\frac{\partial(\tau_{xx}u)}{\partial x}+\frac{\partial(\tau_{xy}v)}{\partial x}+\frac{\partial(\tau_{yx}u)}{\partial y}+\frac{\partial(\tau_{yy}v)}{\partial y}-\frac{\partial(pu)}{\partial x}-\frac{\partial(pv)}{\partial y} \tag{4}$$

where:

$$k=C_p(\frac{\mu}{Pr}+\frac{\varepsilon}{Pr_t}) \tag{5}$$

$$\tau_{xx}=2(\mu+\varepsilon)u_x+\lambda_T(u_x+v_y) \tag{6}$$

$$\tau_{xy}=\tau_{yx}=(\mu+\varepsilon)(u_y+v_x) \tag{7}$$

$$\tau_{yy}=2(\mu+\varepsilon)v_y+\lambda_T(u_x+v_y) \tag{8}$$

Other variable relationships are:

$$F_4=u\tau_{xx}+v\tau_{xy}+C_p(\frac{\mu}{Pr}+\frac{\varepsilon}{Pr_t}) \tag{9}$$

$$G_4=u\tau_{xy}+v\tau_{yy}+C_p(\frac{\mu}{Pr}+\frac{\varepsilon}{Pr_t}) \tag{10}$$

Stokes hypothesis is applied using:

$$\lambda_T=-\frac{2}{3}(\mu+\varepsilon) \tag{11}$$

The perfect gas law is applied using:

$$p=\rho RT=(\gamma-1)[\rho e-\frac{1}{2}\rho(u^2+v^2)] \tag{12}$$

In curvilinear coordinates (ξ,η), the Navier-Stokes equations can be combined as follows:

$$\frac{\partial q}{\partial t}+\xi_x\frac{\partial F}{\partial \xi}+\xi_y\frac{\partial G}{\partial \xi}+\eta_x\frac{\partial F}{\partial \eta}+\eta_y\frac{\partial G}{\partial \eta}=0 \tag{13}$$

where:

$$q = \begin{pmatrix} \rho \\ \rho u \\ \rho v \\ \rho e \end{pmatrix} \tag{14}$$

$$F = \begin{pmatrix} \rho u \\ \rho u^2 + p - \tau_{xx} \\ \rho uv - \tau_{xy} \\ (\rho e + p)u - F_4 \end{pmatrix} \tag{15}$$

$$G = \begin{pmatrix} \rho v \\ \rho uv - \tau_{xy} \\ \rho v^2 + p - \tau_{yy} \\ (\rho e + p)v - G_4 \end{pmatrix} \tag{16}$$

The transformation between the physical domain and the computational domain is illustrated in Figure 2 adapted to an O-grid. The 2-D physical domain (x,y) and the computational domain (ξ, η) are related using chain rule differentiation (2:252).

$$\xi = \xi(x,y) \qquad \eta = \eta(x,y) \tag{17}$$

$$\frac{\partial}{\partial x} = \xi_x \frac{\partial}{\partial \xi} + \eta_x \frac{\partial}{\partial \eta} \tag{18}$$

$$\frac{\partial}{\partial y} = \xi_y \frac{\partial}{\partial \xi} + \eta_y \frac{\partial}{\partial \eta} \tag{19}$$

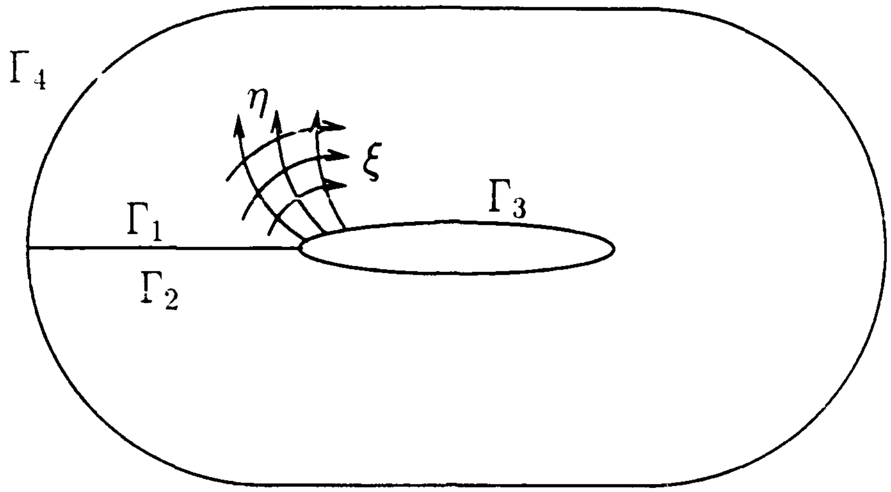

(a) Physical Plane

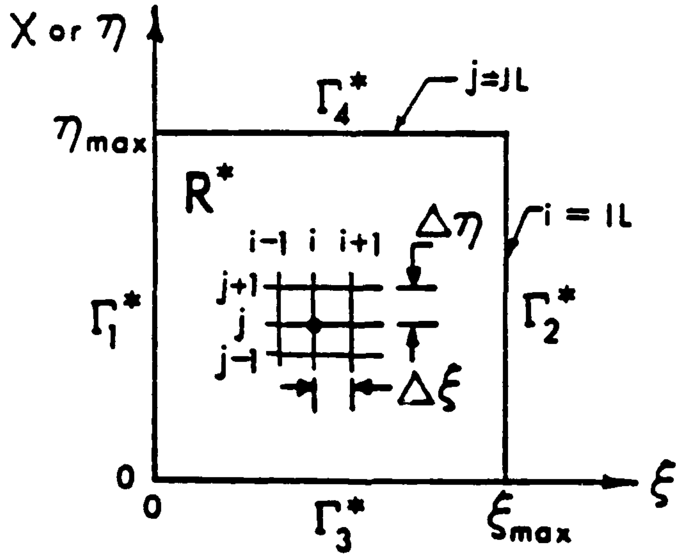

(b) Transformed Plane (16:47)

Figure 2. Physical to Computational Domain Transformation

The metrics are determined by:

$$d\xi = \xi_x dx + \xi_y dy \tag{20}$$

$$d\eta = \eta_x dx + \eta_y dy \tag{21}$$

which in matrix form are:

$$\begin{bmatrix} d\xi \\ d\eta \end{bmatrix} = \begin{bmatrix} \xi_x & \xi_y \\ \eta_x & \eta_y \end{bmatrix} \begin{bmatrix} dx \\ dy \end{bmatrix} \tag{22}$$

and

$$\begin{bmatrix} dx \\ dy \end{bmatrix} = \begin{bmatrix} x_\xi & x_\eta \\ y_\xi & y_\eta \end{bmatrix} \begin{bmatrix} d\xi \\ d\eta \end{bmatrix} \tag{23}$$

Therefore

$$\begin{bmatrix} \xi_x & \xi_y \\ \eta_x & \eta_y \end{bmatrix} = \begin{bmatrix} x_\xi & x_\eta \\ y_\xi & y_\eta \end{bmatrix}^{-1} = J \begin{bmatrix} y_\eta & -x_\eta \\ -y_\xi & x_\xi \end{bmatrix} \tag{24}$$

where the Jacobian (J) is:

$$J = \frac{\partial(\xi,\eta)}{\partial(x,y)} = \begin{vmatrix} \xi_x & \xi_y \\ \eta_x & \eta_y \end{vmatrix} = \xi_x \eta_y - \xi_y \eta_x \tag{25}$$

or equivalently:

$$J = \frac{1}{\frac{\partial(x,y)}{\partial(\xi,\eta)}} = \frac{1}{\begin{vmatrix} x_\xi & x_\eta \\ y_\xi & y_\eta \end{vmatrix}} = \frac{1}{(x_\xi y_\eta - x_\eta y_\xi)} \tag{26}$$

The resulting metrics are:

$$\xi_x = y_\eta J \qquad \xi_y = -x_\eta J \tag{27}$$

$$\eta_x = -y_\xi J \qquad \eta_y = x_\xi J \tag{28}$$

Now the Navier-Stokes Equation 13 can be recast as:

$$\frac{\partial \hat{q}}{\partial t} + \frac{\partial \hat{F}}{\partial \xi} + \frac{\partial \hat{G}}{\partial \eta} = 0 \tag{29}$$

where

$$\hat{q} = \frac{1}{J} q \tag{30}$$

$$\hat{F} = \frac{1}{J}(\xi_x F + \xi_y G) \tag{31}$$

$$\hat{G} = \frac{1}{J}(\eta_x F + \eta_y G) \tag{32}$$

To aid in implicit factorization, Equation 29 is rewritten as:

$$\begin{gathered} \frac{\partial \hat{q}}{\partial t} + \frac{\partial E_1}{\partial \xi} + \frac{\partial E_2}{\partial \eta} = \\ \frac{\partial V_1(\hat{q}, \hat{q}_\xi)}{\partial \xi} + \frac{\partial V_2(\hat{q}, \hat{q}_\eta)}{\partial \xi} + \frac{\partial W_1(\hat{q}, \hat{q}_\xi)}{\partial \eta} + - \frac{\partial W_2(\hat{q}, \hat{q}_\eta)}{\partial \eta} \end{gathered} \tag{33}$$

where:

$$\hat{q} = \frac{1}{J} \begin{pmatrix} \rho \\ \rho u \\ \rho v \\ \rho e \end{pmatrix} \tag{34}$$

$$E_1 = \frac{1}{J} \begin{pmatrix} \rho \mathcal{U} \\ \rho u \mathcal{U} + \xi_x p \\ \rho v \mathcal{U} + \xi_y p \\ (\rho e + p)\mathcal{U} \end{pmatrix} \tag{35}$$

$$E_2 = \frac{1}{J}\begin{pmatrix} \rho\mathcal{V} \\ \rho u\mathcal{V} + \eta_x p \\ \rho v\mathcal{V} + \eta_y p \\ (\rho e + p)\mathcal{V} \end{pmatrix} \tag{36}$$

$$V_1 = \frac{1}{J}\begin{pmatrix} 0 \\ b_1 u_\xi + b_2 v_\xi \\ b_2 u_\xi + b_3 v_\xi \\ b_1 u u_\xi + b_2(v u_\xi + u v_\xi) + b_3 v v_\xi + b_4 T_\xi \end{pmatrix} \tag{37}$$

$$V_2 = \frac{1}{J}\begin{pmatrix} 0 \\ c_1 u_\eta + c_2 v_\eta \\ c_3 u_\eta + c_4 v_\eta \\ c_1 u u_\eta + c_2 u v_\eta + c_3 v u_\eta + c_4 v v_\eta + c_5 T_\eta \end{pmatrix} \tag{38}$$

$$W_1 = \frac{1}{J}\begin{pmatrix} 0 \\ c_1 u_\xi + c_3 v_\xi \\ c_2 u_\xi + c_4 v_\xi \\ c_1 u u_\xi + c_2 v u_\xi + c_3 u v_\xi + c_4 v v_\xi + c_5 T_\xi \end{pmatrix} \tag{39}$$

$$W_2 = \frac{1}{J}\begin{pmatrix} 0 \\ d_1 u_\eta + d_2 v_\eta \\ d_2 u_\eta + d_3 v_\eta \\ d_1 u u_\eta + d_2(v u_\eta + u v_\eta) + d_3 v v_\eta + d_4 T_\eta \end{pmatrix} \tag{40}$$

$\mathcal{U}$ and $\mathcal{V}$ denote the contravariant velocities:

$$\mathcal{U} = \xi_x u + \xi_y v \tag{41}$$

$$\mathcal{V} = \eta_x u + \eta_y v \tag{42}$$

and the viscous coefficients are b_i, c_i, and d_i :

$$\begin{aligned}
b_1 &= (\mu + \varepsilon)(\frac{4}{3}\xi_x^2 + \xi_y^2) \\
b_2 &= \frac{1}{3}(\mu + \varepsilon)\xi_x\xi_y \\
b_3 &= (\mu + \varepsilon)(\xi_x^2 + \frac{4}{3}\xi_y^2) \\
b_4 &= C_p(\frac{\mu}{Pr} + \frac{\varepsilon}{Pr_t})(\xi_x^2 + \xi_y^2)
\end{aligned} \tag{13}$$

$$\begin{aligned}
c_1 &= -(\mu + \varepsilon)(\frac{4}{3}\xi_x\eta_x + \xi_y\eta_y) \\
c_2 &= -(\mu + \varepsilon)(\frac{2}{3}\xi_x\eta_y - \xi_y\eta_x) \\
c_3 &= (\mu + \varepsilon)(\xi_x\eta_y - \frac{2}{3}\xi_y\eta_x) \\
c_4 &= -(\mu + \varepsilon)(\xi_x\eta_x + \frac{4}{3}\xi_y\eta_y) \\
c_5 &= -C_p(\frac{\mu}{Pr} + \frac{\varepsilon}{Pr_t})\xi_x\eta_x + \xi_y\eta_y)
\end{aligned} \tag{14}$$

$$\begin{aligned}
d_1 &= (\mu + \varepsilon)(\frac{4}{3}\eta_x^2 + \eta_y^2) \\
d_2 &= \frac{1}{3}(\mu + \varepsilon)\eta_x\eta_y \\
d_3 &= (\mu + \varepsilon)(\eta_x^2 + \frac{4}{3}\eta_y^2) \\
d_4 &= C_p(\frac{\mu}{Pr} + \frac{\varepsilon}{Pr_t})(\eta_x^2 + \eta_y^2)
\end{aligned} \tag{15}$$

2.2 *Implicit Navier-Stokes Algorithm*

The Navier-Stokes solver used in the analysis was developed by Dr. M.R. Visbal of the Wright Research and Devlopment Center (WRDC) (16, 17, 18). The implicit algorithm uses the approximate factorizaion technique developed by Beam and Warming (4) to solve the strong conservation Navier-Stokes Equation 33. The first-order Euler time differencing scheme in delta form is written as:

$$\left\{ I + \Delta t \left[\frac{\partial A^n}{\partial \xi} - \frac{\partial^2 \mathcal{M}^n}{\partial \xi^2} \right] \right\} \left\{ I + \Delta t \left[\frac{\partial B^n}{\partial \eta} - \frac{\partial^2 \mathcal{N}^n}{\partial \eta^2} \right] \right\} \Delta \hat{q}^n = - \Delta t \left[\frac{\partial}{\partial \xi} (E_1 - V_1 - V_2)^n + \frac{\partial}{\partial \eta} (E_2 - W_1 - W_2)^n \right] \quad (46)$$

and:

$$\hat{q}^{n+1} = \hat{q}^n + \Delta \hat{q}^n \quad (47)$$

where n denotes the temporal index (i.e. $\hat{q}^n = \hat{q}(n \ \Delta t)$) and the Jacobian matrices are:

$$A = \frac{\partial E_1}{\partial \hat{q}} \qquad B = \frac{\partial E_2}{\partial \hat{q}} \quad (48)$$

$$\mathcal{M} = \frac{\partial V_1}{\partial \hat{q}_\xi} \qquad \mathcal{N} = \frac{\partial W_2}{\partial \hat{q}_\eta} \quad (49)$$

Spatial derivatives are discretized using using second order central differencing, while explicit and implicit damping terms have been added to capture embedded shocks. Because a steady state condition is desired, a variable time step may be used throughout the grid for faster convergence (16:19-21) . The mass-averaged Navier-Stokes equations have been a very successful tool in numerically analyzing the flow-field. The governing equations for two-dimensional compressible flow are described below, followed by a description of the technique used to solve them. The boundary conditions, turbulence model, airfoil configuration, and the grid generation are then discussed.

2.3 *Boundary Conditions*

The conditions on the physical domain boundaries must be related to the boundary conditions in the computational domain. This relationship is shown in Figure 3. The boundary conditions to be met are the inflow and outflow at the

O-grid exterior, the matching conditions at the grid cut line, and the airfoil surface with the wall-jet slots.

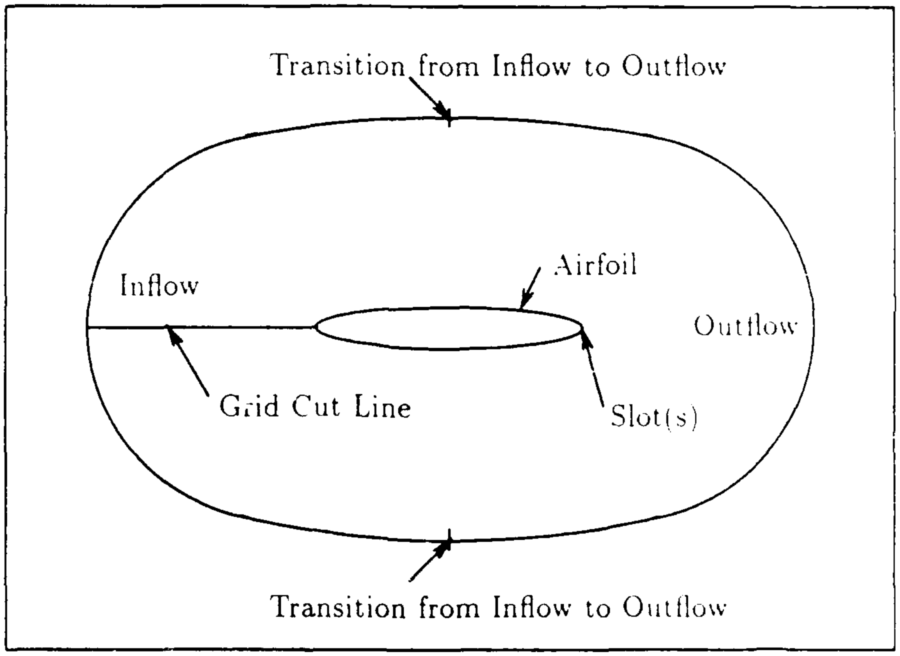

Figure 3. Boundary Conditions

For the O-grid inflow condition, the air has the reference free-stream values at a specified angle of attack. These are given by:

$$u = U_\infty \cos \alpha \tag{50}$$

$$v = U_\infty \sin \alpha \tag{51}$$

$$p = p_\infty \tag{52}$$

$$\rho = \rho_\infty \tag{53}$$

For the outflow conditions, the flow is subsonic with no gradients in the x-direction. The inflow to outflow transition occurs near the maximum and minimum coordinates of the O-grid in the y direction, see Figure 3. The outflow conditions are enforced using:

$$p = p_\infty \tag{54}$$

$$\frac{\partial}{\partial x}\begin{pmatrix} \rho \\ u \\ v \end{pmatrix} = 0 \tag{55}$$

Along the O-grid cut line, the grid is overlapped two points past the cut in both directions, allowing enforcement of a periodic boundary condition. On the overlapped grid points, the flow variables are set equal.

The airfoil has two types of boundary conditions, one for the airfoil surface, and the second for the wall-jet slots. On the airfoil surface, adiabatic, no-slip conditions are enforced using:

$$u = v = 0 \tag{56}$$

$$\frac{\partial}{\partial \eta}\begin{pmatrix} p \\ T \end{pmatrix} = 0 \tag{57}$$

The wall-jet slot is modeled using assumptions based on Shrewsbury's work (15:4). The flow from the wall-jet slots is assumed to be isentropic, and have constant total pressure and temperature across the slot exit. The flow from the slot is limited to less than or equal to sonic velocity. The boundary conditions are enforced using:

$$\frac{\partial p}{\partial \xi} = 0 \tag{58}$$

$$T = T_t\left(1 + \frac{\gamma - 1}{2}M^2\right)^{-1} \tag{59}$$

$$u = M\left(\gamma RT\right)^{\frac{1}{2}}\cos\phi \tag{60}$$

$$v = M\left(\gamma RT\right)^{\frac{1}{2}}\sin\phi \tag{61}$$

Once pressure is calculated using Equation 58, the Mach number is determined. For the subsonic flow, Equations 60 and 61 are applied to the flow-field. For pressure ratios indicating supersonic flow, the flow is assumed choked and is set to critical conditions.

The parameter used for measuring slot blowing is the blowing momentum coefficient:

$$C_\mu = \frac{\dot{m}_j V_j}{q_\infty c} \tag{62}$$

where V_j is the velocity the jet would have if isentropically expanded to the free-stream pressure. For two wall-jets, the total C_{μ_T} is the sum of each slot:

$$C_{\mu_T} = C_{\mu_1} + C_{\mu_2} \tag{63}$$

The drag coefficient is offset by the additional momentum from the wall-jet (7) by the following relationship:

$$C_d = C_{d_f} + C_{d_p} - C_{\mu_T} \tag{64}$$

C_{d_f} and C_{d_p} are the section drag terms due to friction and pressure, respectively. Notice that for high values of blowing momentum, C_{μ_T}, it is possible to have negative values of drag.

2.4 *Turbulence Model*

The Baldwin-Lomax turbulence model (3) was used this analysis, with an empirical correction factor suggested by Bradshaw (5:68-71) for convex surfaces. The algebraic Baldwin-Lomax turbulence model is used because of its accuracy over a wide range of applications. A modification for curvature effects has been suggested from theory and from experiment (5). For the Baldwin-Lomax model, the turbulent eddy viscosity for the inner region is:

$$(\mu_t)_{inner} = \rho|\omega|l^2 \tag{65}$$

The curvature correction factor suggested by Bradshaw adjusts the mixing length (l) by a factor:

$$F_B = 1 - \Theta S \tag{66}$$

where

$$S = \frac{\left(\frac{U}{r}\right)}{\left(\frac{\partial U}{\partial \eta}\right)} \tag{67}$$

and Θ is an empirical constant. Bradshaw suggested that $6 < \Theta < 14$ for a convex wall jet and that

$$1 - (0.05)\Theta < F_B < 1 + (0.05)\Theta$$

limits the value of F_B. Williams (19) found that for his analysis, a value of $\Theta = 3.2$ matched wind tunnel C_l data best. The value of $\Theta = 3.2$ was used in this analysis.

The boundary layer transition is based on the more stringent of two conditions, the first based on the Pohlhousen method (12) and the second based on adverse pressure gradient. The most forward location for the two cases is then used as the boundary layer transition point. This may produce higher drag coefficients than experiment because transition may not always occur with a small adverse pressure gradient.

2.5 *Airfoil Configurations*

The airfoil used in this study is a modified version of the 103RE circulation control airfoil designed and wind tunnel tested by the David Taylor Navel Ship Research and Development Center (DTNSRDC) (1). The 103RE airfoil is a modified ellipse with a maximum chamber of 1% chord located at 70% chord and a maximum thickness of 16% chord. The leading and trailing edges have a reduced radius, varying at the trailing edge from 4.6% chord to 2.8%. The airfoil has one wall-jet slot at 96.88% chord with an operating slot height of (0.0023)c . The trailing-edge for the one-slotted 103RE is shown in Figure 4. The research by Harvell and Franke (8, 9)

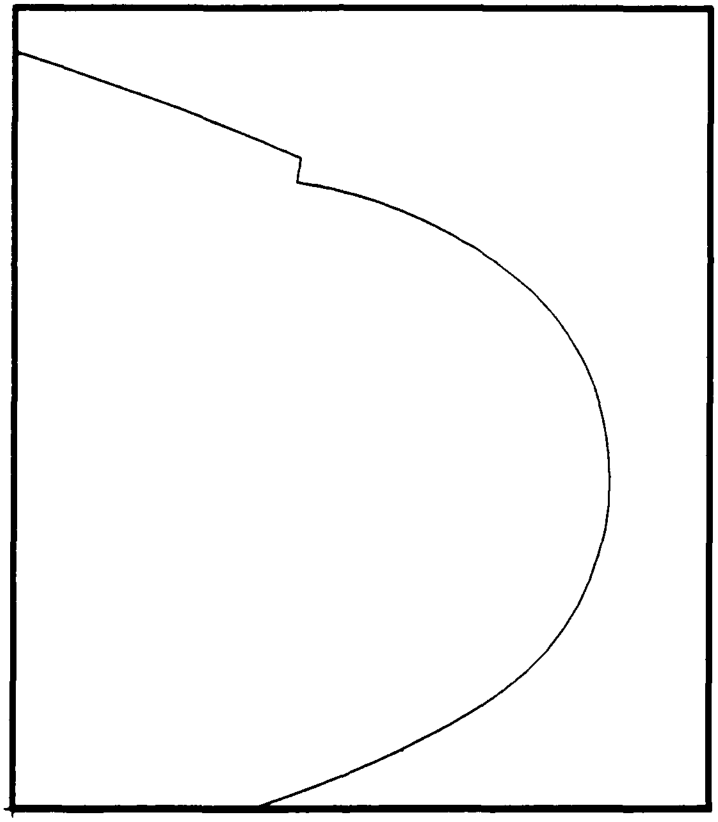

Figure 4. 103RE One-Slot Airfoil Trailing-Edge

demonstrated that a greater lift coefficient, C_l, could be obtained by dividing the blowing momentum, C_μ, between two slots near the Coanda surface. Lift characteristics were determined with the second slot at various locations, with a free-stream velocity of 100 ft/sec. They found that the first slot was effective in keeping the flow attached to the surface until reaching the second slot. The second slot produced higher lift , C_l, per unit blowing momentum, C_μ, at an angle, β, of 73.5 deg . The angle β is measured clockwise from was a vertical line through the center of the circular surface.

The 103RE airfoil was modified to add a second wall-jet blowing slot identical in size to the original slot. The second slot location was selected graphically on the trailing-edge at 73 deg from a similarly sized circle, due to the variance in radius of curvature for an ellipse. The angle β for this point was 70.2 deg based on the radius of curvature at selected point. At the selected second slot location, the existing airfoil surface between the first slot and second slot was then translated outward (0.00247)c in the direction normal to the airfoil, as shown in Figure 5. The opening size of (0.00247)c was due to a slot height of (0.0023)c and a slot opening lip of (0.00017)c, identical to that of the original slot. This shifted airfoil surface, however, reduced the original slot height of the first slot. The reduction was determined, and the airfoil surface preceding the first slot was modified to increase the first slot height to (0.0034)c. The final first slot height for the two-slot configuration was (0.0023)c after the airfoil modifications. The resulting two-slot airfoil trailing-edge is shown in Figure 6.

2.6 Grid Generation

The O-grid for the analysis was generated using the interactive grid-generation program (INGRID) developed at the Arnold Engineering Development Center (AEDC) (6). Elliptical smoothing was used to refine the grid into more orthogonal sections. The O-grid outer boundary is a circle with a radius of 14 airfoil chords from the airfoil . Figure 7 shows the entire and Figure 8 shows the inner portion. Due to the sharp corners at the slot exits , the grid is somewhat skewed near these points, as seen in

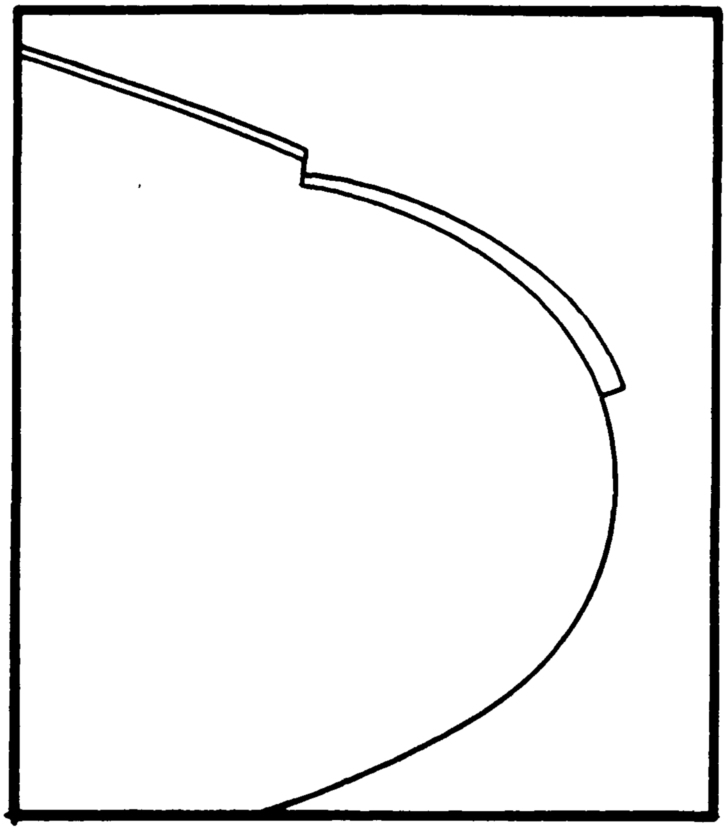

Figure 5. 103RE Airfoil Modification - One-Slot to Two-Slot

Figures 9, 10,and 11. The grid has 254 points along the airfoil, and 80 points normal to the airfoil. Hyperbolic tangent stretching was used to concentrate grid points in the regions near the surface and the jet slots.

Williams' analysis of the O-grid for the one-slot configuration found that a 176 by 80 grid was sufficiently dense to accurately model the wind tunnel results. The O-grid for the two-slot configuration has the same spacing normal to the airfoil as the one-slot grid, using 80 grid points. Along the airfoil surface, additional points are required to model the second jet slot. Grid points were added between the slots and on the trailing-edge in order to maintain the grid density used in the one-slot analysis. The addition of grid points was due to the grid angle required to model the flow near the second slot, as shown in Figure 9.

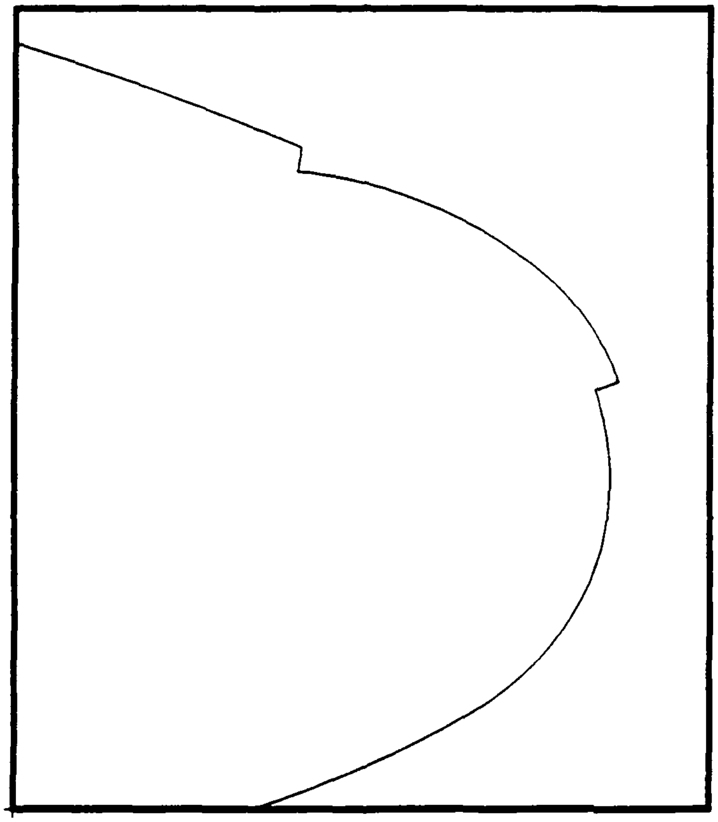

Figure 6. Modified 103RE Two-Slot Airfoil Trailing-Edge

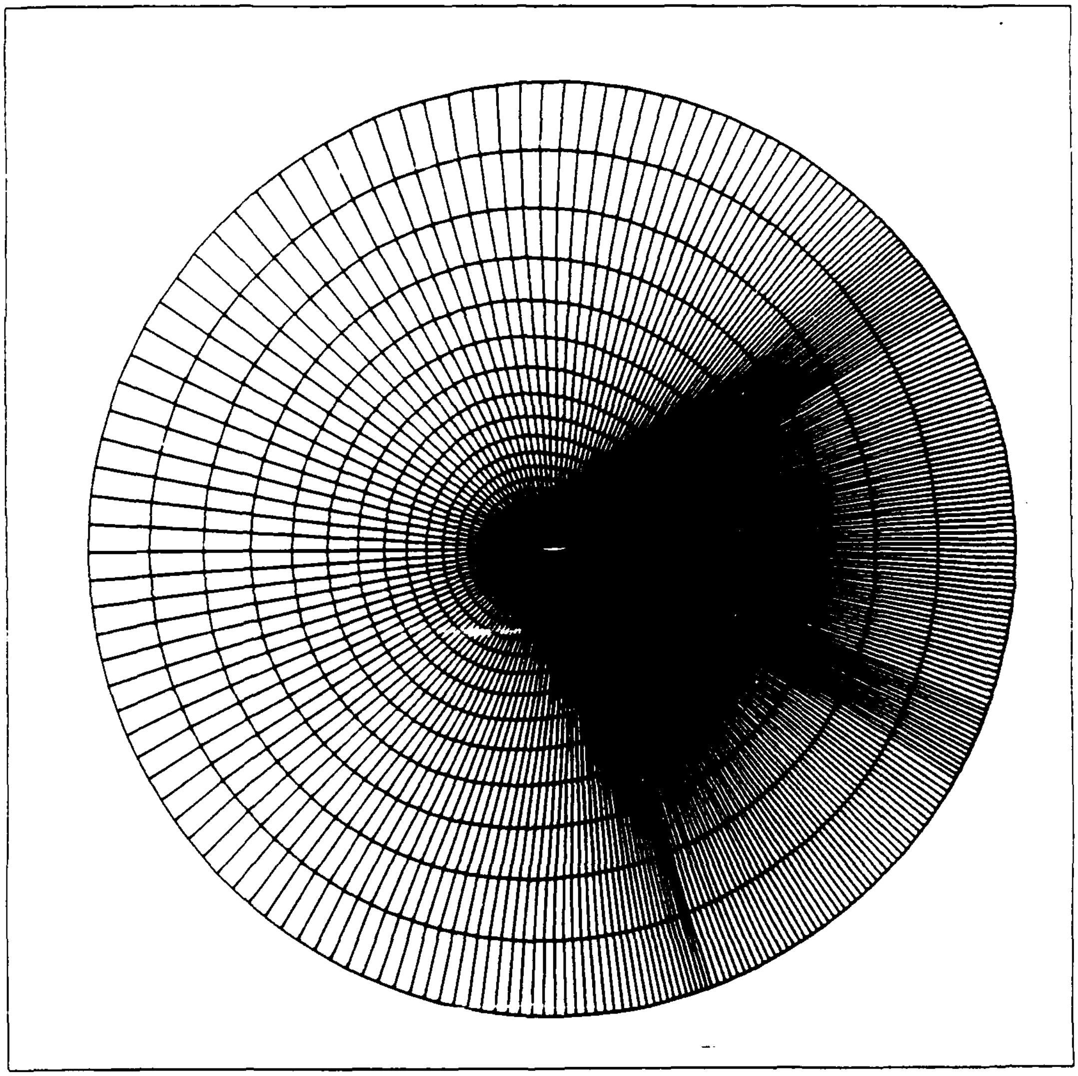

Figure 7. O-Grid Overview - Complete Grid

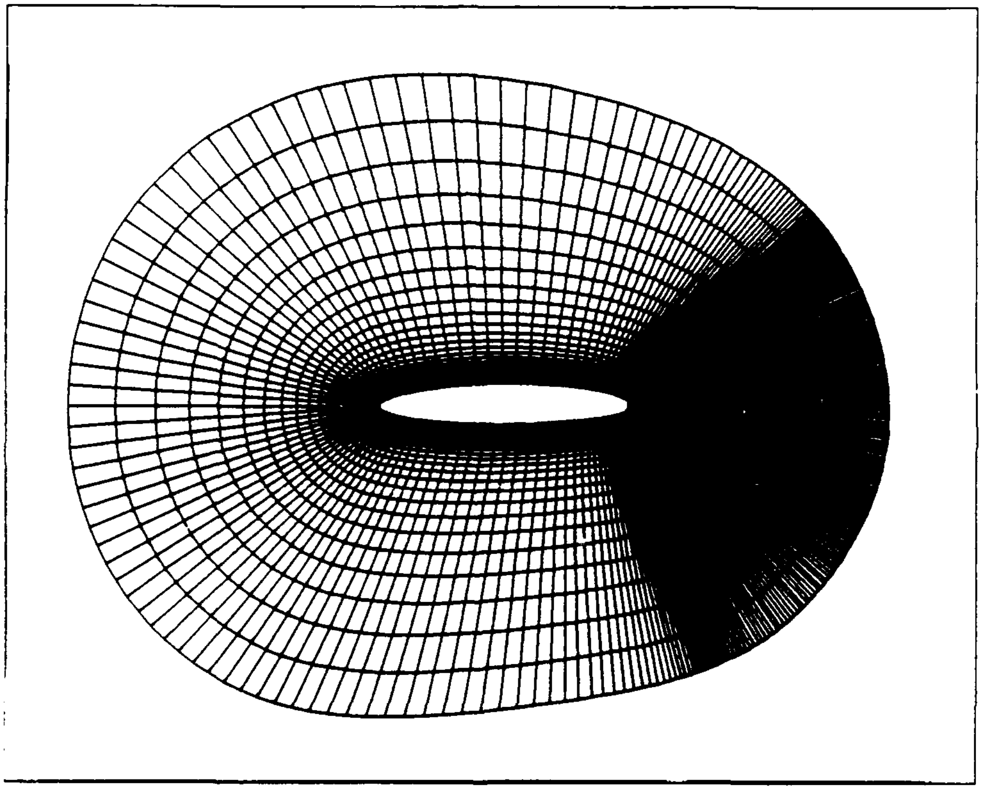

Figure 8. O-Grid Overview - Interior Section

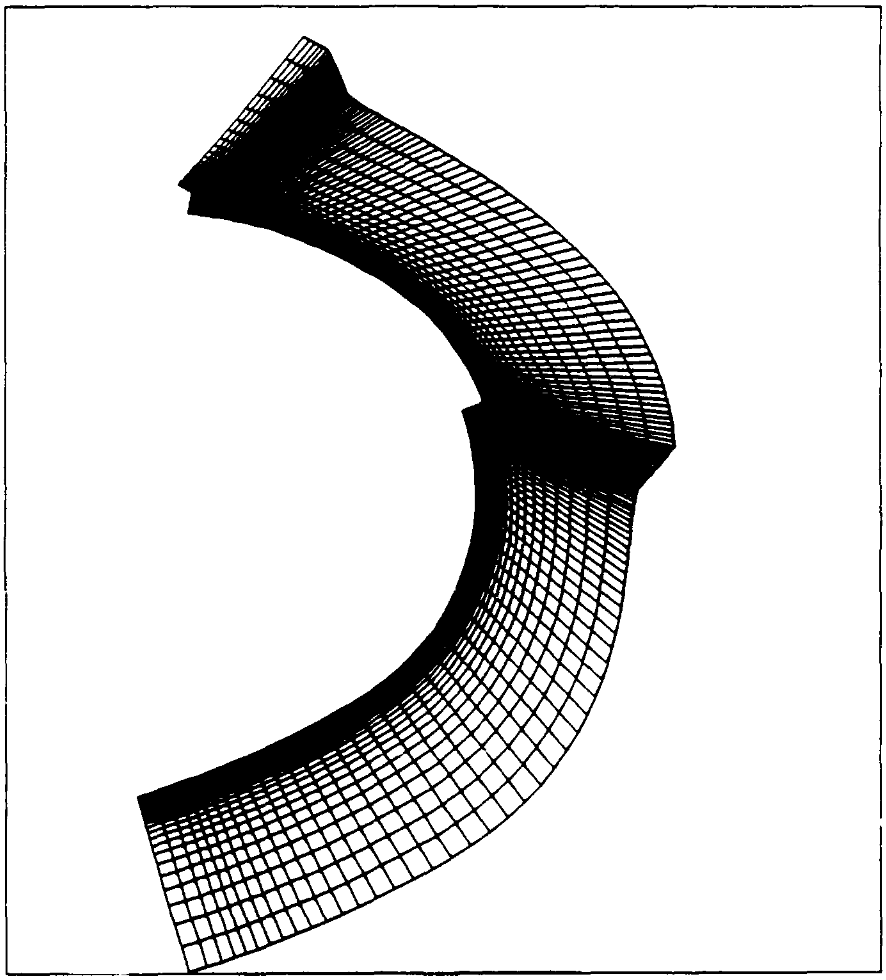

Figure 9. O-Grid Detail - Trailing Edge

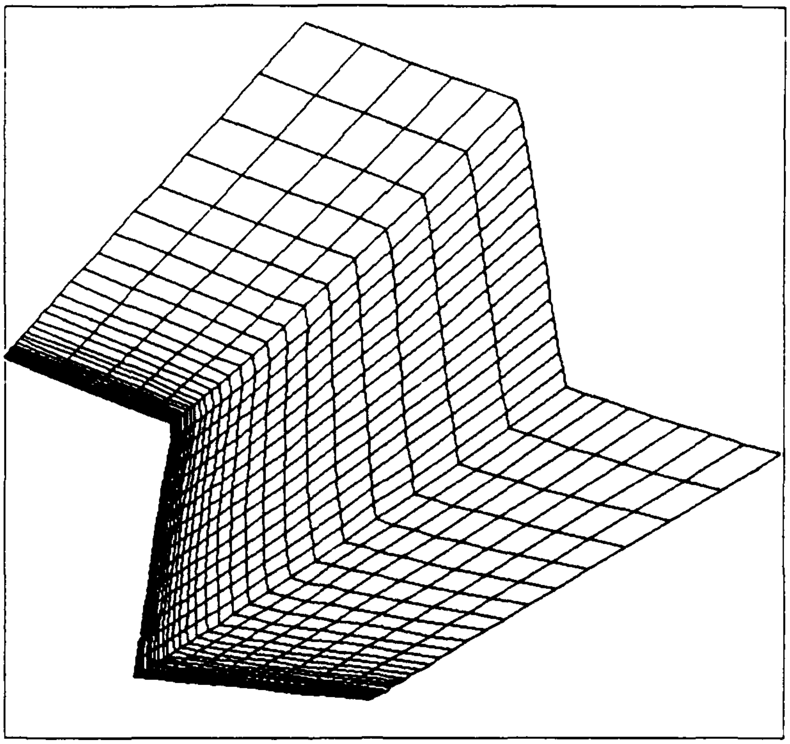

Figure 10. O-Grid Detail - Slot 1

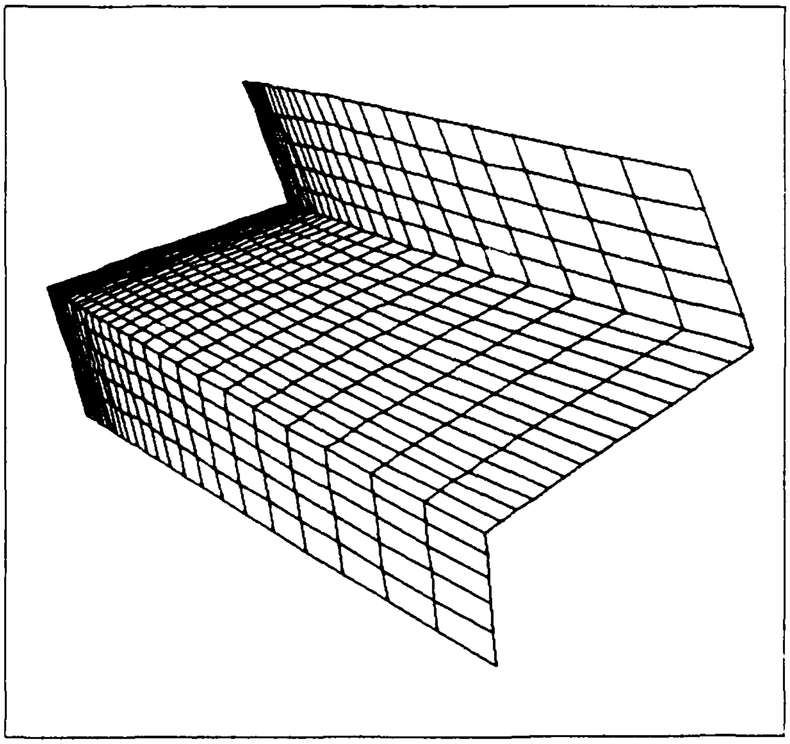

Figure 11. O-Grid Detail - Slot 2

III. Results and Discussion

3.1 Slot Blowing Conditions

The 103RE airfoil has been extensively wind tunnel tested by DTNSRDC (1), and was analyzed in Williams' research (19). The test conditions referenced are for Mach number 0.3, and an angle of attack α of 0. The wind tunnel test results for the one-slot airfoil are designated as Points 33, 35, 36, and 38 for various blowing rates. The wall-jet slot blowing momentum coefficient, C_μ, was varied using a reference total pressure in the slot plenum, and the measured temperature. The blowing conditions for Points 33, 35, 36, and 38 correspond to the two-slot analysis conditions of A, B, C, and D. Point 37 was used to further investigate lift trends, and was designated as E, even though the pressure lies between conditions C and D.

The analysis used combinations of the four different blowing rates (A, B, C, D) for each of the two slots. The case designator for each two-slot combination is a two letter reference, where the first letter is the blowing condition for the first slot, and the second letter for the second slot.

The blowing rate is varied by adjusting the total pressure and temperature, but C_μ will be affected by flow-field conditions. Williams' analysis had been done using an effective angle of attach (α_{eff}) and Reynolds number, Re, adjusted for wind tunnel effects. Both α_{eff} and Re were proportional to C_l, which is itself proportional to C_μ. Effective values were used in order to adjust for wind tunnel effects, allowing comparison to wind tunnel data from DTNSRDC (1) for $\alpha = 0$. Because no reference data existed for the two-slot airfoil conditions being analyzed, linear interpolation was used to obtain the reference (α_{eff}) and Re. The linear relationships used to select the reference conditions are:

$$\alpha_{eff} = -.25 - 72.3(C_{\mu_T}) \qquad (68)$$

$$Re = [3.12 - 1.81(C_{\mu_T})]10^6 \qquad (69)$$

where C_{μ_T} is given by Equation 63 , and C_μ values for Points 33, 35, 36 and 38 were used. Because C_{μ_T} is dependent on the flow-field solution, an estimate of C_{μ_T} was made using C_μ values from the one-slot solutions. These estimates of C_{μ_T} varied from the final values by 0.033% to 9.31%. The values used as inputs are listed in Table 1.

3.2 Results

The results of the analysis at the various blowing rate combinations are displayed in Table 2 and in Figures 12 to 15.

To aid in the result analysis, the cases were grouped with those of constant first slot blowing conditions (i.e. Cases BA, BB, BC, BD). In Figures 12 to 15 the solid lines connect cases with constant first slot blowing conditions, allowing the second slot blowing conditions to change. For comparison, the dashed lines in Figures 12 to 15 connect cases with constant second slot blowing conditions (i.e. Cases AB, BB, CB , DB), allowing the first slot blowing conditions to change.

The single slot cases are included as a reference. The Mach number profiles, trailing edge velocity vectors, and C_p vs. x/c for the two-slot cases are included in the Appendix.

The lift characteristics were very dependent on the first slot blowing momentum coefficient. The lift coefficient, C_l, vs. C_{μ_T} is shown in Figure 12. For cases without blowing from the first slot, (Cases AA, AB), the flow separated before reaching the second slot and lift decreased with additional blowing from the second slot. Cases AC and AD were not examined because of flow separation. It can be noted that if the airfoil has two slots, blowing may be required from the first slot in order for the flow to remain attached until reaching the second slot.

The lowest level of blowing considered for the first slot (Cases BA, BB, BC, BD)

Table 1. Analysis Input Values

Case	α_{eff}	Re(10^{-6})	Slot 1			Slot 2		
			P_T/P_∞	T_T/T_∞	C_{μ_1}	P_T/P_∞	T_T/T_∞	C_{μ_2}
33	−0.25	3.12	1.0	1.0	0.0000	n/a	n/a	n/a
35	−0.92	3.10	1.137	0.956	0.0096	n/a	n/a	n/a
36	−1.66	3.09	1.284	0.934	0.0187	n/a	n/a	n/a
38	−2.65	3.06	1.573	0.905	0.0332	n/a	n/a	n/a
AA	−0.25	3.12	1.000	1.000	0.0000	1.000	1.000	0.0000
AB	−0.94	3.10	1.000	1.000	0.0000	1.137	0.956	0.0096
BA	−0.94	3.10	1.137	0.956	0.0096	1.000	1.000	0.0000
BB	−1.64	3.09	1.137	0.956	0.0096	1.137	0.956	0.0096
BC	−2.30	3.09	1.137	0.956	0.0096	1.284	0.934	0.0187
BE	−2.77	3.06	1.137	0.956	0.0096	1.432	0.956	0.0253
BD	−3.34	3.04	1.137	0.956	0.0096	1.573	0.905	0.0332
CA	−1.60	3.09	1.284	0.934	0.0187	1.000	1.000	0.0000
CB	−2.30	3.09	1.284	0.934	0.0187	1.000	1.000	0.0000
CC	−2.95	3.05	1.284	0.934	0.0187	1.284	0.934	0.0187
CD	−4.00	3.03	1.284	0.934	0.0187	1.573	0.905	0.0332
DA	−2.65	3.06	1.573	0.905	0.0332	1.000	1.000	0.0000
DB	−3.34	3.04	1.573	0.905	0.0332	1.137	0.956	0.0096
DC	−4.00	3.03	1.573	0.905	0.0332	1.284	0.934	0.0187
DD	−5.05	3.00	1.573	0.905	0.0332	1.573	0.905	0.0332

Table 2. Analysis Output Values

Case	$C_{\Delta T}$	C_l	C_d	C_m	$\beta(deg)$	C_{μ_1}	C_{μ_2}
33	0.00000	0.032	0.01467	−0.01685	7.9	0.0000	n/a
35	0.00956	0.553	0.00752	−0.03794	69.8	0.00956	n/a
36	0.01880	1.094	0.00612	−0.06345	84.6	0.01880	n/a
38	0.03315	1.764	0.00624	−0.10150	95.2	0.03315	n/a
AA	0.00000	0.040	0.01331	−0.01438	5.6	0.00000	0.00000
AB	0.01022	−0.019	0.00580	−0.04641	5.6	0.00000	0.01022
BA	0.00929	0.501	0.00658	−0.03516	57.9	0.00929	0.00000
BB	0.02058	1.149	0.00071	−0.05729	112.7	0.01018	0.01040
BC	0.03052	1.609	0.00252	−0.07510	134.0	0.01017	0.01986
BE	0.03815	2.098	0.01018	−0.08489	163.7	0.01121	0.02694
BD	0.04454	2.353	0.01496	−0.09787	173.0	0.01153	0.03301
CA	0.01852	0.635	0.00295	−0.05841	67.1	0.01852	0.00000
CB	0.03003	1.446	−.00733	−0.07710	96.1	0.01881	0.01122
CC	0.03975	1.905	−.00860	−0.09810	120.9	0.01940	0.02035
CD	0.05263	2.558	0.01424	−0.12143	172.3	0.01964	0.03299
DA	0.03309	0.738	−0.01062	−0.09165	70.7	0.03309	0.00000
DB	0.04472	1.580	−0.02042	−0.10658	90.5	0.03310	0.01162
DC	0.05345	1.932	−0.01086	−0.13239	109.0	0.03316	0.02029
DD	0.06676	2.353	−0.02053	−0.17282	120.9	0.03316	0.03302

demonstrated approximately the same lift characteristics for a given C_{μ_T} as the single slot case. The lift curve is extended farther because a higher C_{μ_T} is available because of the two slots. This may be an advantage if slot height caused choking, as it does in the higher blowing cases.

At intermediate levels of blowing from the first slot, (Cases CA, CB, CC, CD), additional second slot blowing did increase C_l. However, the increase in blowing from the first slot was not as effective as increasing the second slot blowing instead. Consider, for example, the initial condition for Case BB. If additional blowing is added to the first slot (Case CB), C_l increases from 1.149 to 1.446, with C_{μ_T} = 0.03052, shown in Figure 12 as a dashed line from BB to CB. If the additional blowing is instead applied to the second slot (Case BC), C_l increases from 1.149 to 1.609, with C_{μ_T} = 0.03005, shown in Figure 12 as a solid line from BB to BC.

At the highest level of blowing for the first slot, (Cases DA, DB, DC, DD), lift only increased marginally for Cases DA and DB, and actually decreased for Cases DC and DD. This appears to be due to flow separation. Additional first slot blowing can actually reduce lift in these cases.

For comparison to the one-slot configuration, consider the cases where no blowing is applied to the second slot (Cases AA, BA, CA, DA). Notice in Figure 12 that for the same total blowing momentum, C_{μ_T}, the lift is less for these two-slot cases than for the one-slot configuration. This would indicate that lift and flow separation angle for a circulation control airfoil is very sensitive to to the airfoil smoothness at the trailing-edge. Small protrusions could cause premature flow separation and decreased lift.

The drag characteristics were influenced by the first slot blowing momentum coefficient. The drag coefficient, C_d, vs. C_{μ_T} is shown in Figure 13. The drag did decrease enough to become negative at intermediate blowing rates, but drag increased for higher blowing momentum. For the cases in which drag increased (Cases BC, BD, BE, CD, DC), single precision computations were used. This may have influenced the drag values more than the other values because the drag term, C_d, is small compared to the lift coefficient, C_l.

The moment characteristics were dependent on the total blowing momentum. The moment coefficient, C_m, vs. C_{μ_T} is shown in Figure 14. For all cases, except those with no blowing on the first slot, the moment had a smaller magnitude than the one-slot airfoil. The lowest level of first slot blowing produced the smallest magnitude for moment coefficient. The difference in moment depends more on the total blowing momentum than on how the blowing is divided between the two slots.

The flow separation angles were influenced by the total blowing momentum and how the blowing was divided between the two slots. The separation angle, β vs. C_{μ_T} is shown in Figure 15. For the same blowing momentum, C_{μ_T}, the two-slot configuration had significantly higher separation angles. The exceptions were for the cases with no blowing from the first slot (Cases AA,AB). In these cases, the flow separated immediately after reaching the first slot. If the blowing momentum for the first slot increases past condition B, the separation angle decreases for cases with constant second slot blowing.

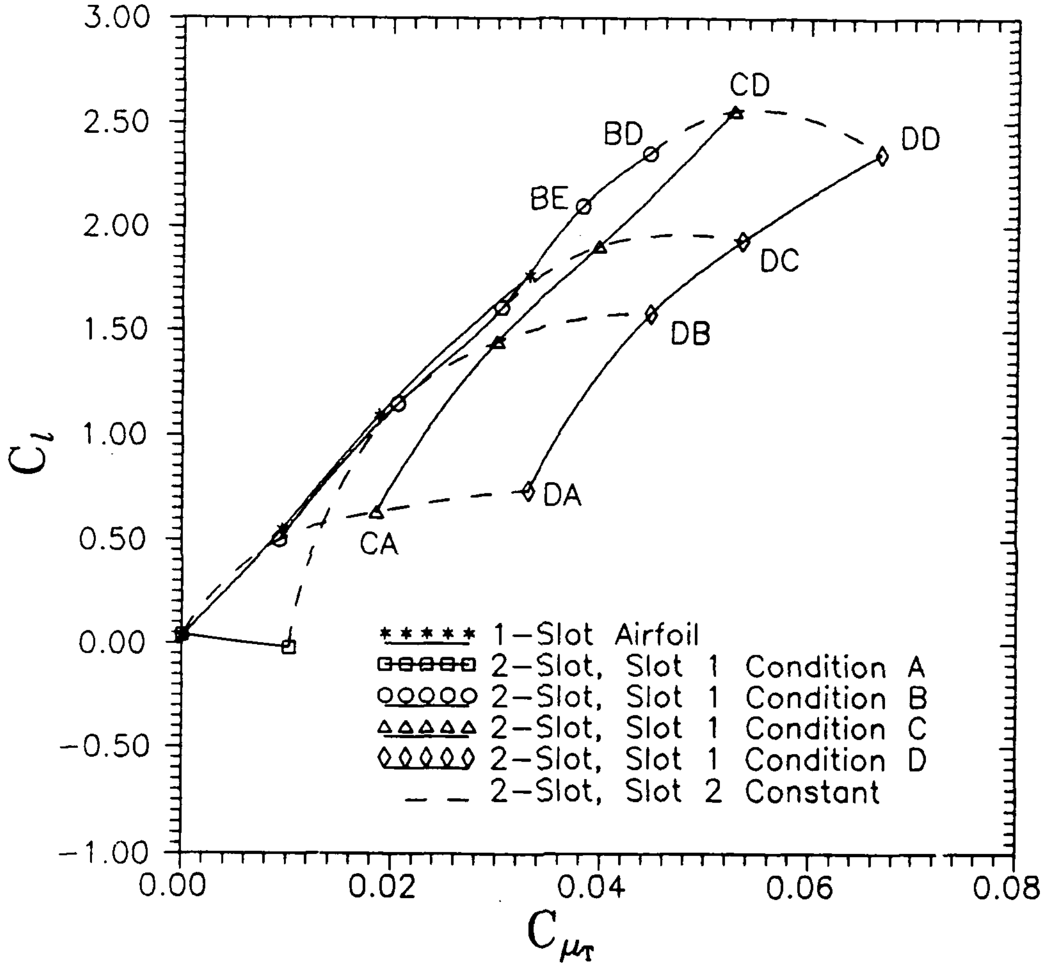

Figure 12. Effect of Blowing on Lift Coefficient, (C_l) vs. (C_μ)

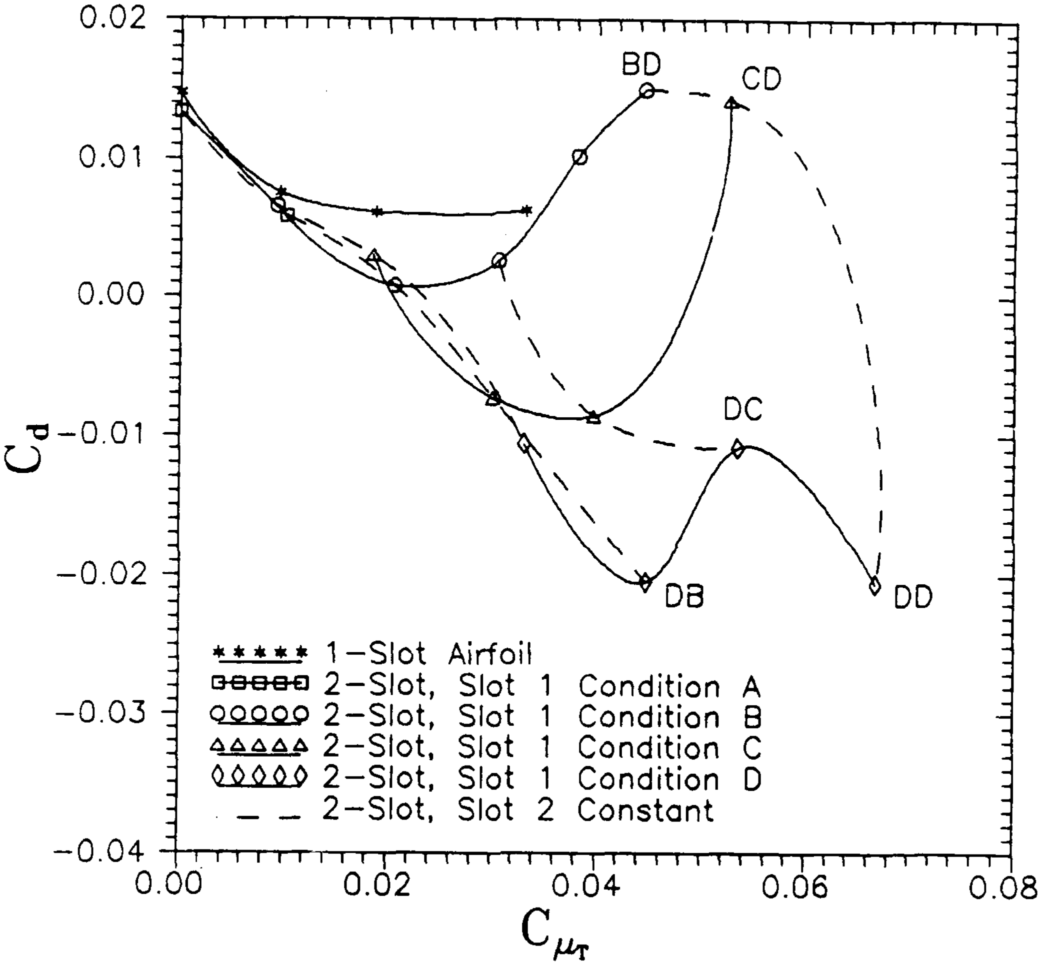

Figure 13. Effect of Blowing on Drag Coefficient, (C_d) vs. (C_μ)

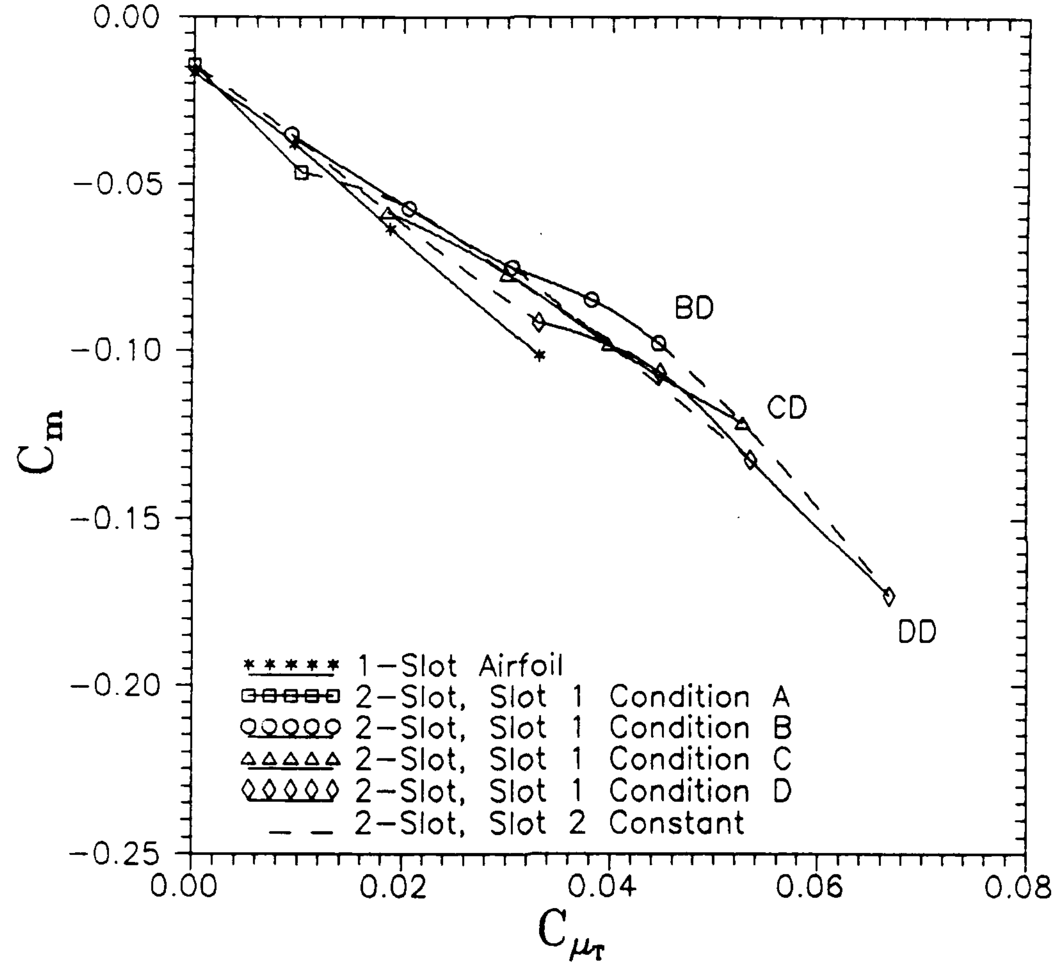

Figure 14. Effect of Blowing on Moment Coefficient, (C_m) vs. (C_μ)

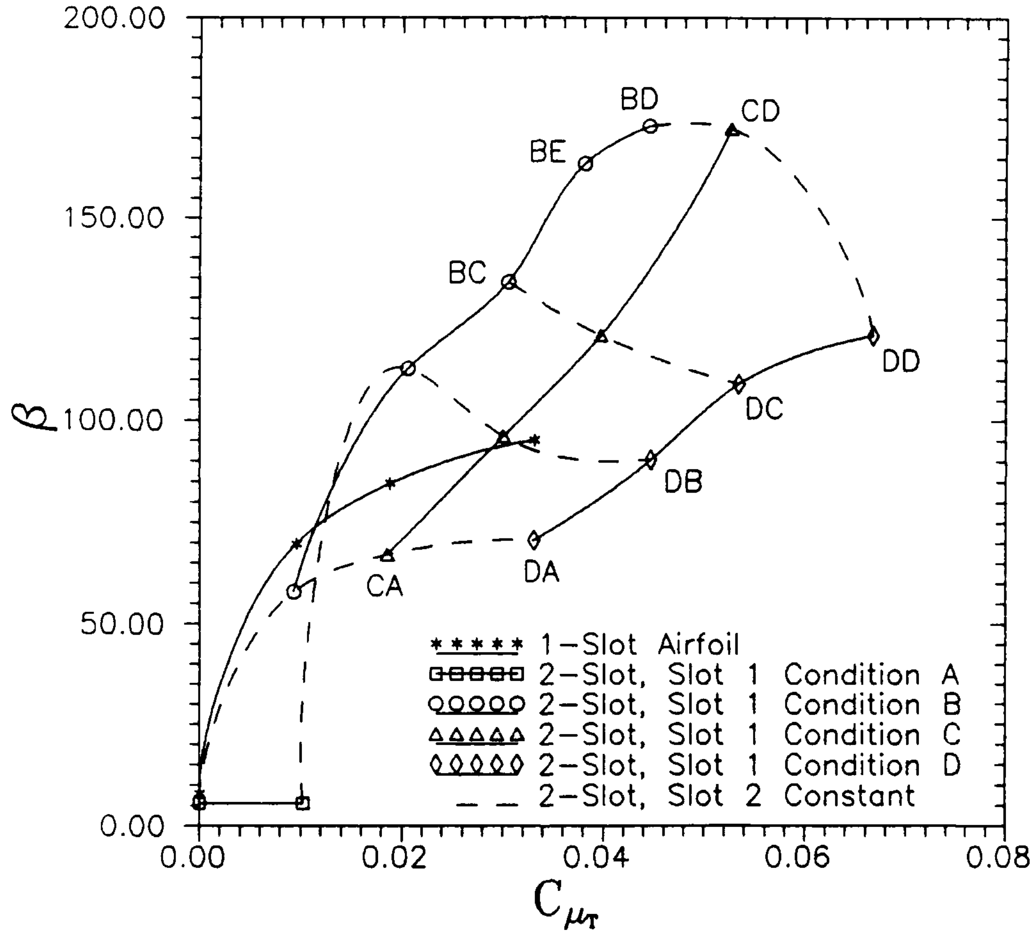

Figure 15. Effect of Blowing on Separation Angle, (β) vs. (C_μ)

3.3 Discussion

The lift coefficient did not increase for the same total blowing momentum coefficient for the two-slot case, which did occur in the research by Harvell and Franke (8, 9) with a different airfoil and Reynolds number. The lift characteristics were quite similar to those found by Harvell and Franke. The first slot blowing was important in keeping the flow attached until reaching the second slot. Once attached, the lift was increased and separation delayed primarily by the second slot. When the two-slot case is compared to Williams' one-slot analysis (19), the lift characteristics showed the same trends. The lift curve was extended to higher maximum lift values, $C_{l_{max}}$, because a higher total blowing momentum was reached using two slots. However, because of the different trailing-edge and interference between slots, increased first slot blowing did not effectively increase lift.

The drag results were typical of what Williams found (19), that the model overpredicted the drag. In cases where the blowing was closest to experimental values, the drag for two slots was less than a one slot case for the same blowing.

3.4 Computer Resources

The primary computational tool for the analysis was the Aeronautical Systems Division CRAY XMP-12 through the sponsorship of Dr. Joe Shang WRDC/FIMM. Each run was approximately 2500 iterations, with change in C_l determining convergence. For Cases BC, BE, BD, CD, and DC some computation was required at AFIT's computer facility on the ELXSI-6400. The CRAY computations were in double precision, and averaged 3.3 x 10^{-6} (seconds)/[(grid point)(iteration)]. The ELXSI computations were in single precision with a performance level of 3.6 x 10^{-3} (seconds)/[(grid point)(iteration)]. The data was transferred to the AFIT computer systems and post processed using the DI-3000 software package. Data transfer and storage was difficult to say the least, and the DI-3000 software package is no longer being supported at AFIT.

IV. Conclusions and Recommendations

4.1 Conclusions

The Navier-Stokes analysis of a two-slot circulation control airfoil demonstrated that the maximum lift coefficient, $C_{l_{max}}$, can be extended over that of the one-slot airfoil, but the lift per total blowing momentum coefficient did not increase over the one-slot airfoil. The lift coefficient,C_l, and angle of separation, β, show greatest increases as additional blowing is applied to the second slot, provided the first slot blowing has sufficient blowing to maintain flow attachment flow between slots. When no blowing is applied to the first slot, separation occurs before reaching the second slot. Thus, if two slots exist, some blowing must be applied to the first slot. When no blowing is applied to the second slot of a two-slot airfoil, lift and separation angle are significantly less than for the same blowing applied to a one-slot circulation control airfoil. This indicates that lift and flow separation are very sensitive to small protrusions on the trailing-edge.

Drag showed similar characteristics to that of the one-slot configuration, but no conclusion can be drawn from the trends. The moment coefficient was less dependent on which slot blowing was applied.

4.2 Recommendations

Based on the analysis, these recommendations follow:

1. Investigate what minimum level of blowing is required for the flow to remain attached between slots and how various free-stream conditions affect attachment.
2. Use the Navier-Stokes code to model existing two-slot airfoil data. The present method may not be able to model flow below Mach numbers of 0.25.
3. Analyze various flight conditions, such as Mach number or angle of attack, in order to evaluate the effect on the airfoil aerodynamic characteristics. Analysis can be done on the influence of the effective angle of attack, and analysis done without using effective values.
4. Investigate the effects of a different O-grid generation program, and if the skewness of the grid near the slots could be reduced, improving analysis.
5. Investigate a configuration the could be analyzed both experimentally and computationally for a two-slot, elliptical airfoil.

Appendix A. *Cases with Slot 1 at Condition A*

A.1 Case AA Data

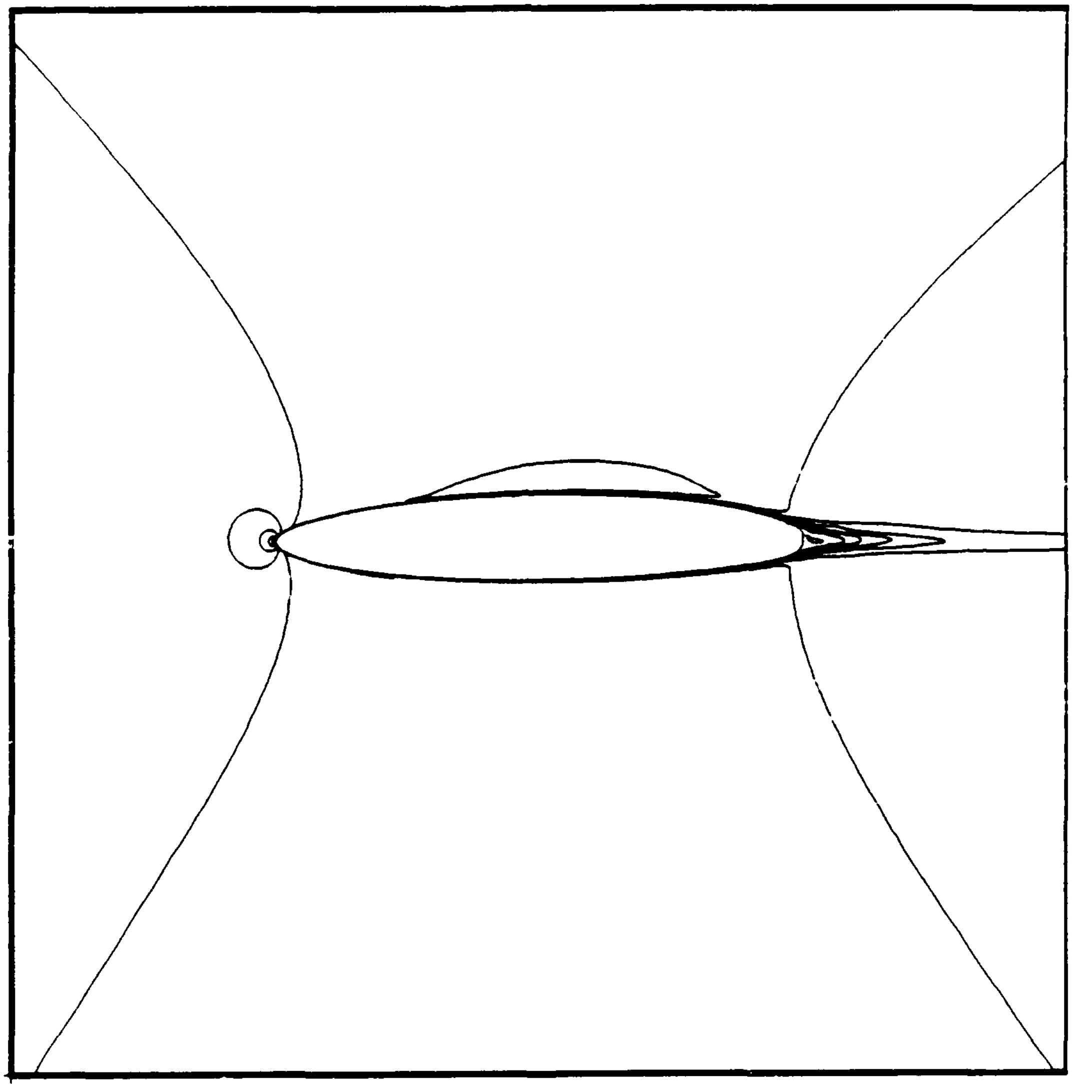

Figure 16. Case AA Mach Contour - Overview

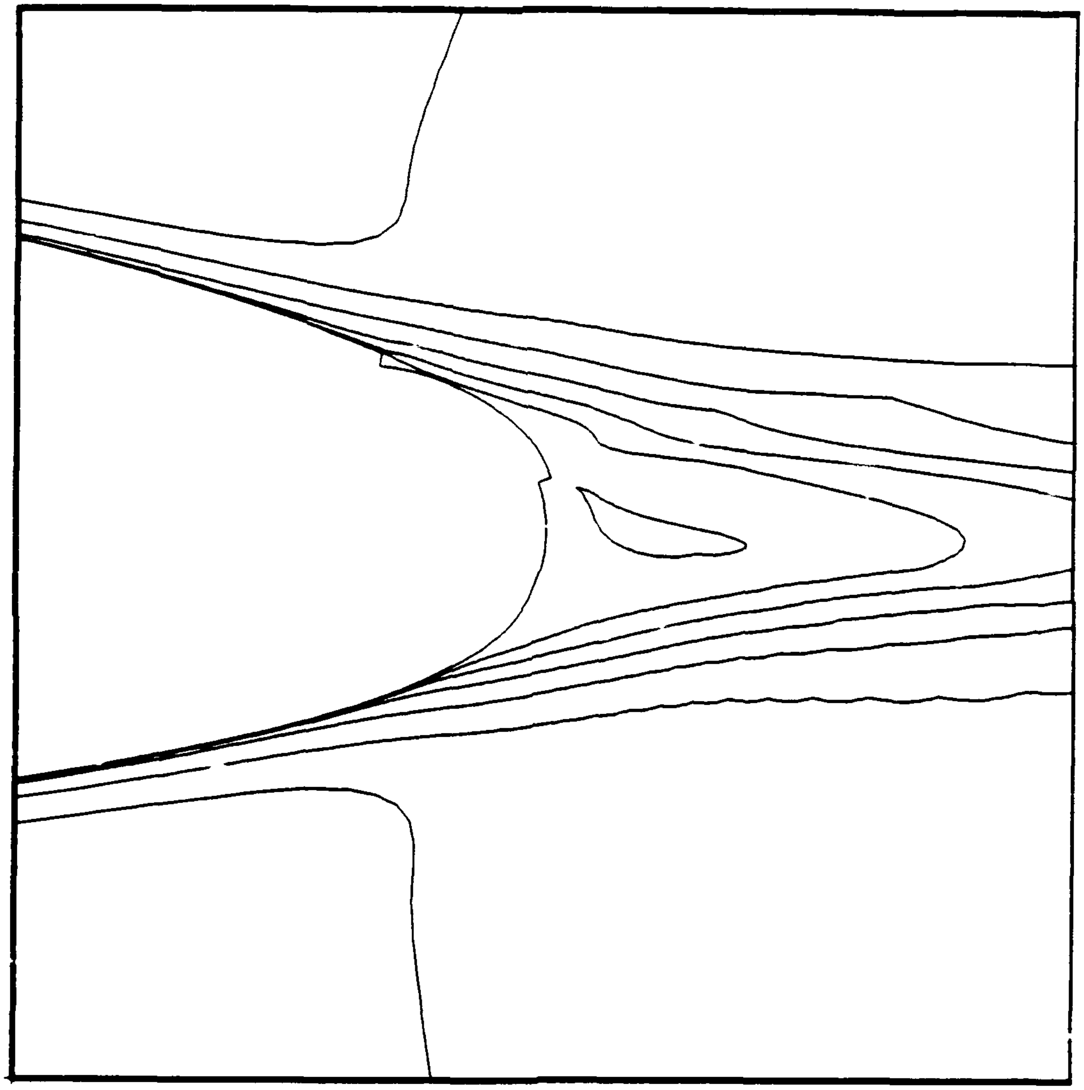

Figure 17. Case AA Mach Contour - Trailing Edge

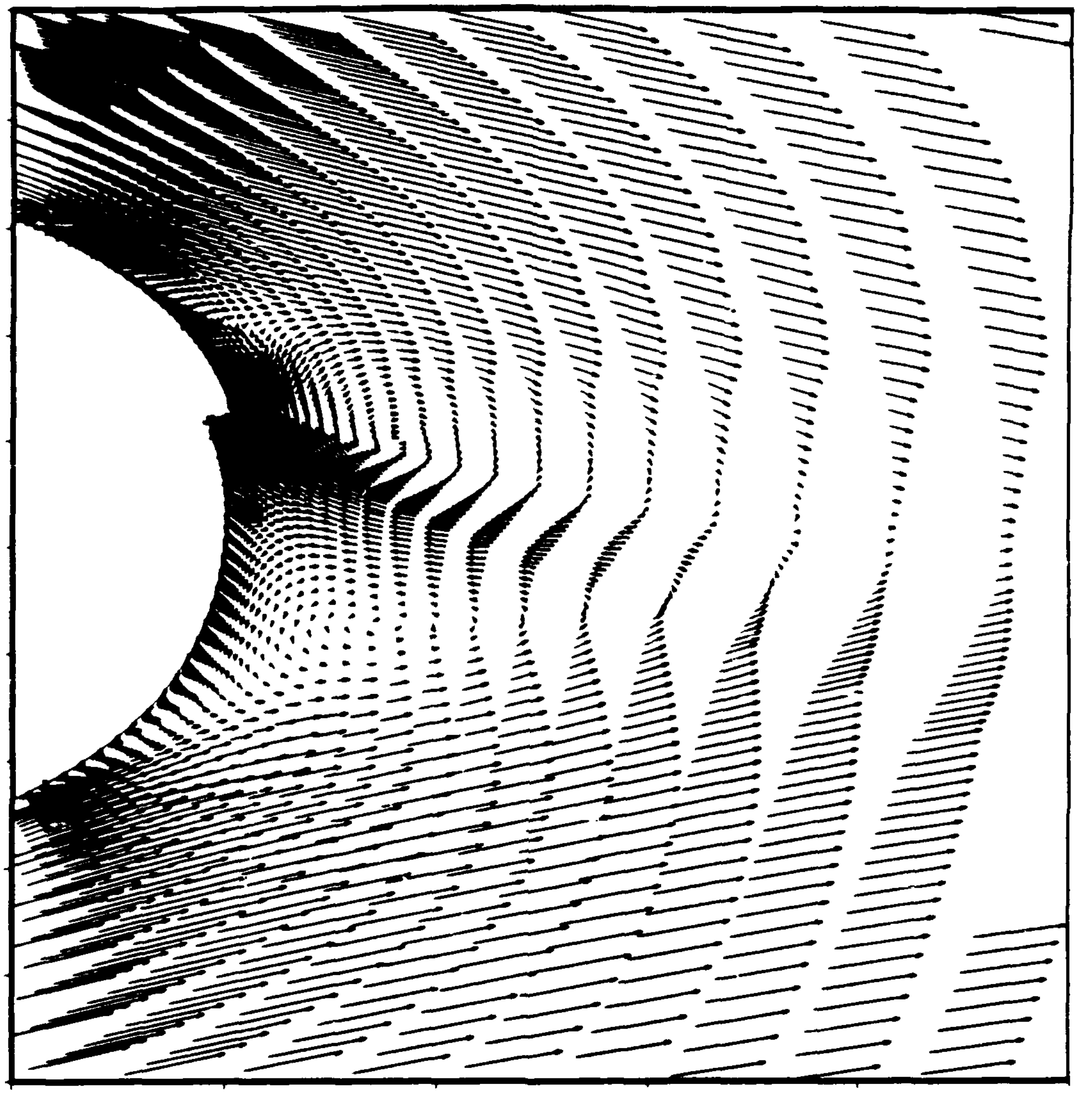

Figure 18. Case AA Trailing Edge Velocity Vector Field

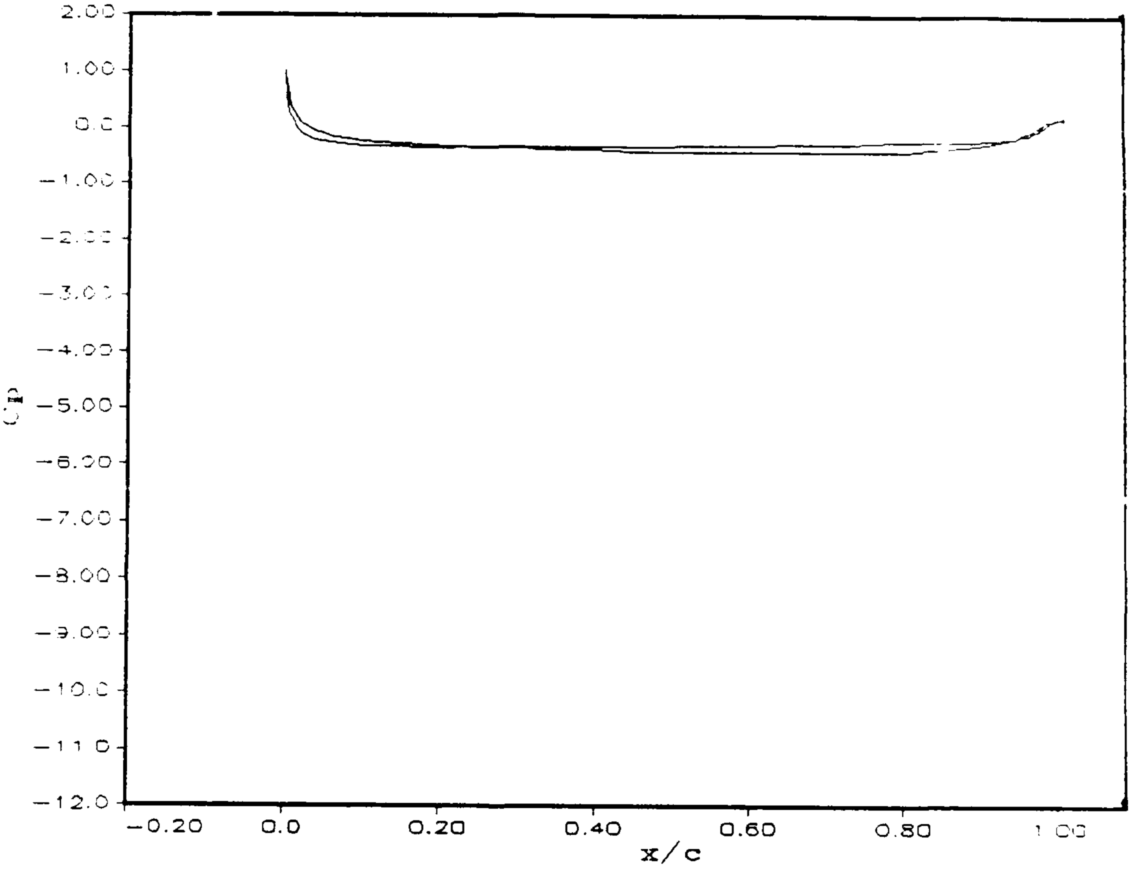

Figure 19. Case AA Pressure Coefficient (C_p) vs. x/c

A.2 *Case AB Data*

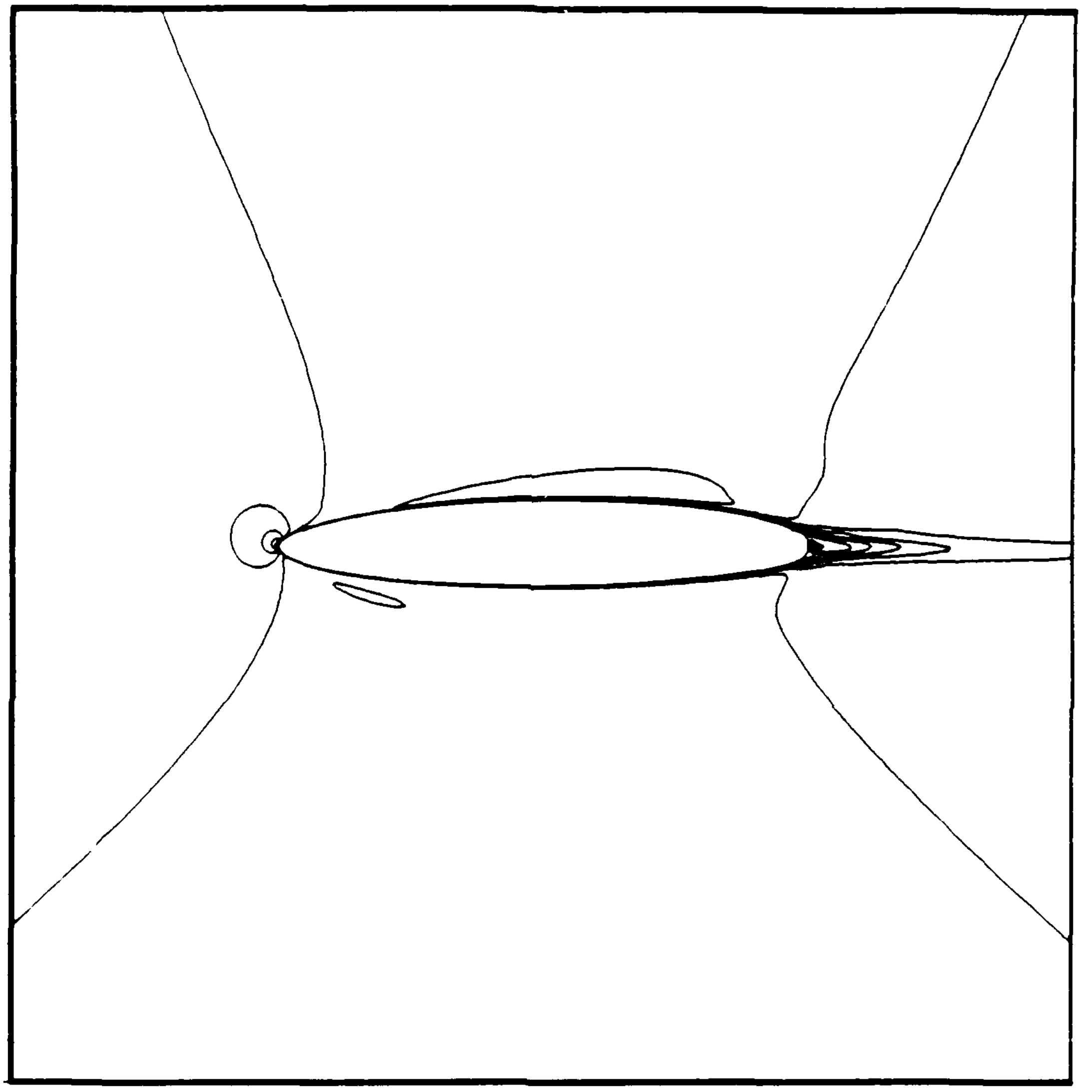

Figure 20. Case AB Mach Contour - Overview

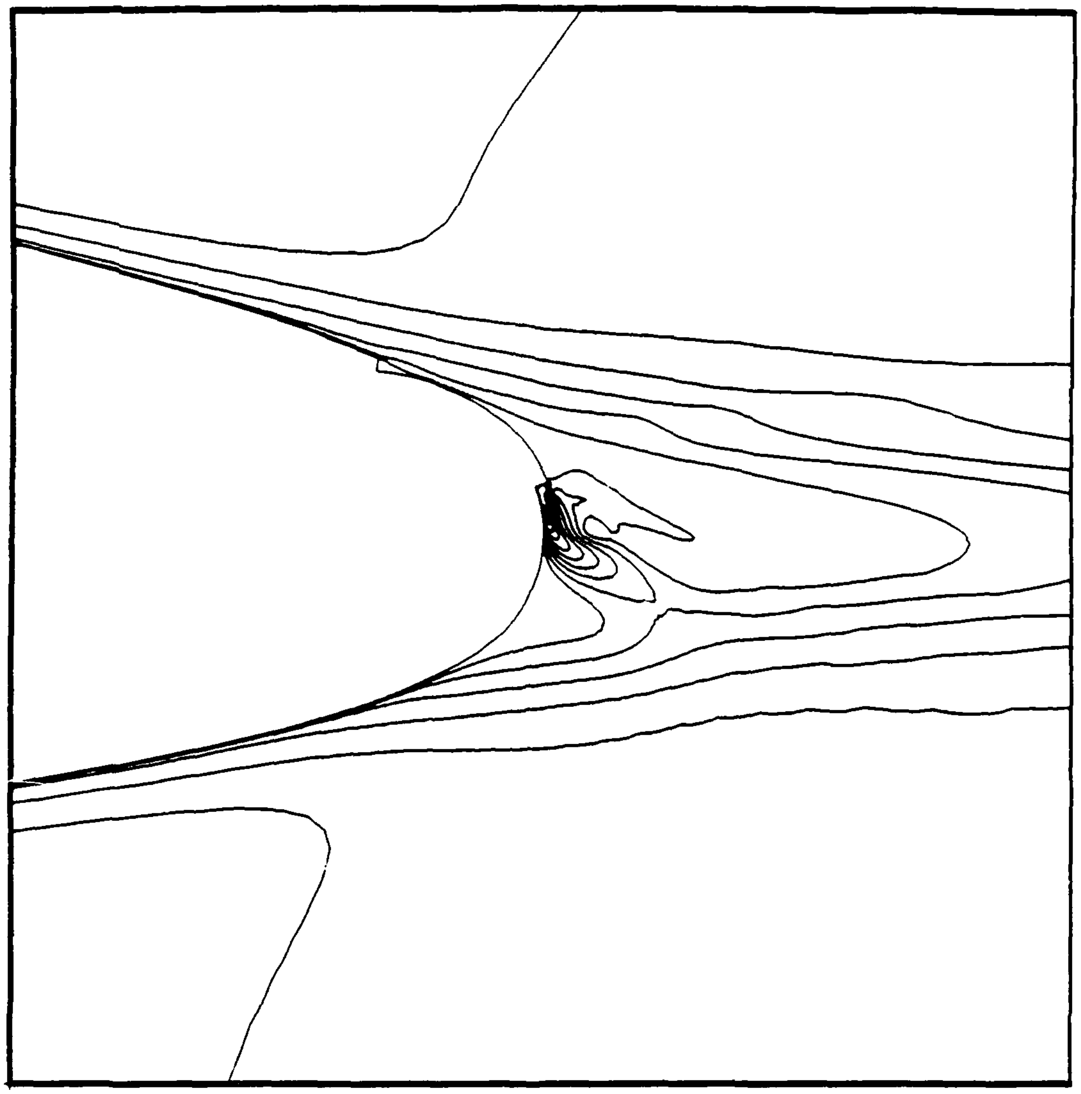

Figure 21. Case AB Mach Contour - Trailing Edge

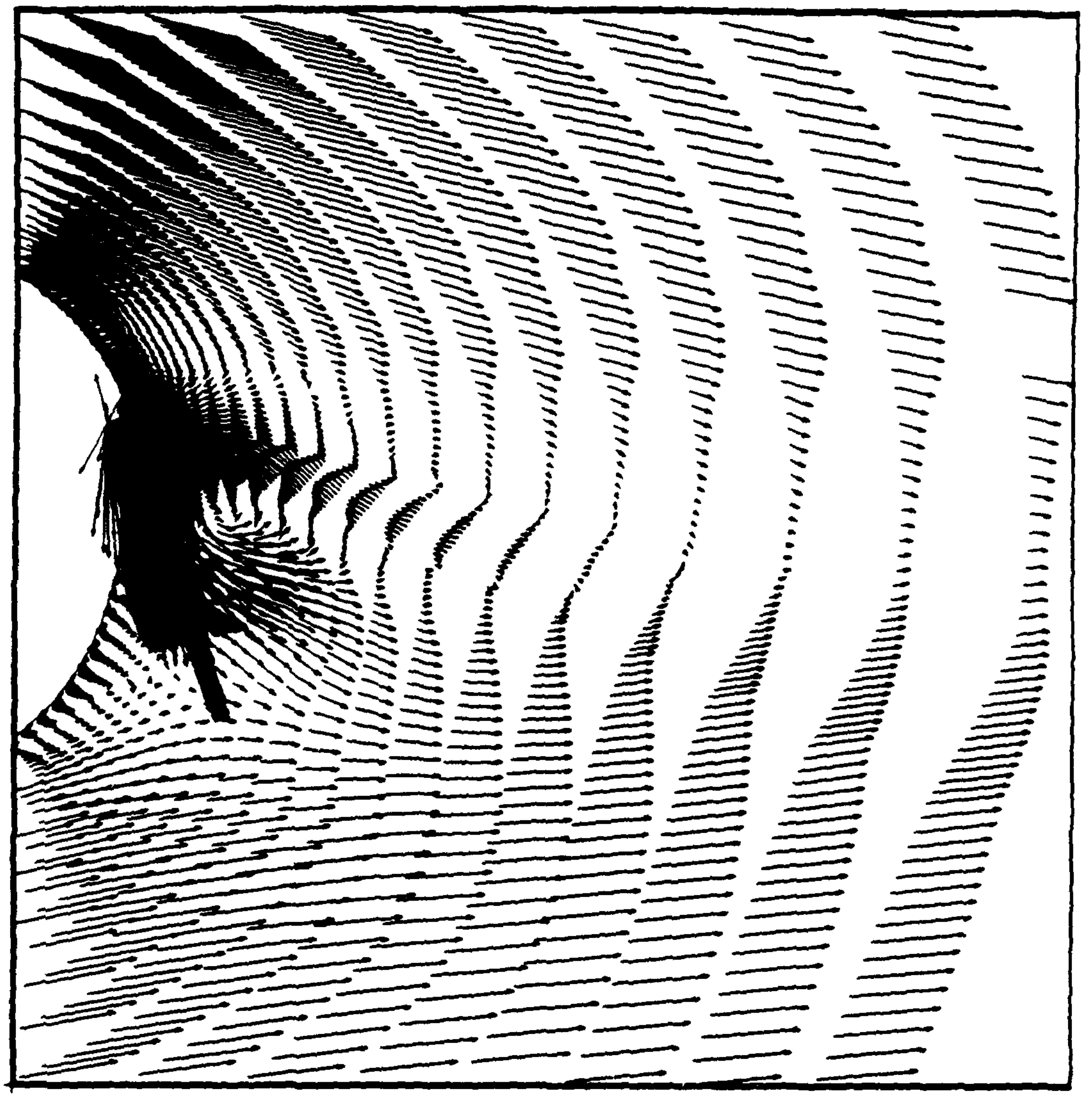

Figure 22. Case AB Trailing Edge Velocity Vector Field

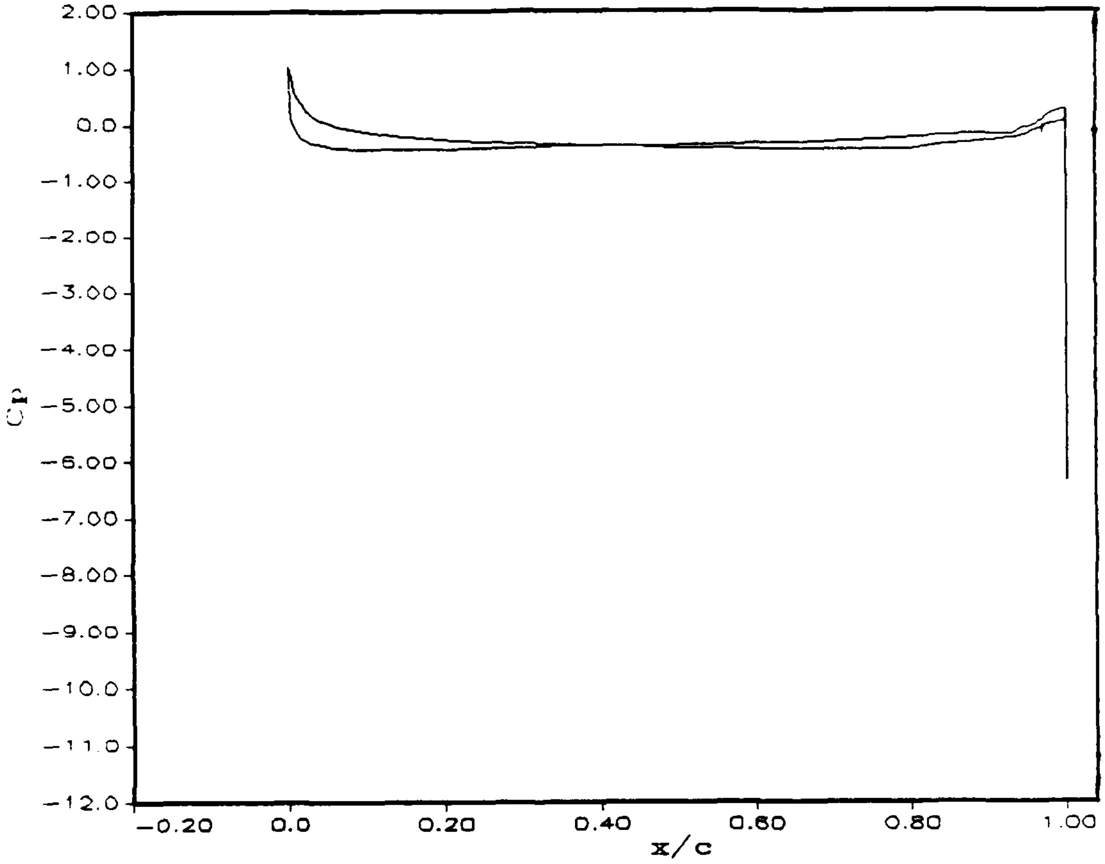

Figure 23. Case AB Pressure Coefficient (C_p) vs. x/c

Appendix B. *Cases with Slot 1 at Condition B*

B.1 Case BA Data

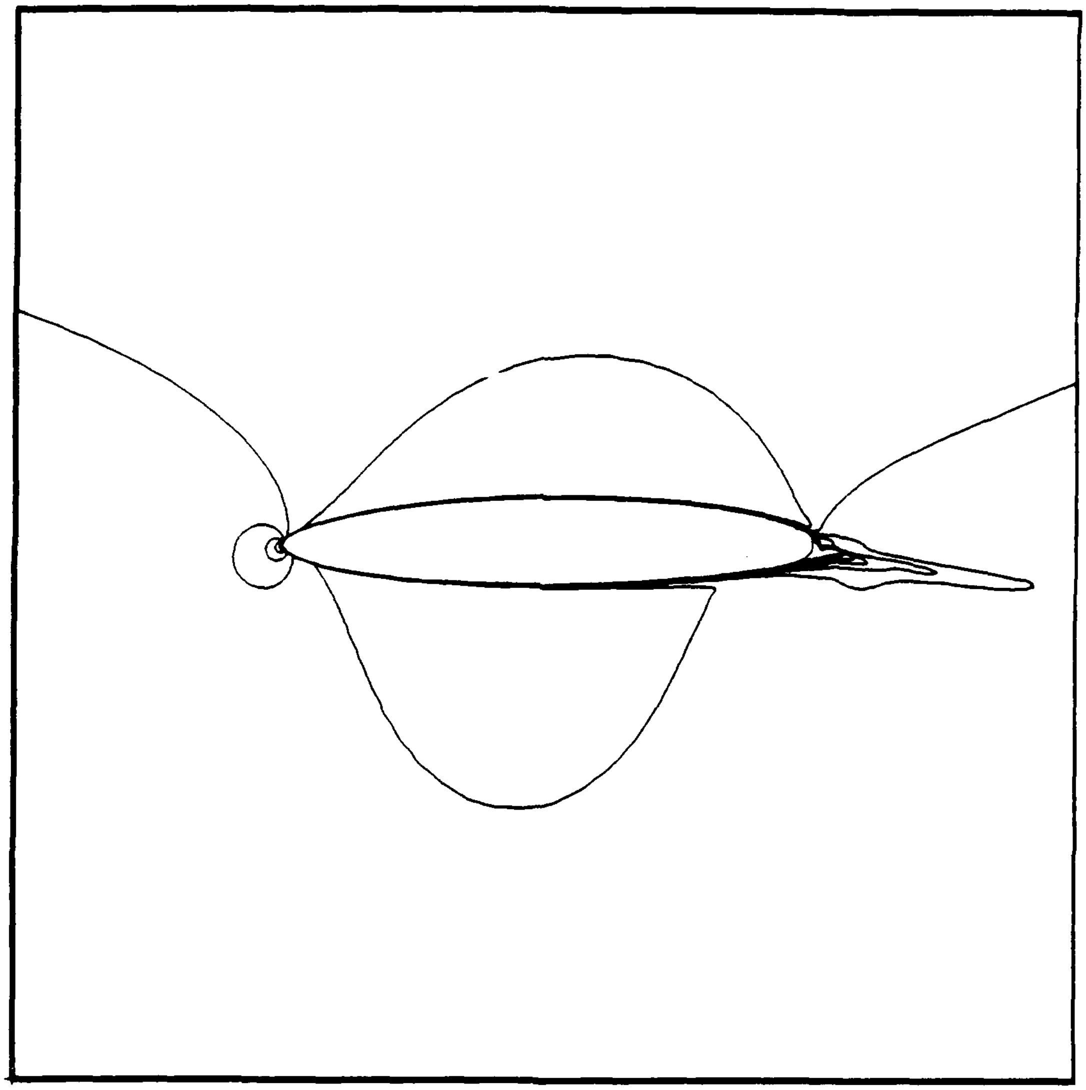

Figure 24. Case BA Mach Contour - Overview

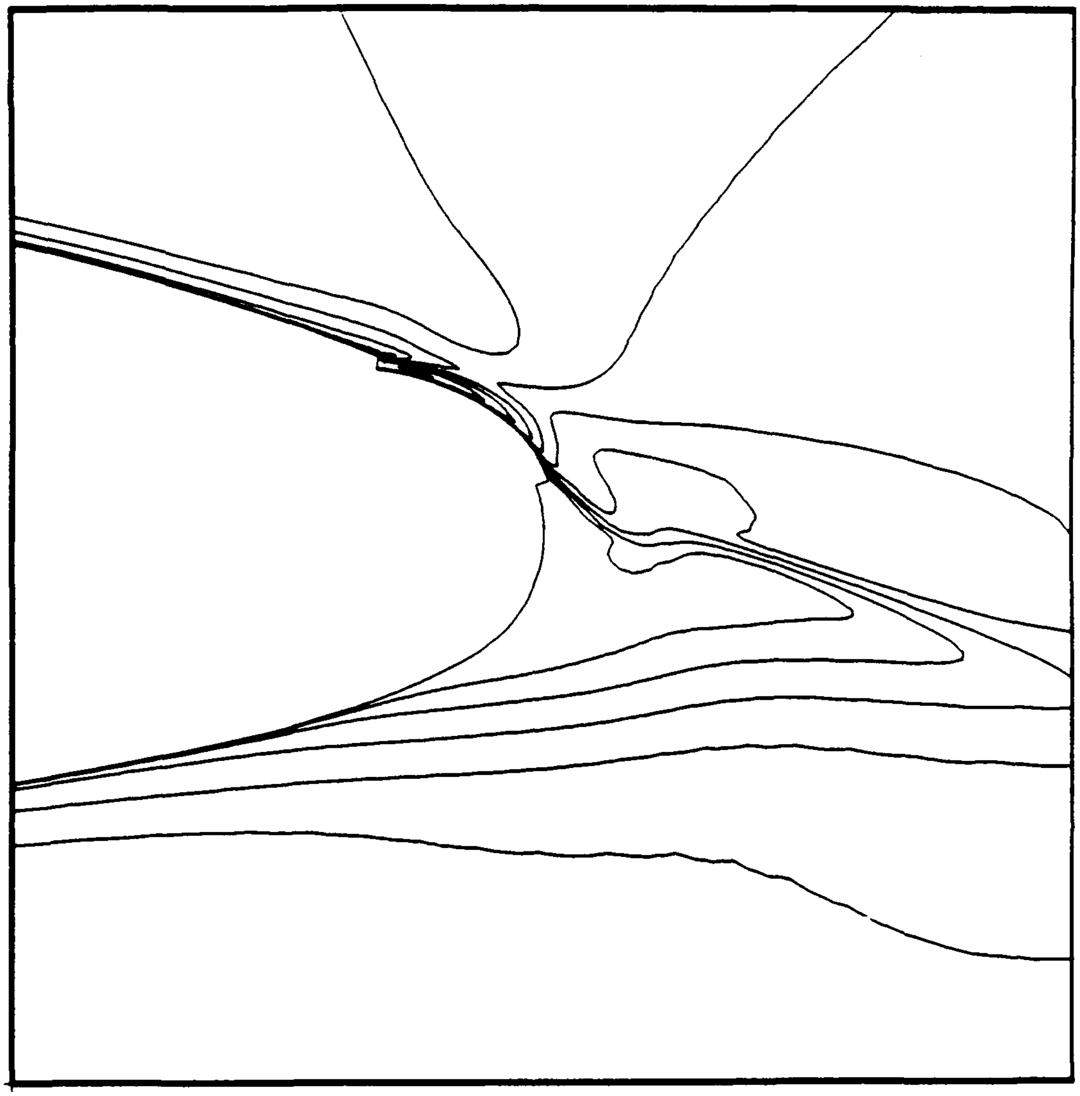

Figure 25. Case BA Mach Contour - Trailing Edge

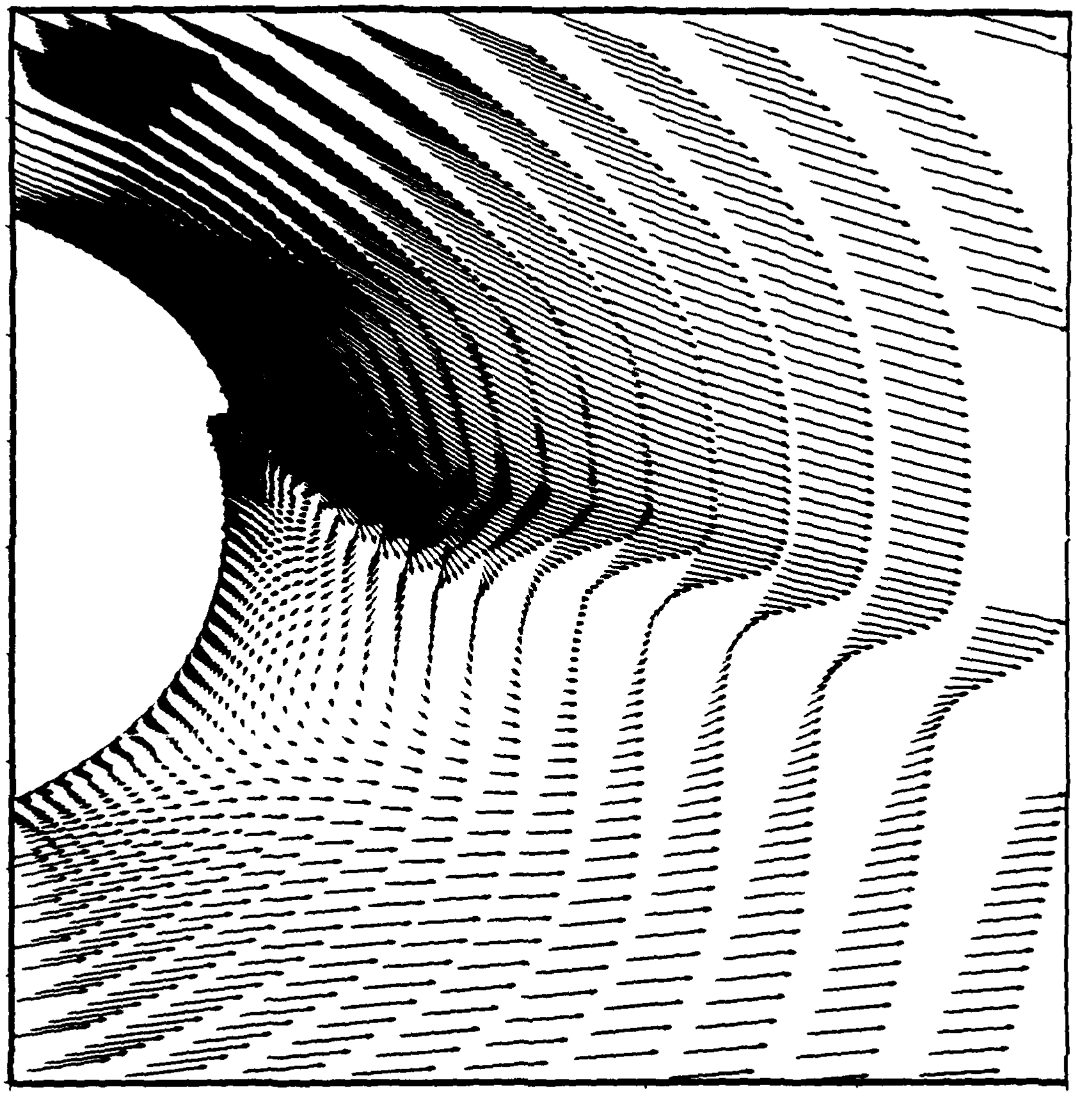

Figure 26. Case BA Trailing Edge Velocity Vector Field

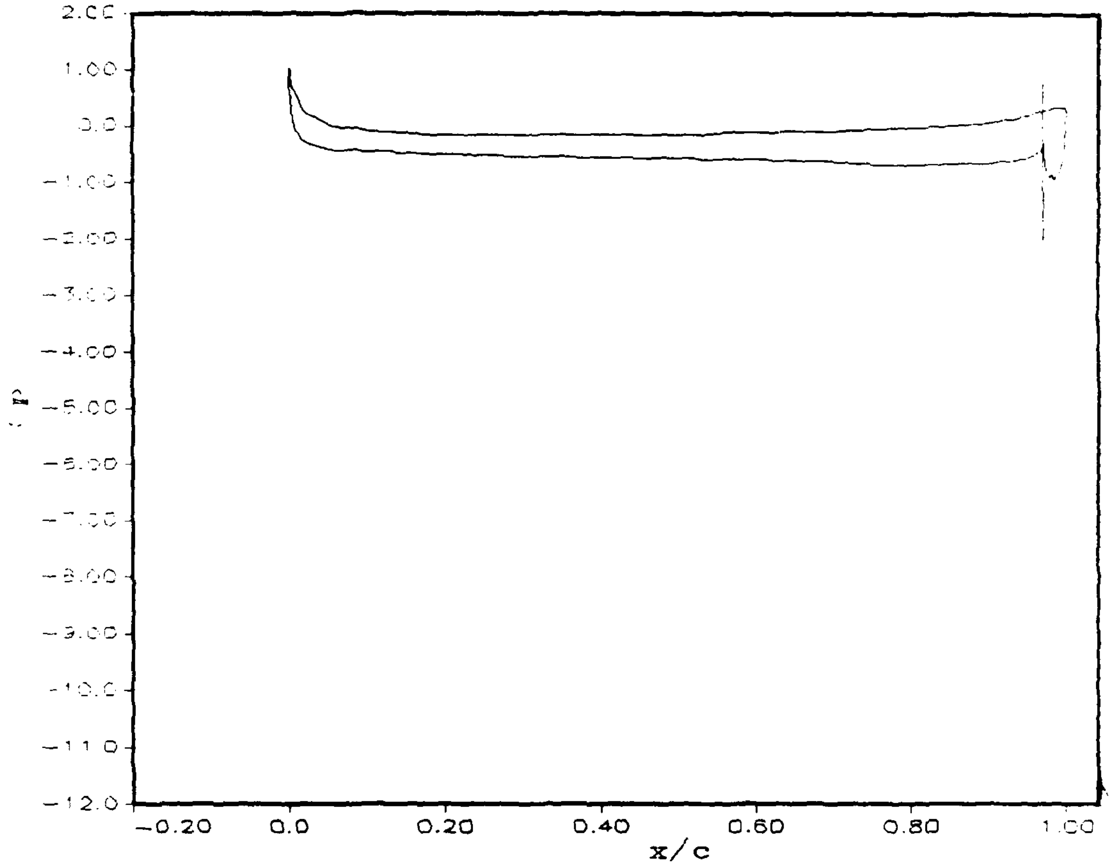

Figure 27. Case BA Pressure Coefficient (C_p) vs. x/c

B.2 Case BB Data

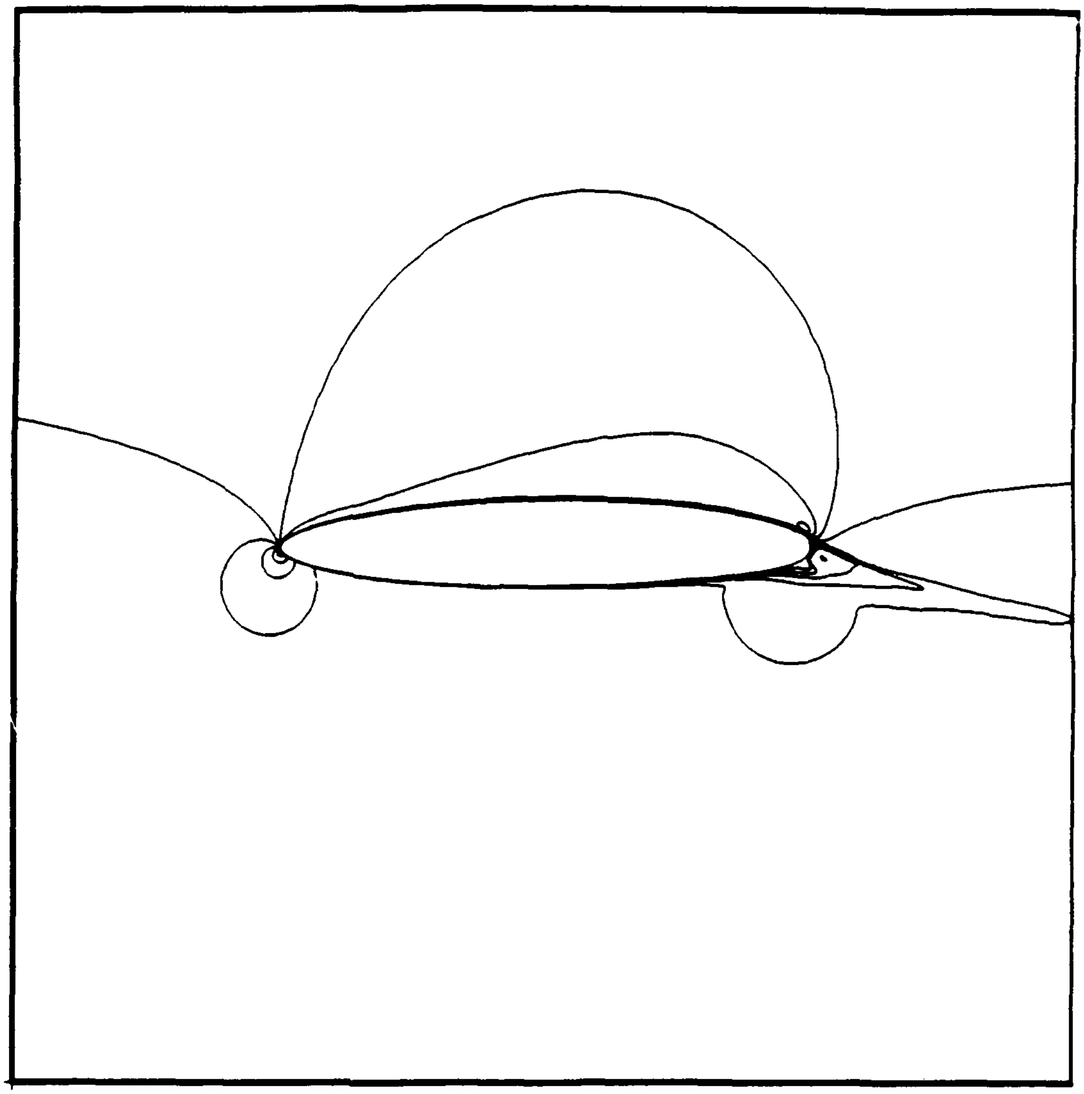

Figure 28. Case BB Mach Contour - Overview

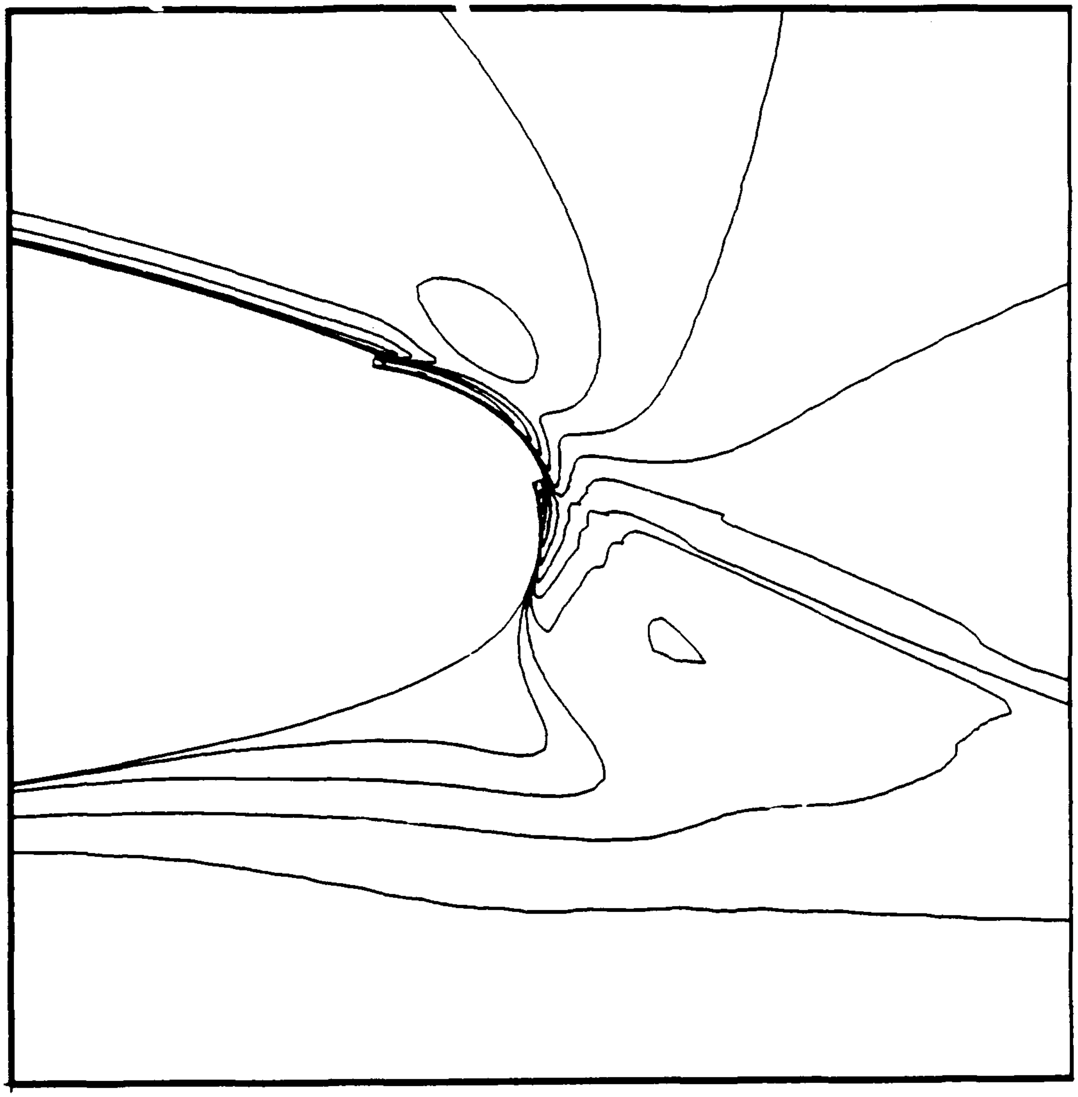

Figure 29. Case BB Mach Contour - Trailing Edge

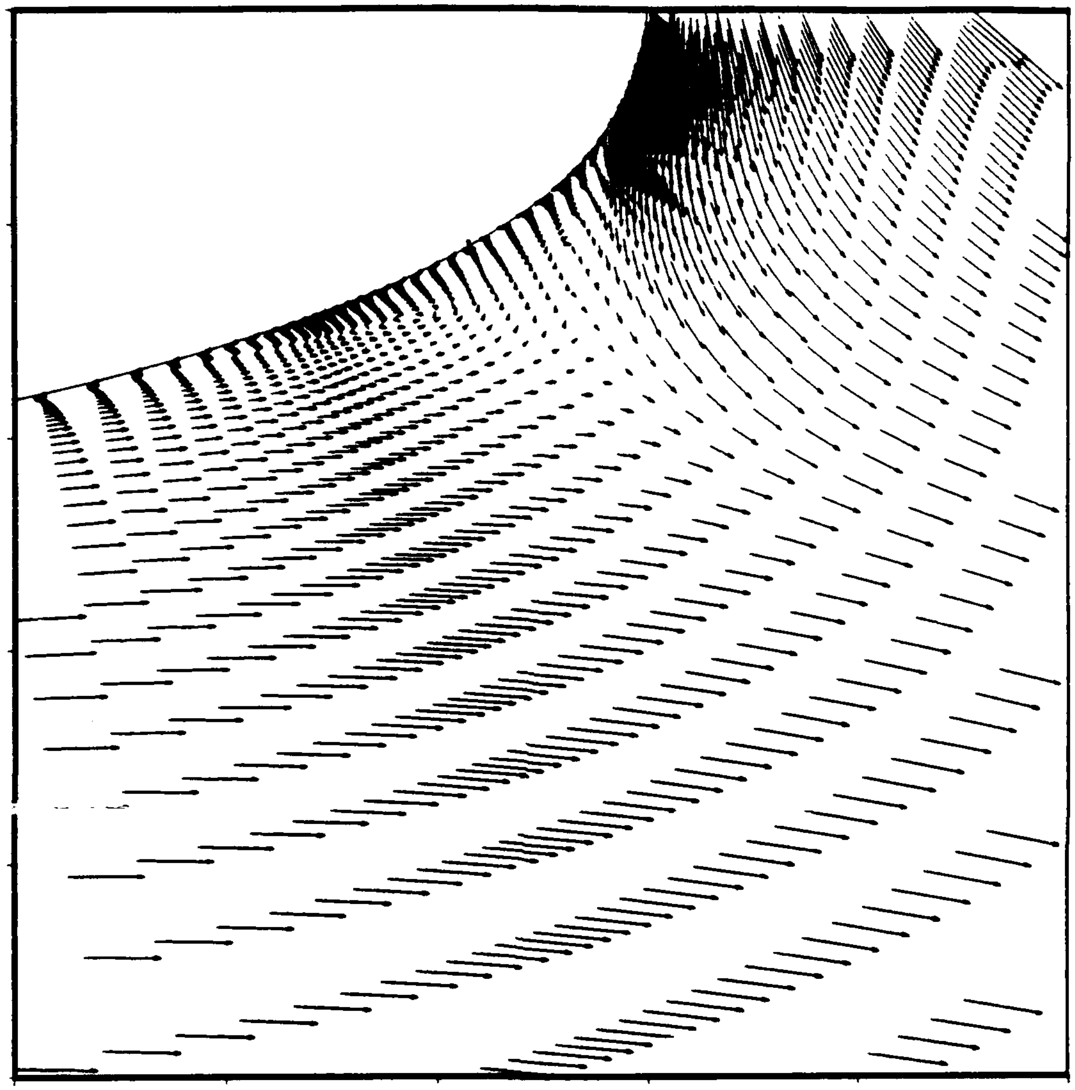

Figure 30. Case BB Trailing Edge Velocity Vector Field

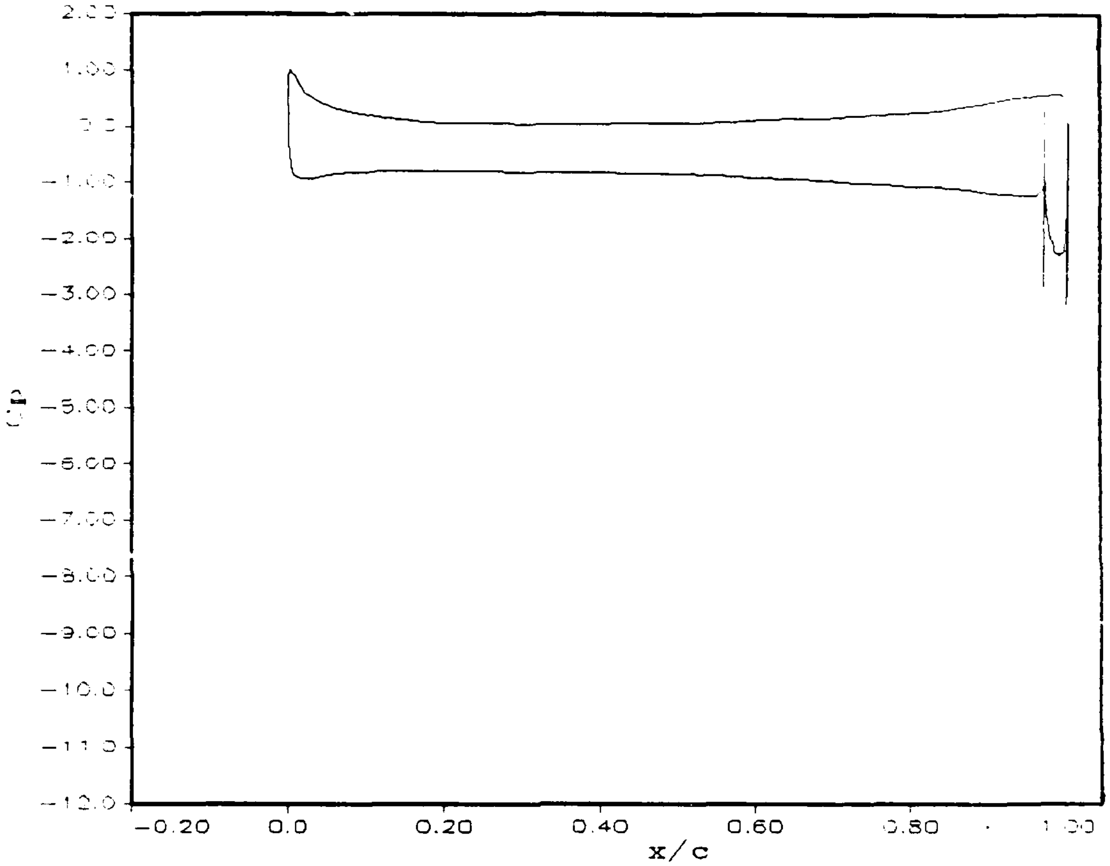

Figure 31. Case BB Pressure Coefficient (C_p) vs. x/c

B.3 Case BC Data

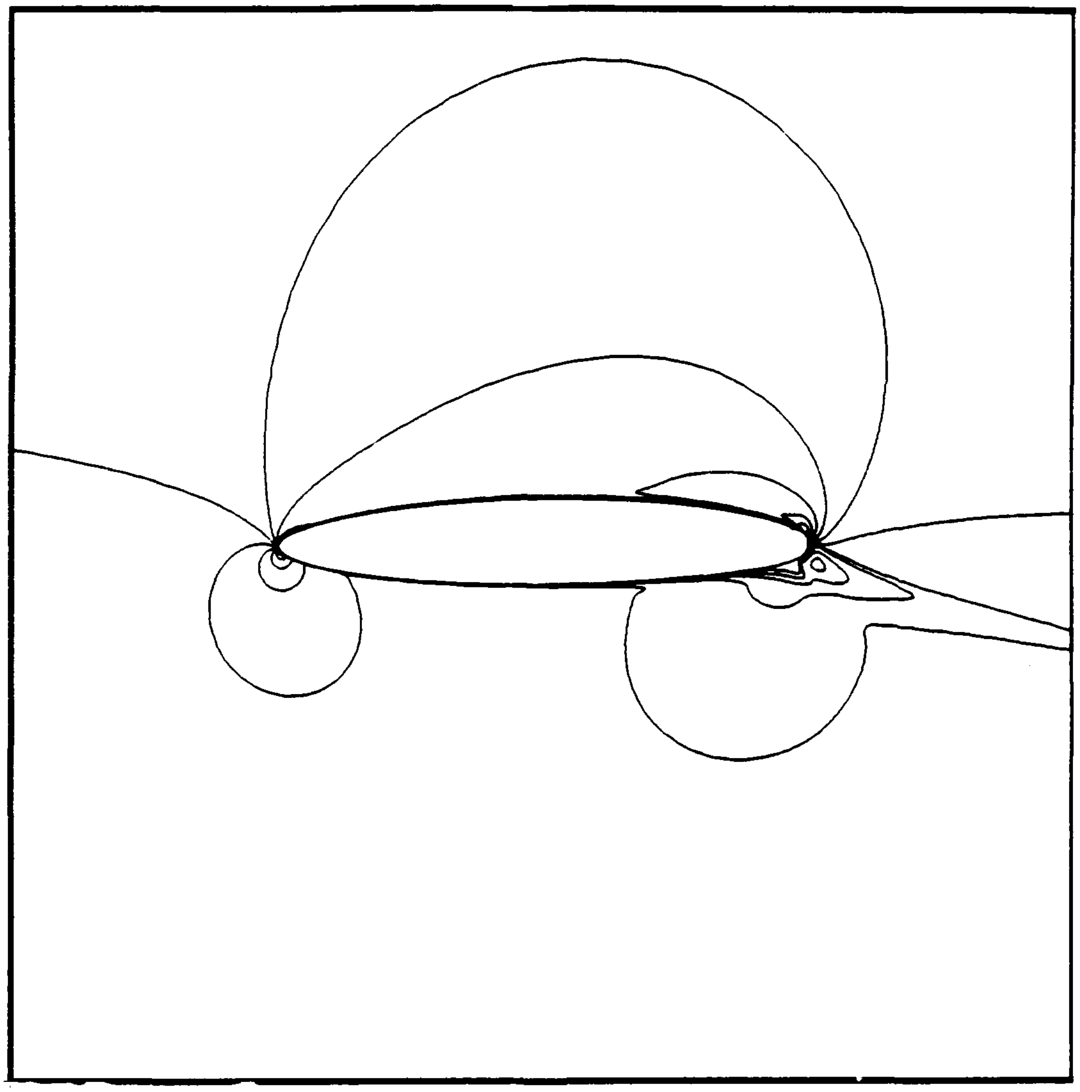

Figure 32. Case BC Mach Contour - Overview

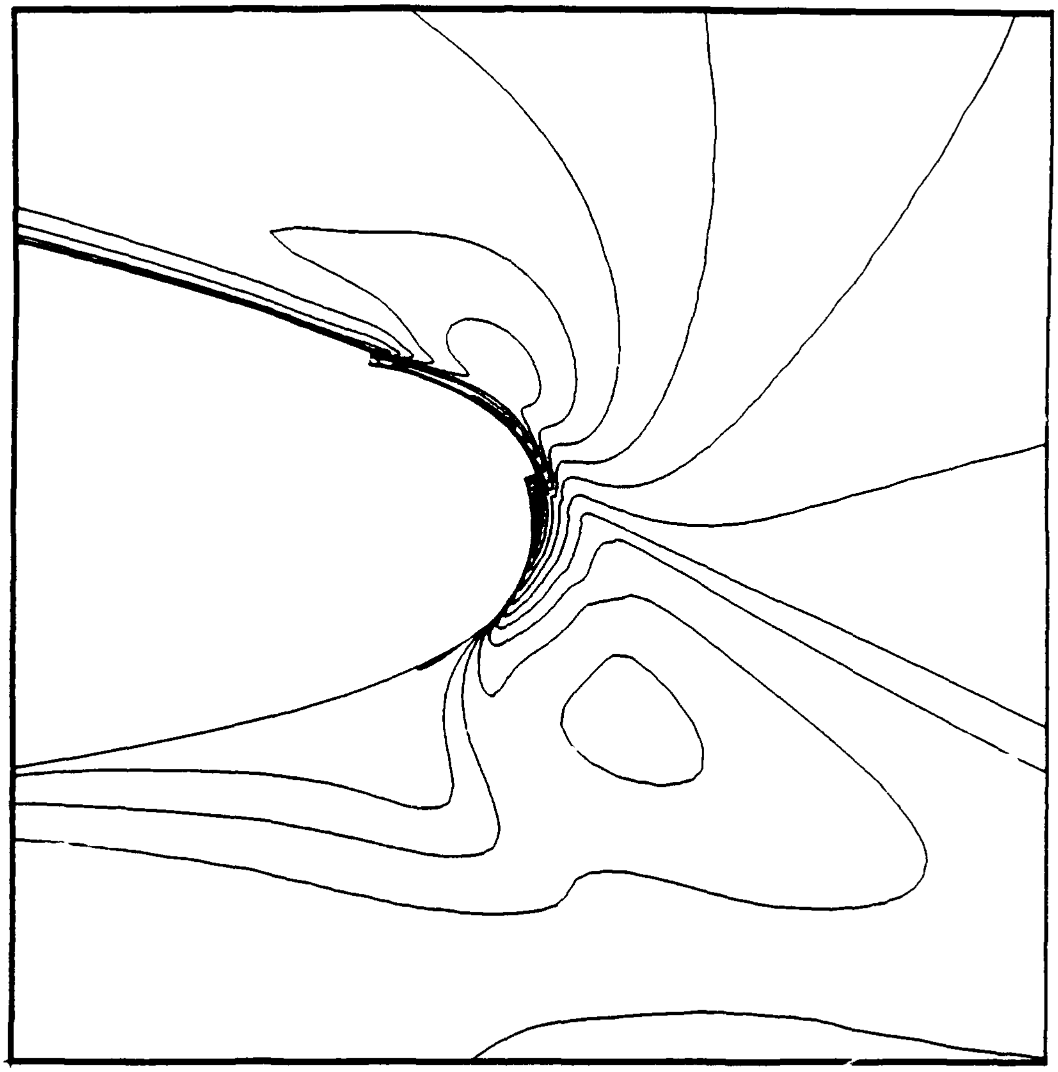

Figure 33. Case BC Mach Contour - Trailing Edge

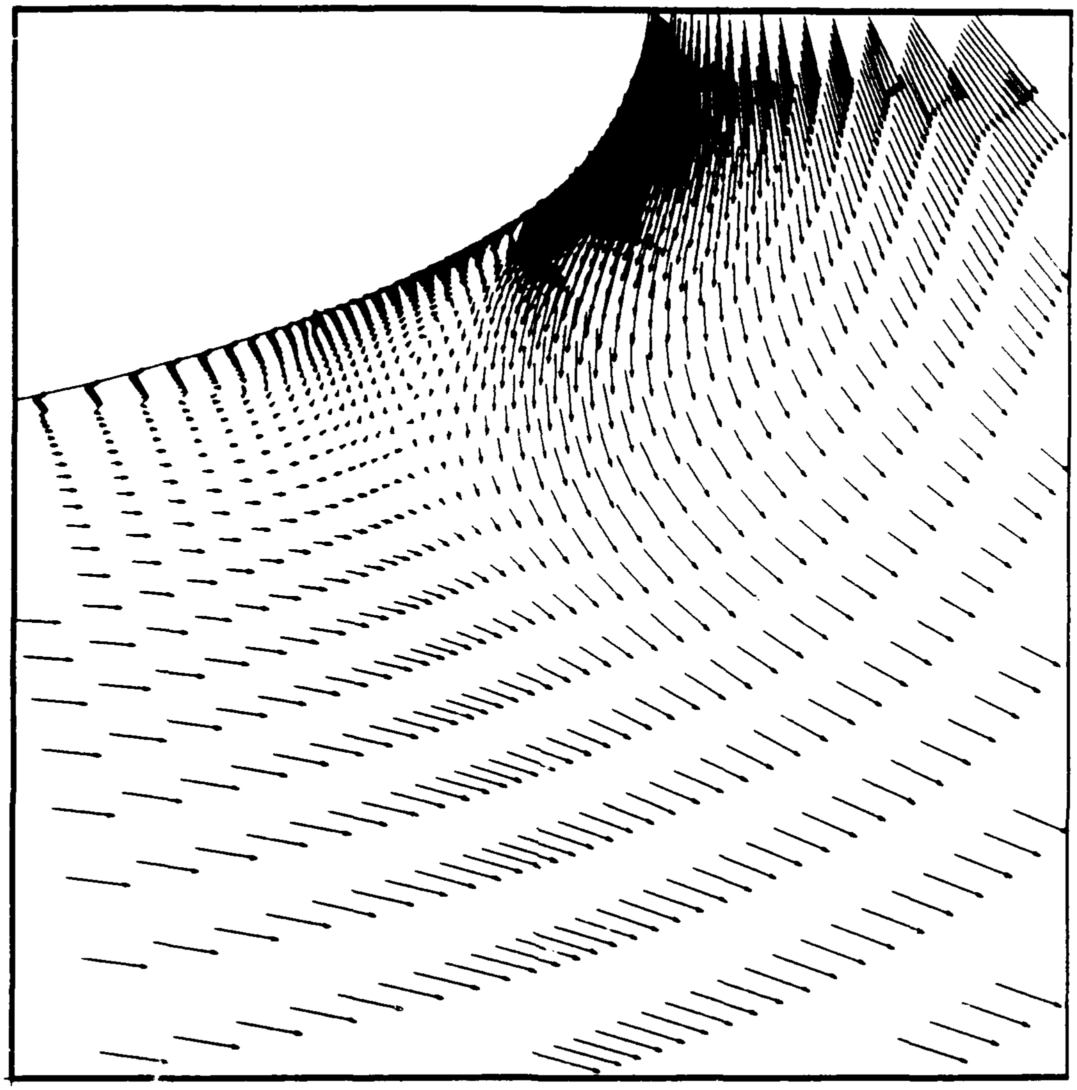

Figure 34. Case BC Trailing Edge Velocity Vector Field

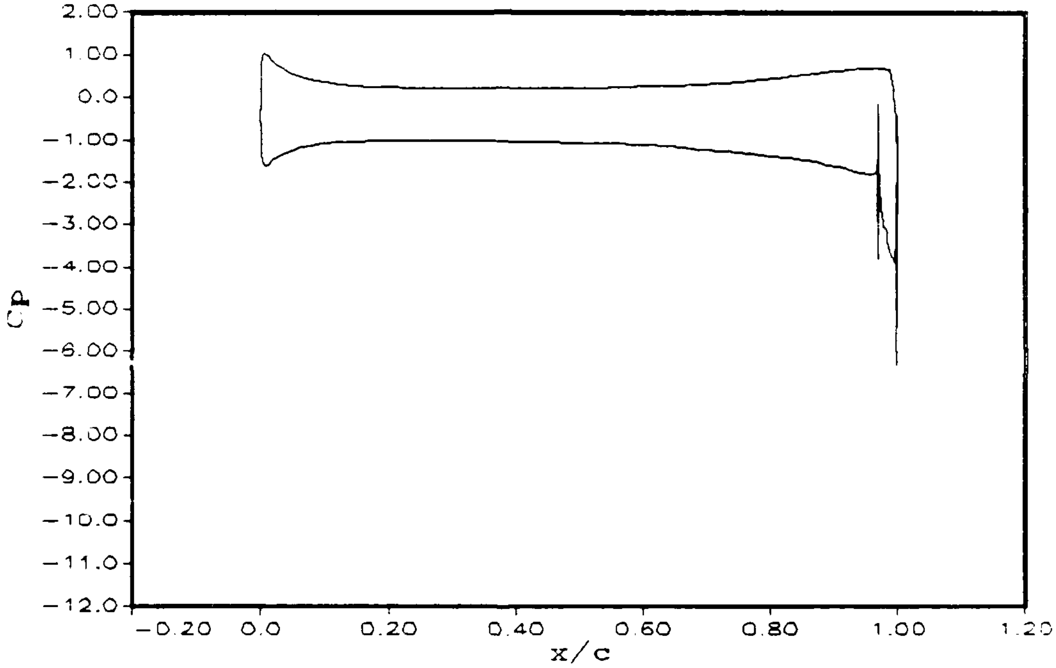

Figure 35. Case BC Pressure Coefficient (C_p) vs. x/c

B.4 Case BE Data

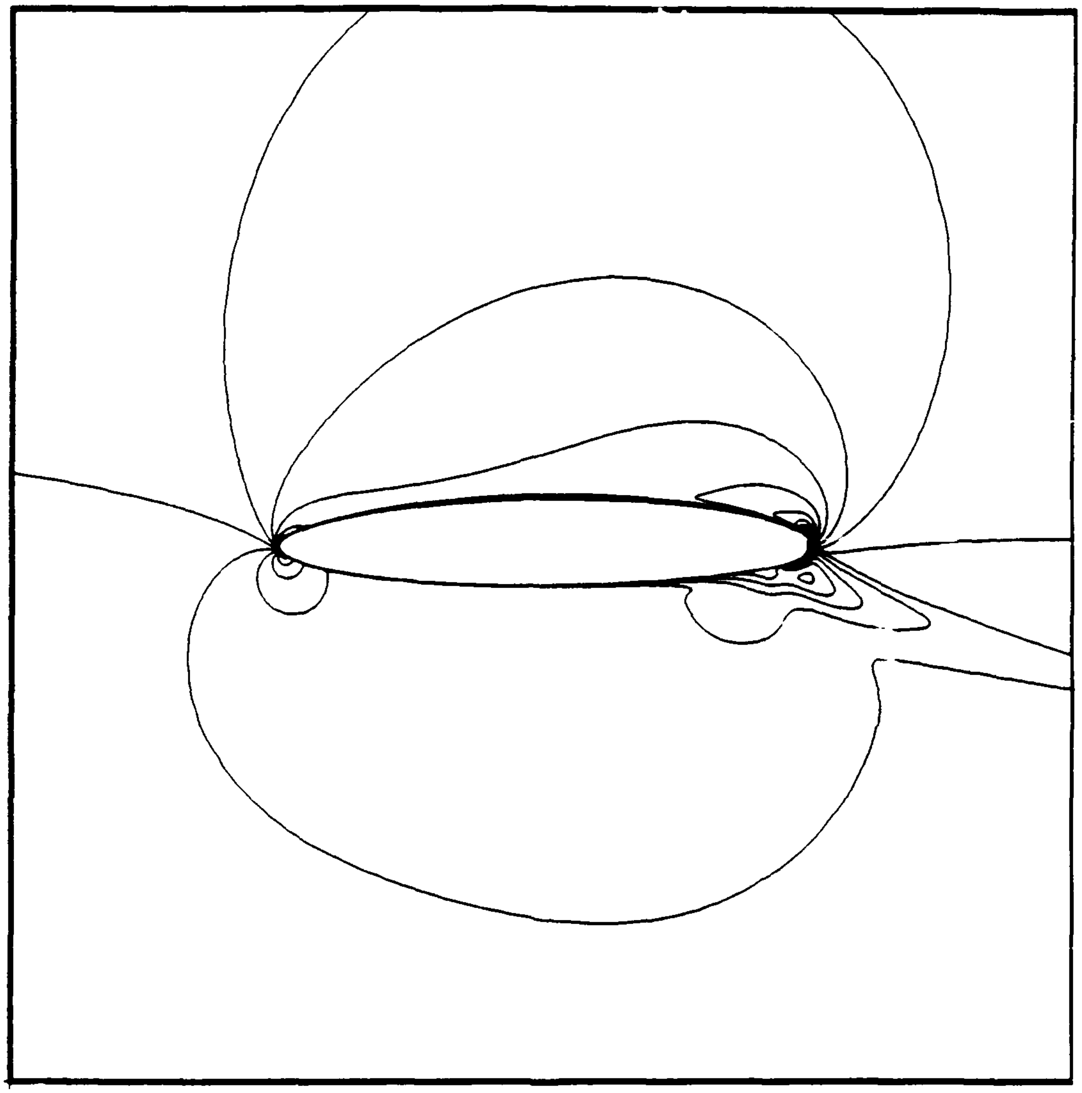

Figure 36. Case BE Mach Contour - Overview

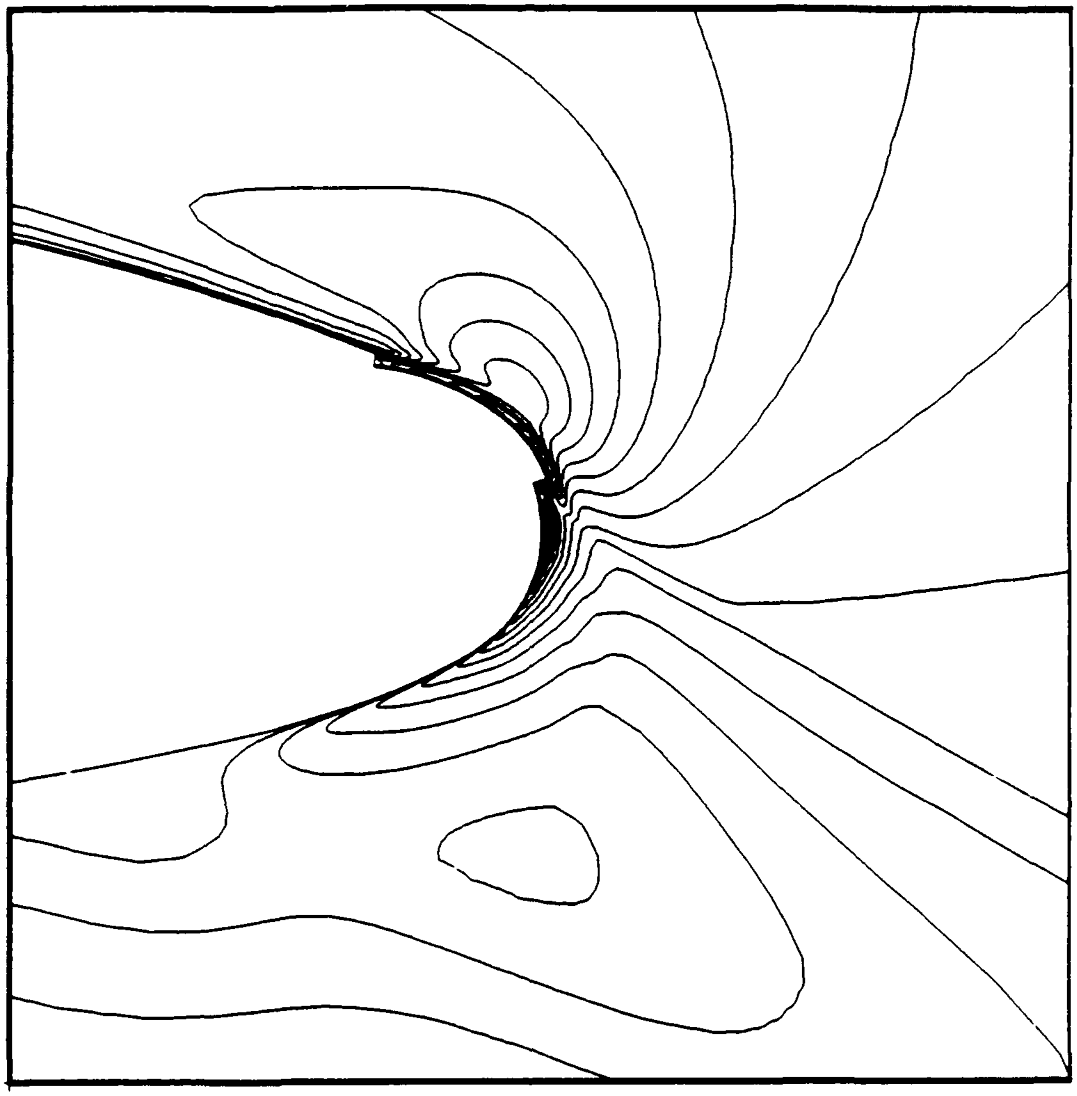

Figure 37. Case BE Mach Contour - Trailing Edge

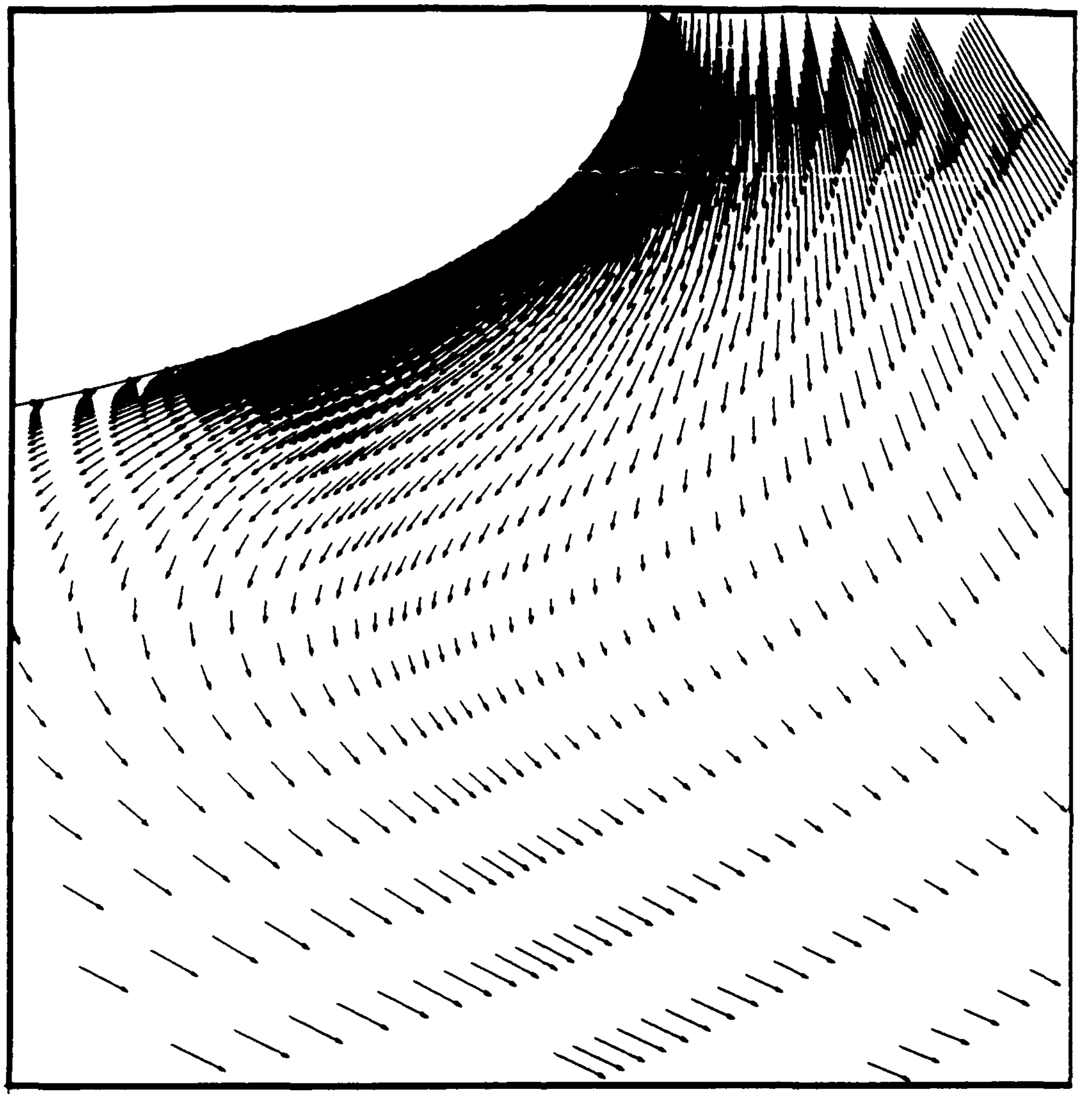

Figure 38. Case BE Trailing Edge Velocity Vector Field

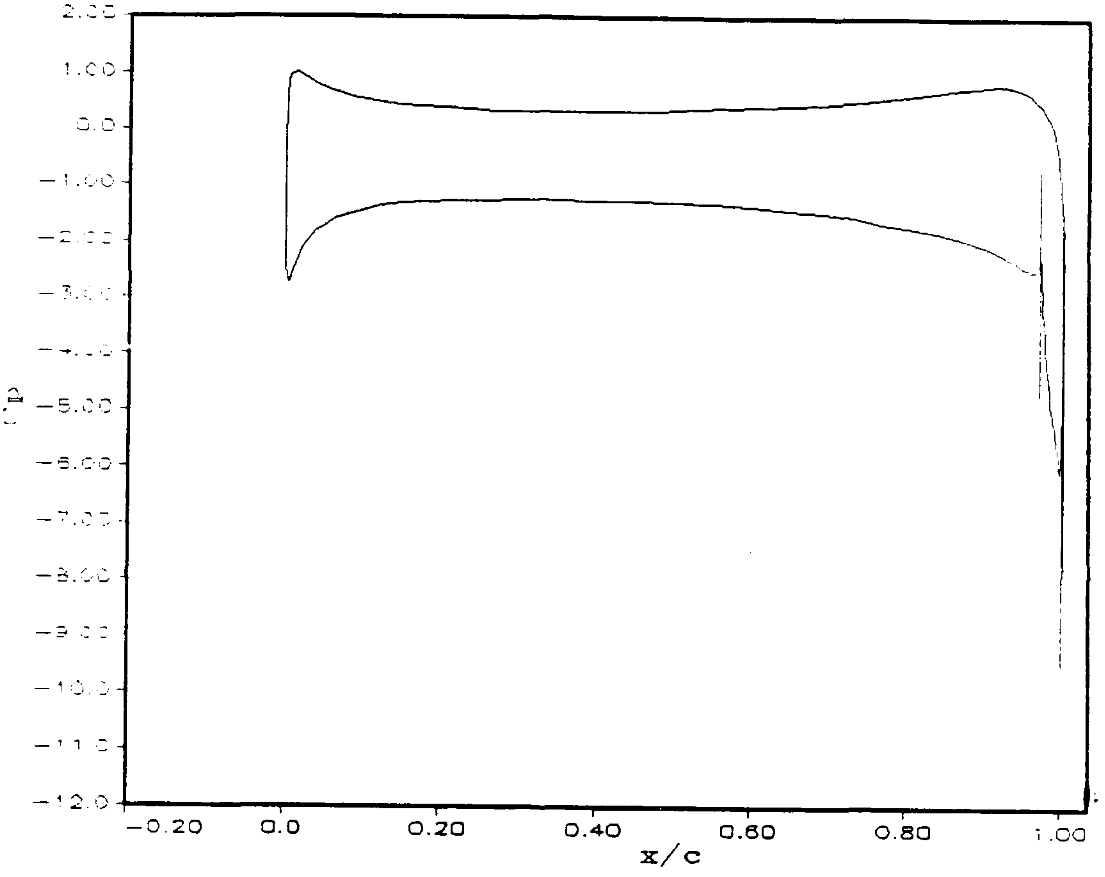

Figure 39. Case BE Pressure Coefficient (C_p) vs. x/c

B.5 Case BD Data

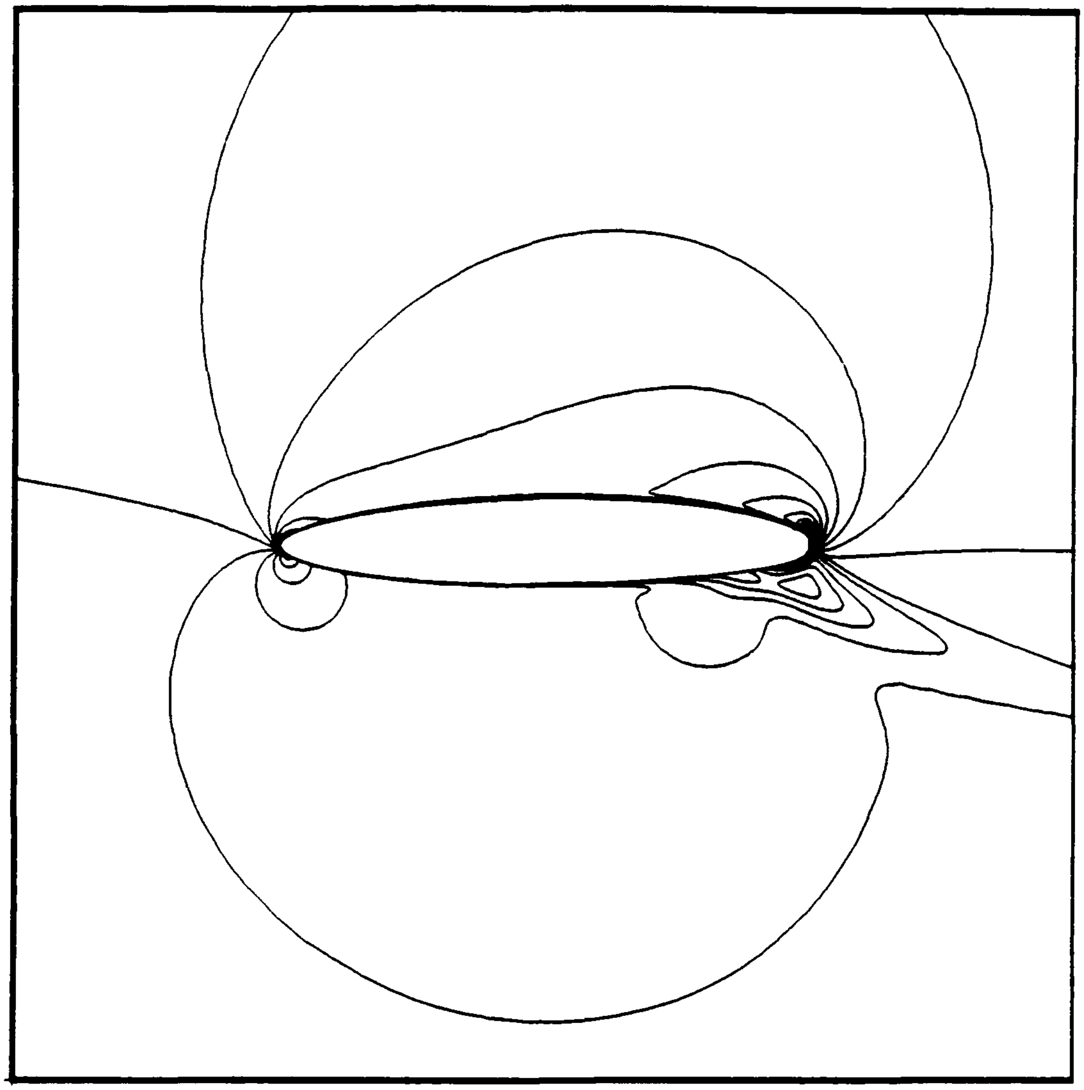

Figure 40. Case BD Mach Contour - Overview

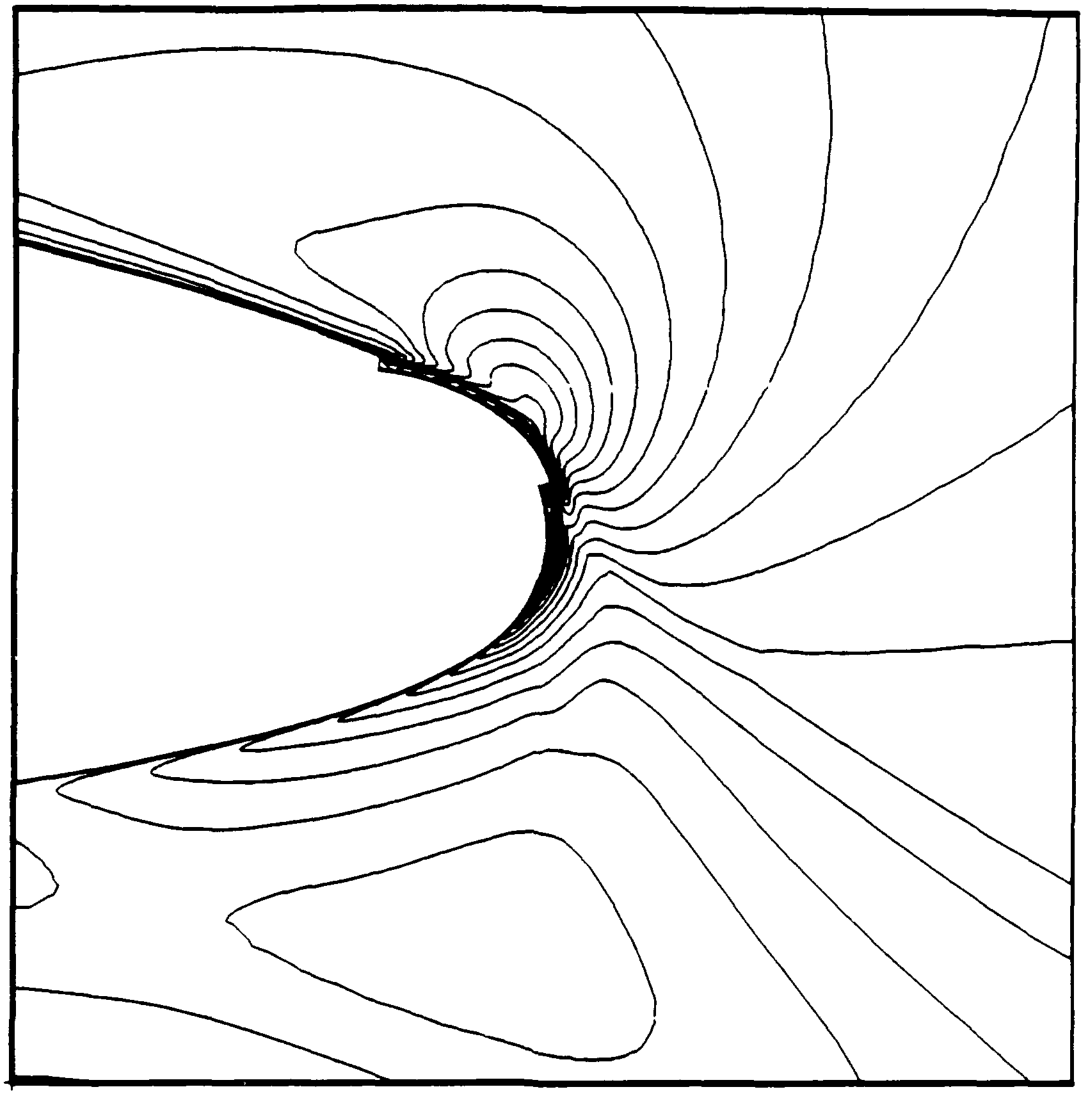

Figure 41. Case BD Mach Contour - Trailing Edge

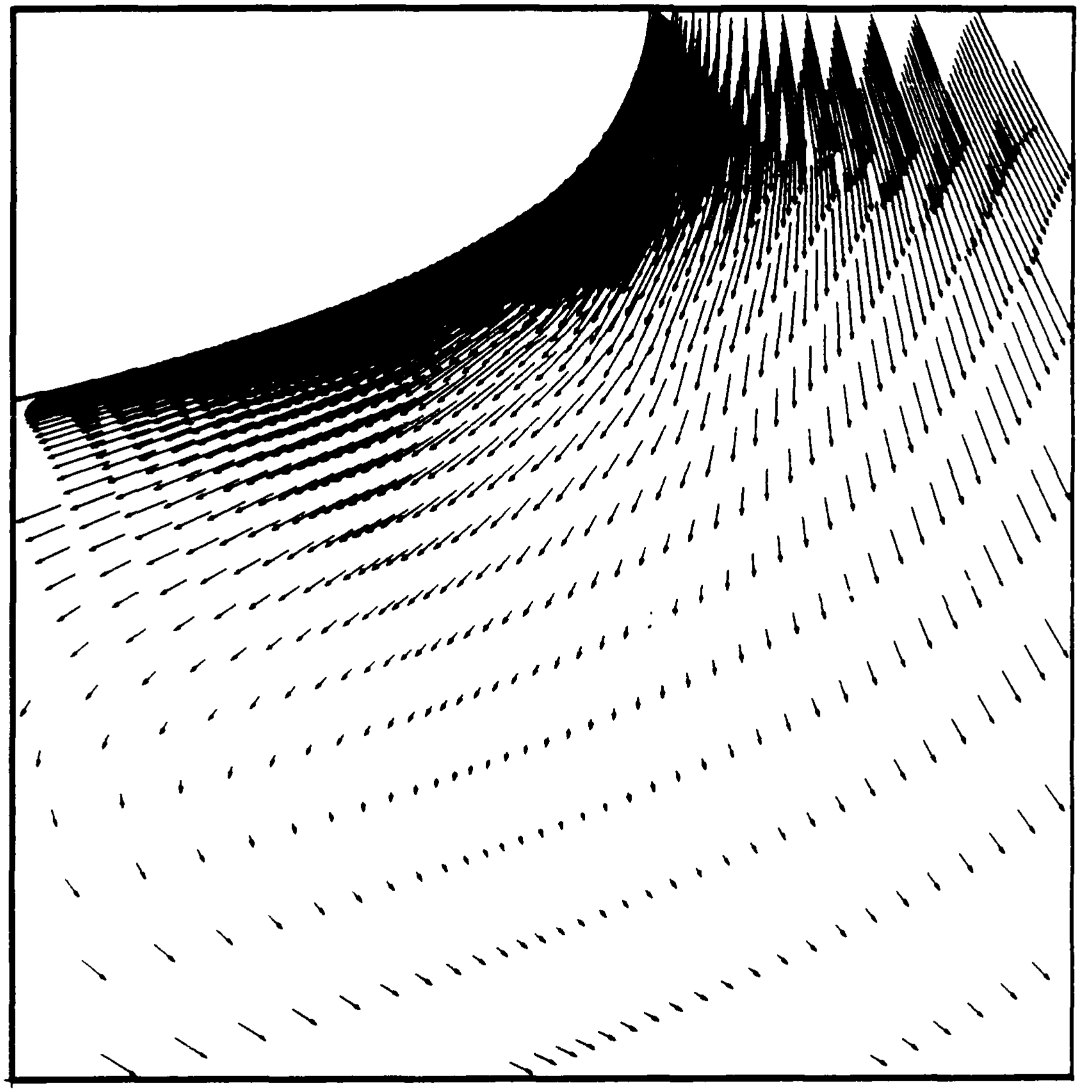

Figure 42. Case BD Trailing Edge Velocity Vector Field

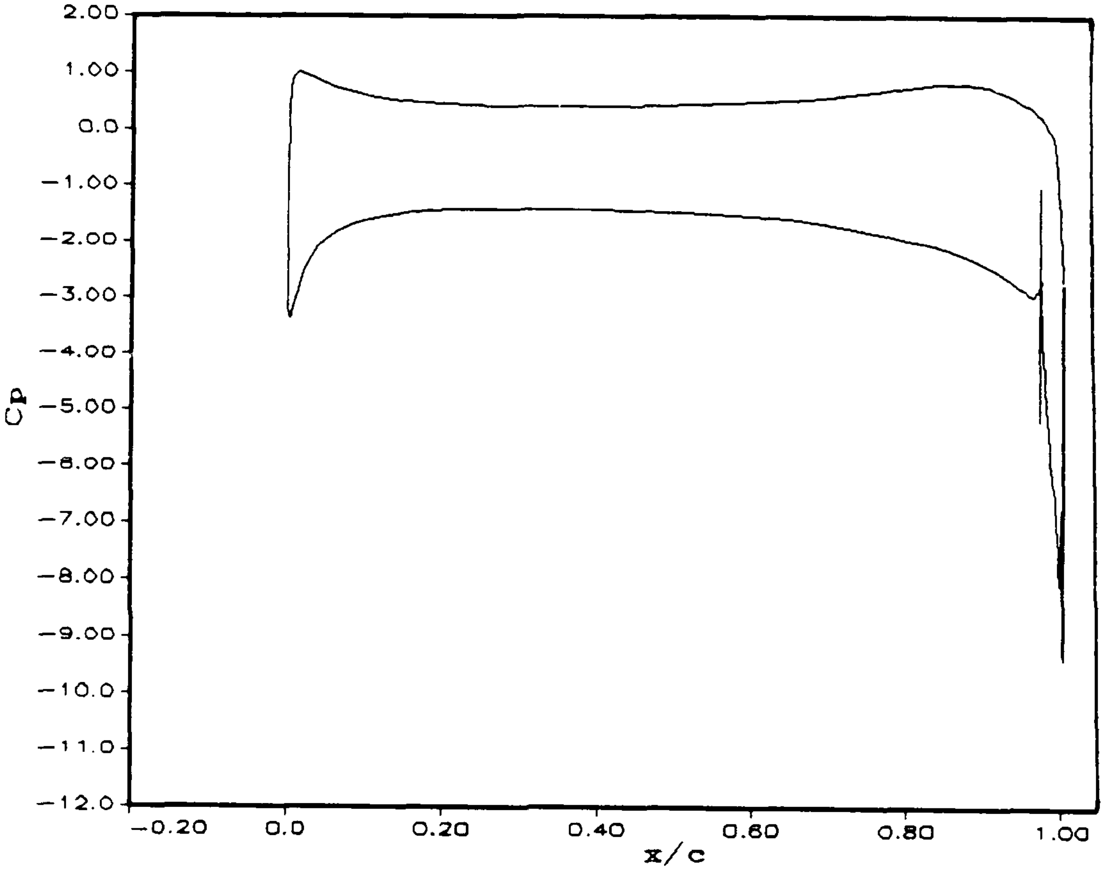

Figure 43. Case BD Pressure Coefficient (C_p) vs. x/c

Appendix C. *Cases with Slot 1 at Condition C*

C.1 Case CA Data

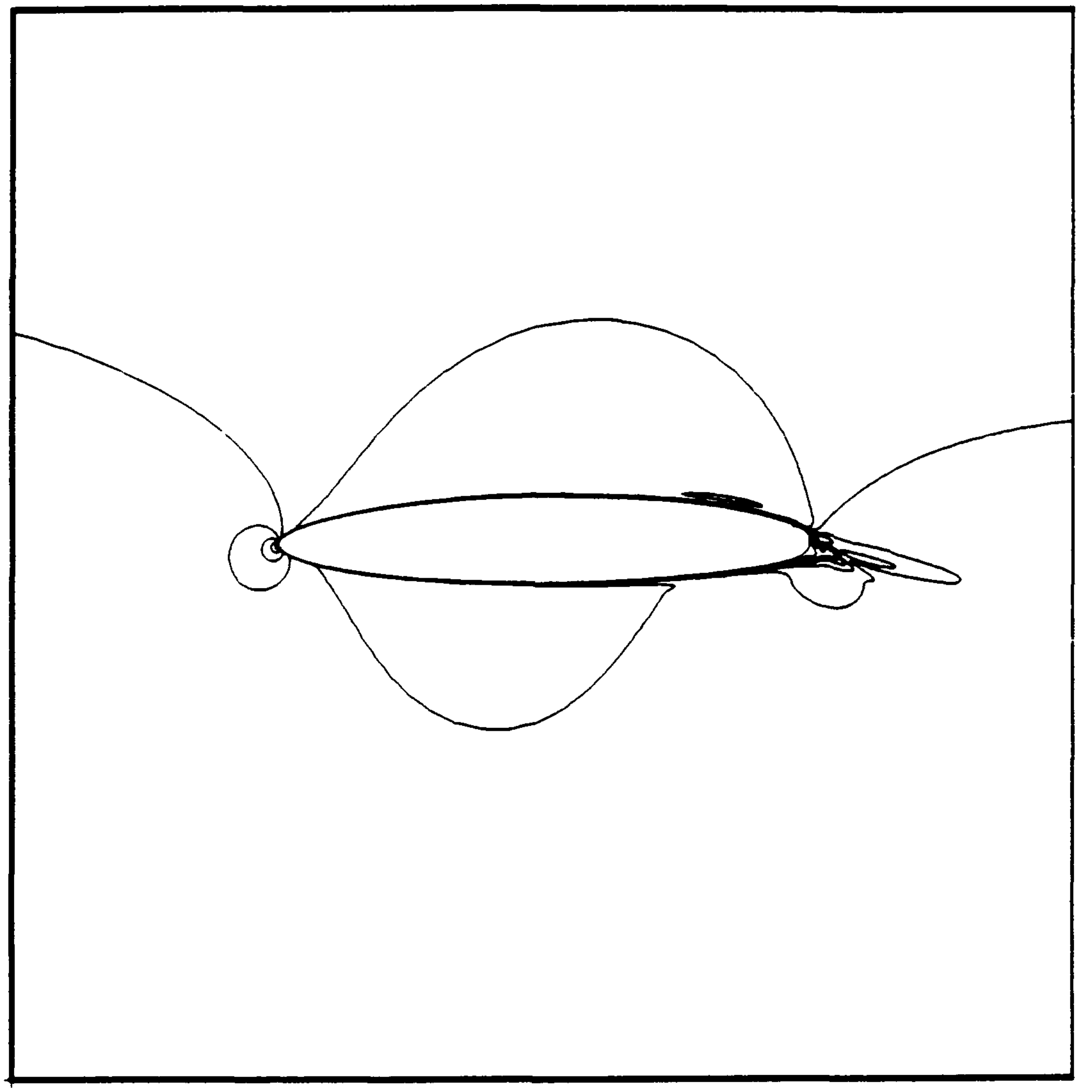

Figure 44. Case CA Mach Contour - Overview

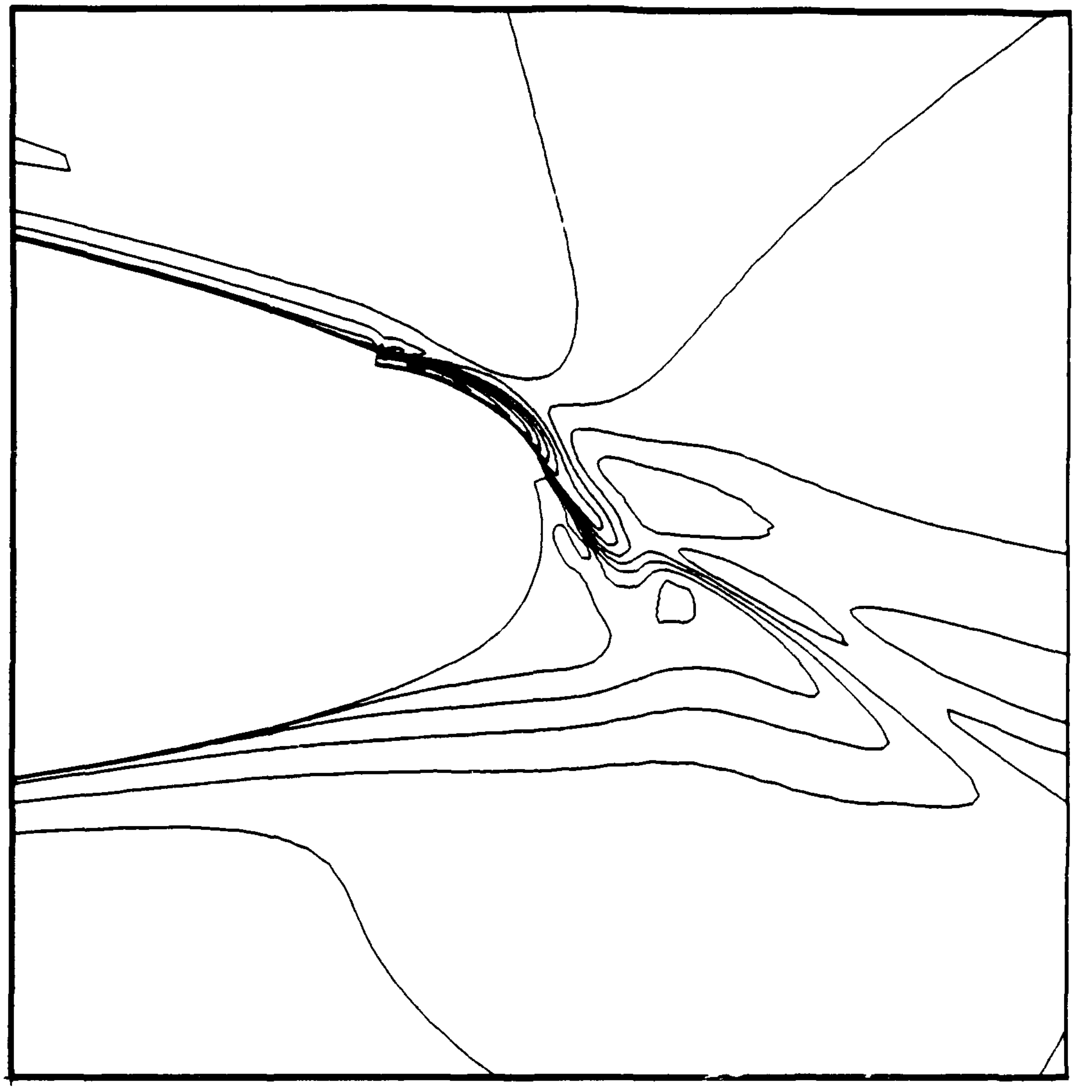

Figure 45. Case CA Mach Contour - Trailing Edge

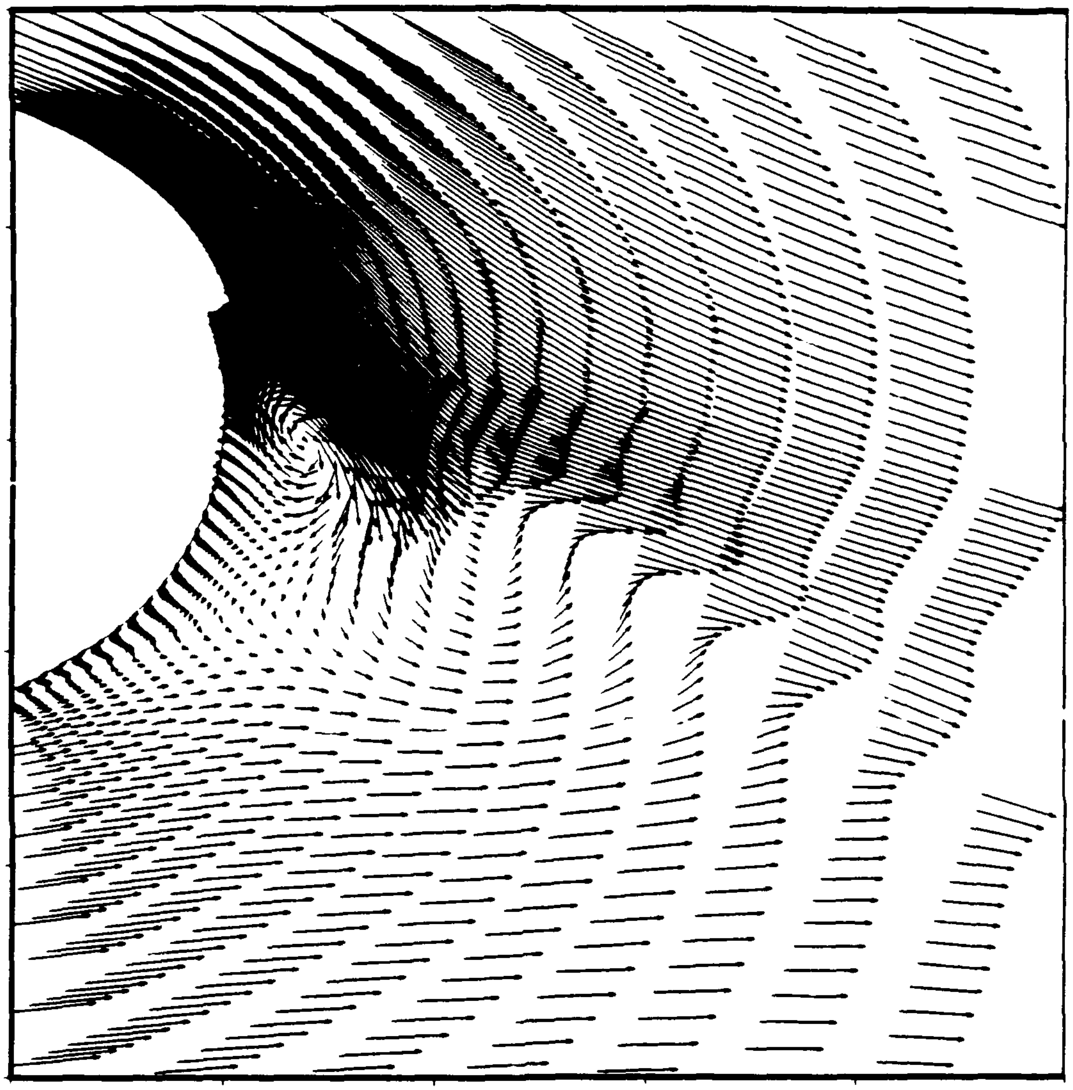

Figure 46. Case CA Trailing Edge Velocity Vector Field

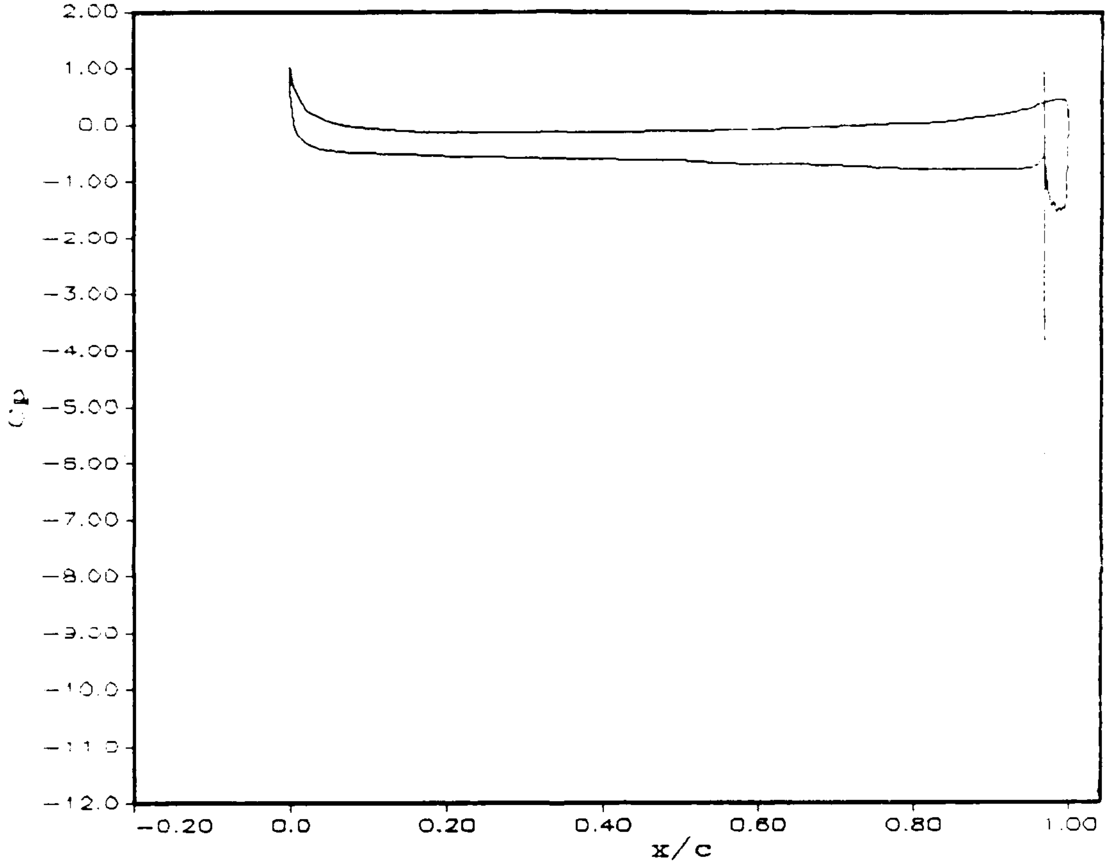

Figure 47. Case CA Pressure Coefficient (C_p) vs. x/c

C.2 Case CB Data

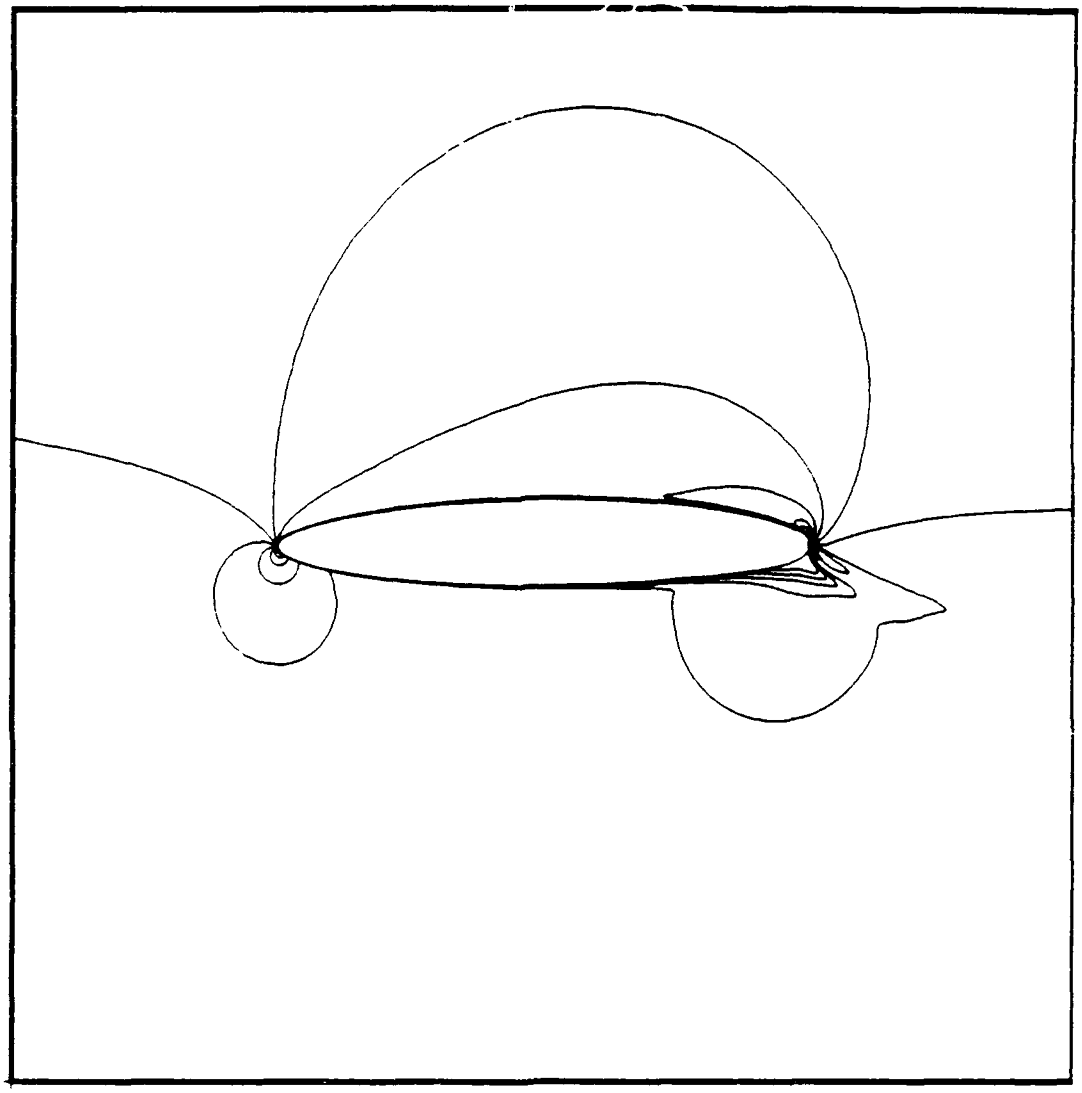

Figure 48. Case CB Mach Contour - Overview

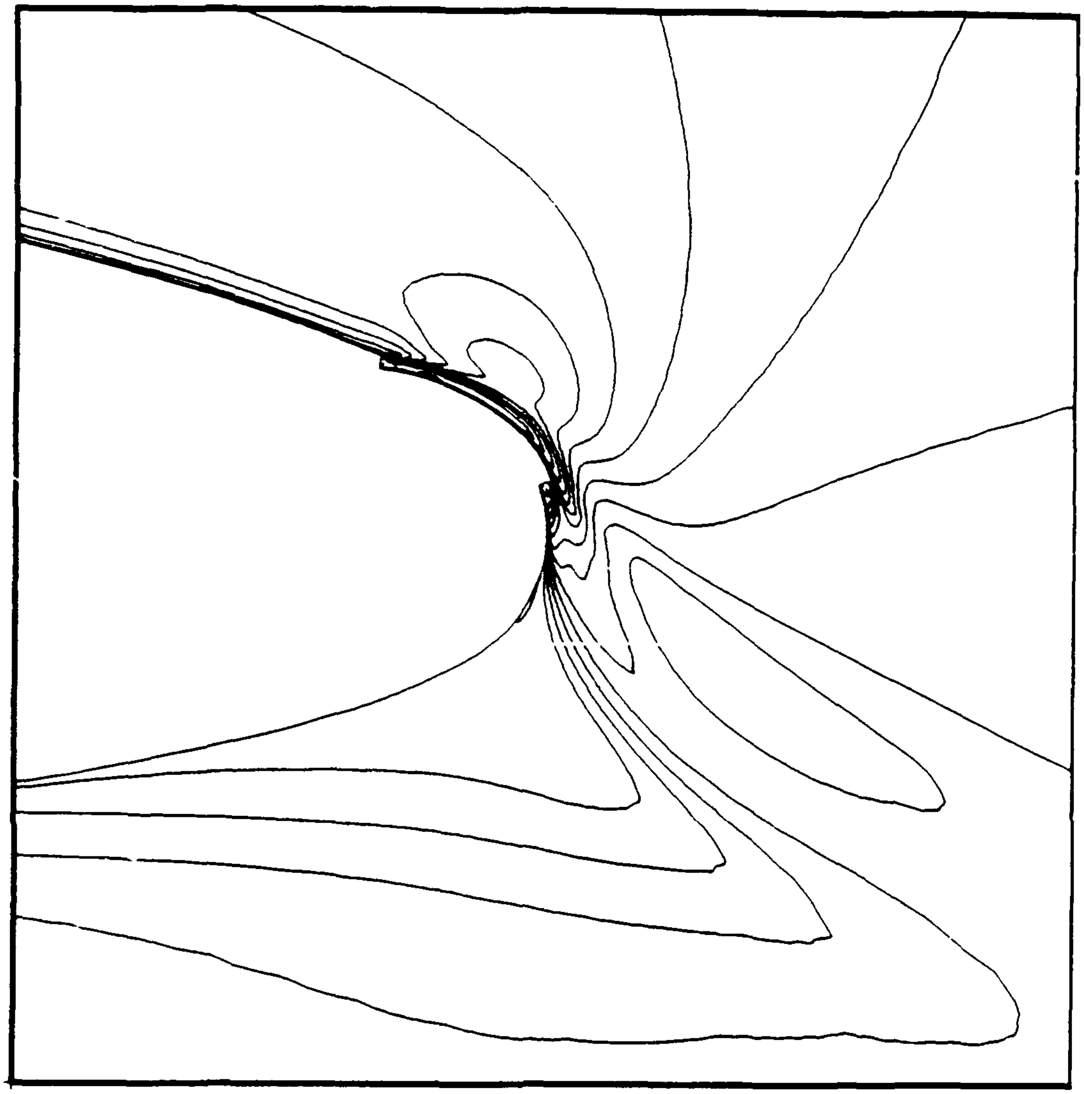

Figure 49. Case CB Mach Contour - Trailing Edge

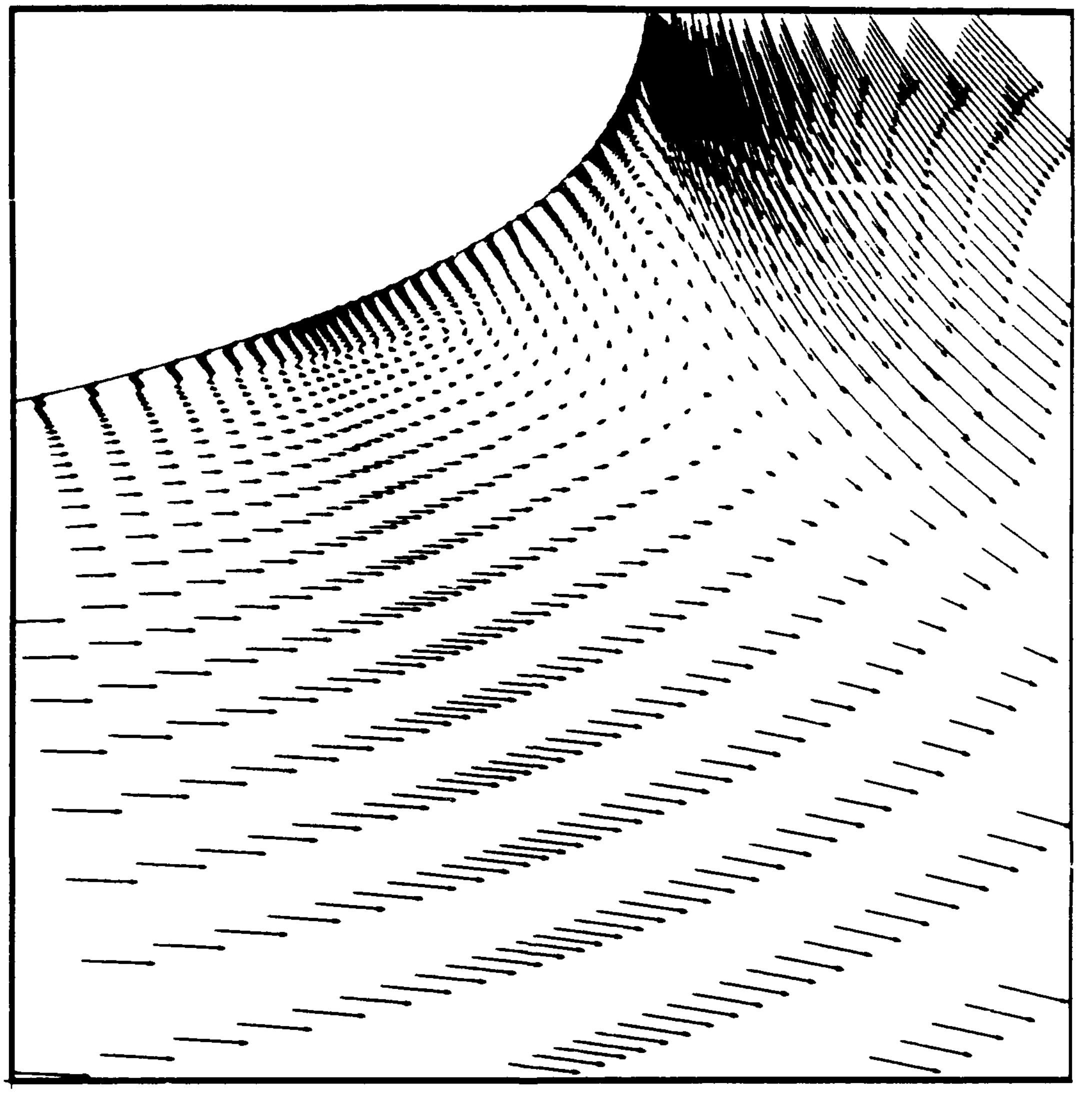

Figure 50. Case CB Trailing Edge Velocity Vector Field

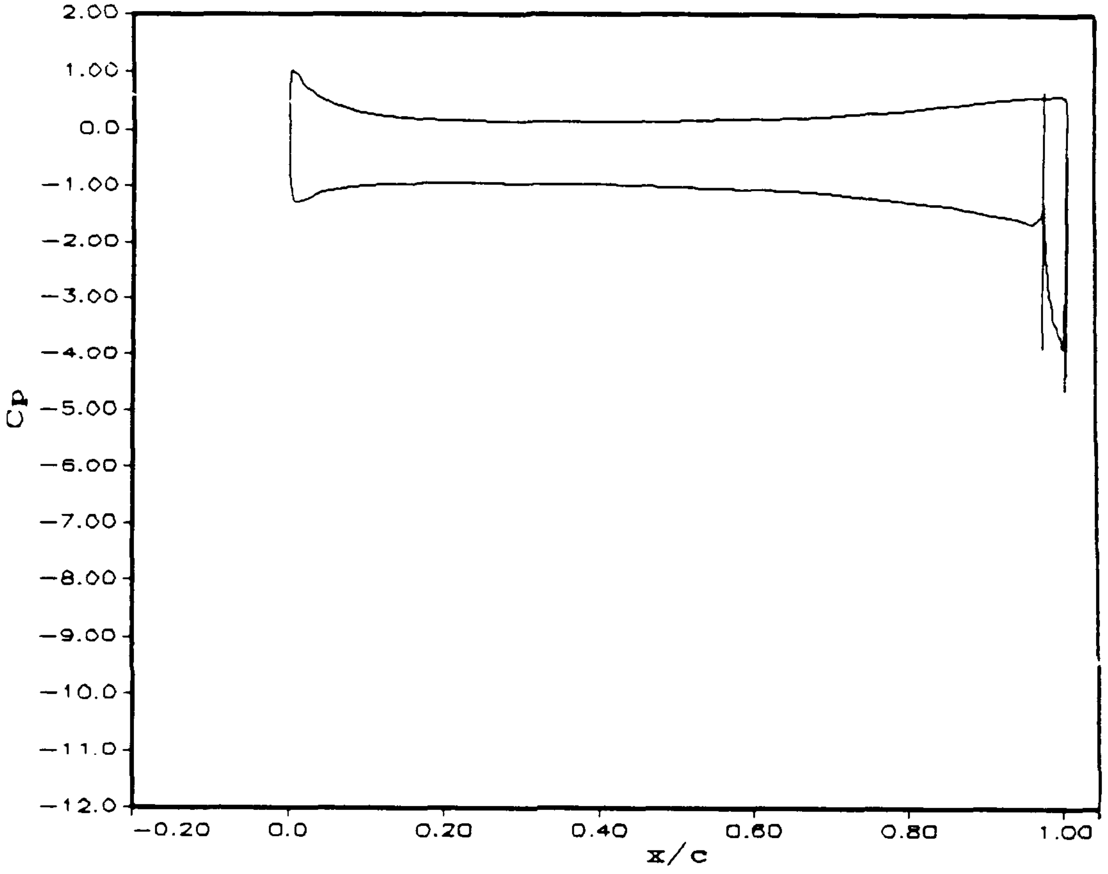

Figure 51. Case CB Pressure Coefficient (C_p) vs. x/c

C.3 Case CC Data

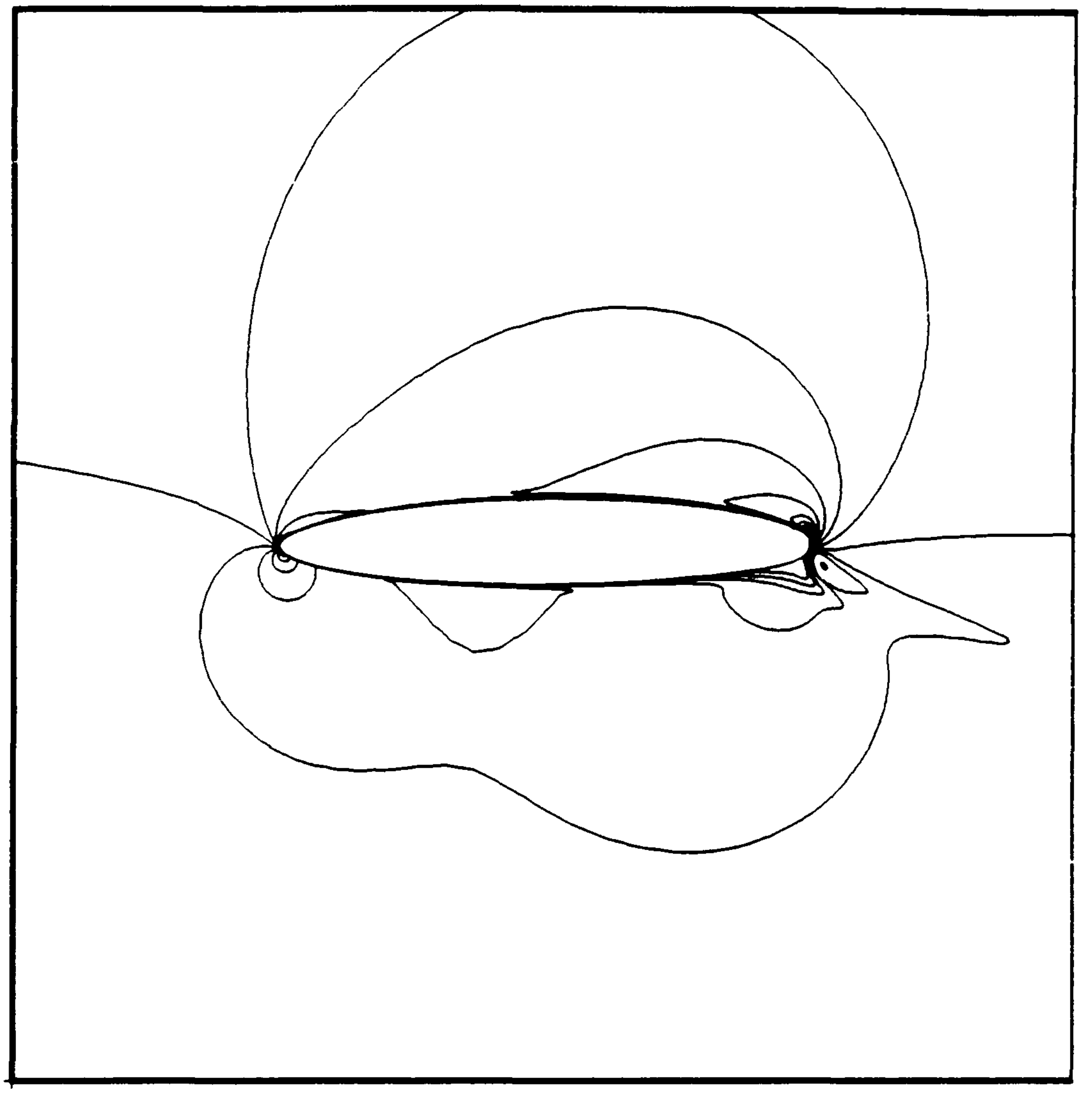

Figure 52. Case CC Mach Contour - Overview

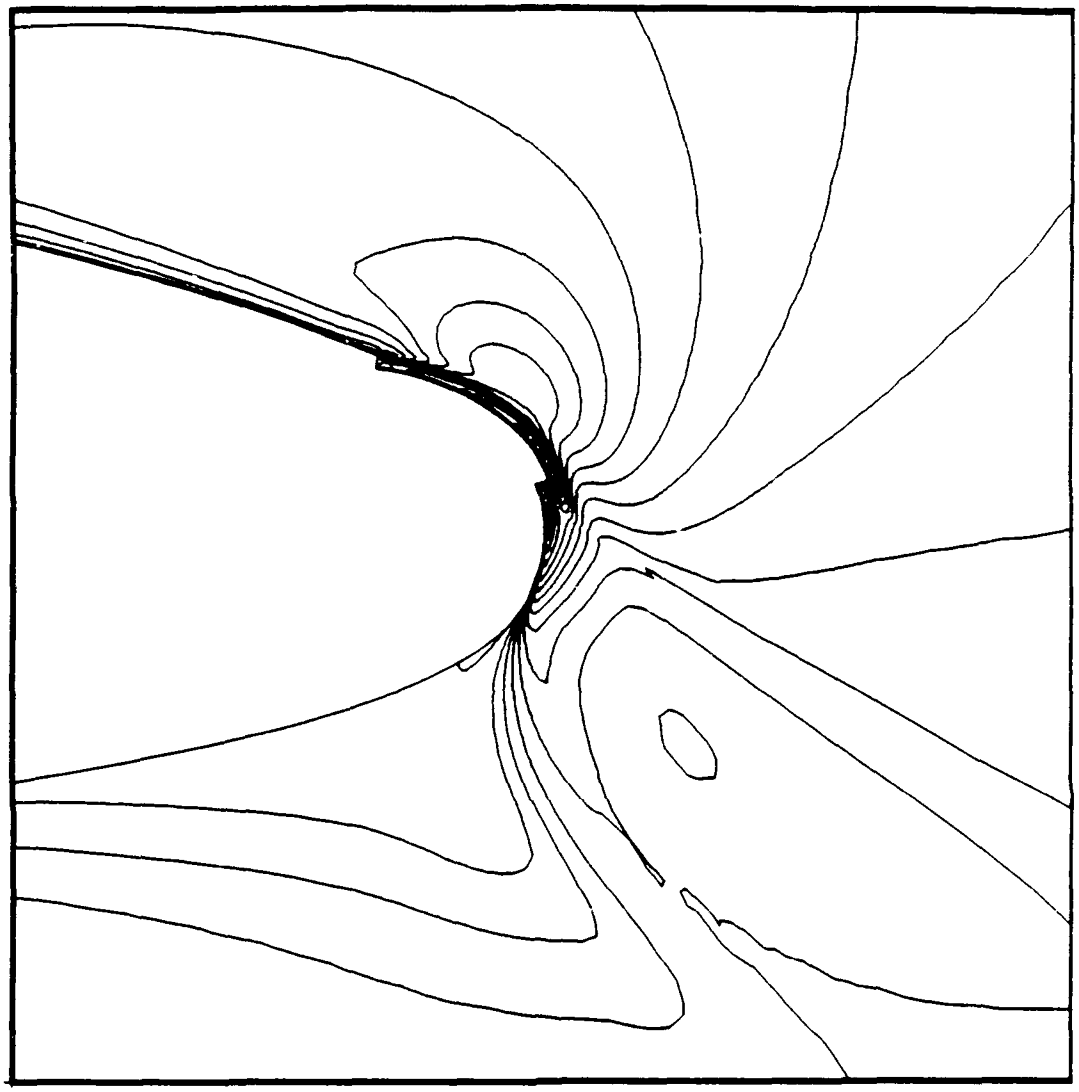

Figure 53. Case CC Mach Contour - Trailing Edge

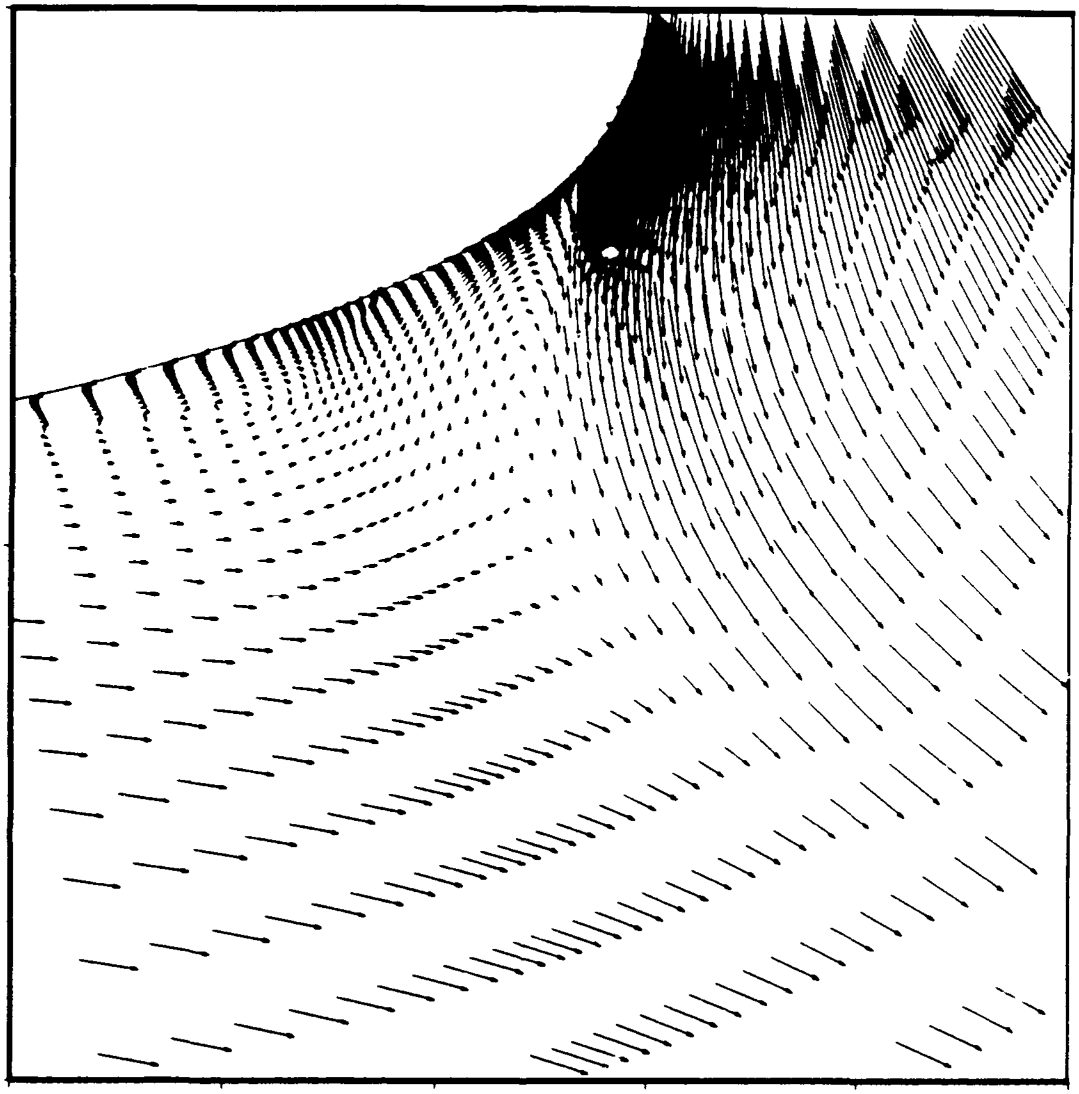

Figure 54. Case CC Trailing Edge Velocity Vector Field

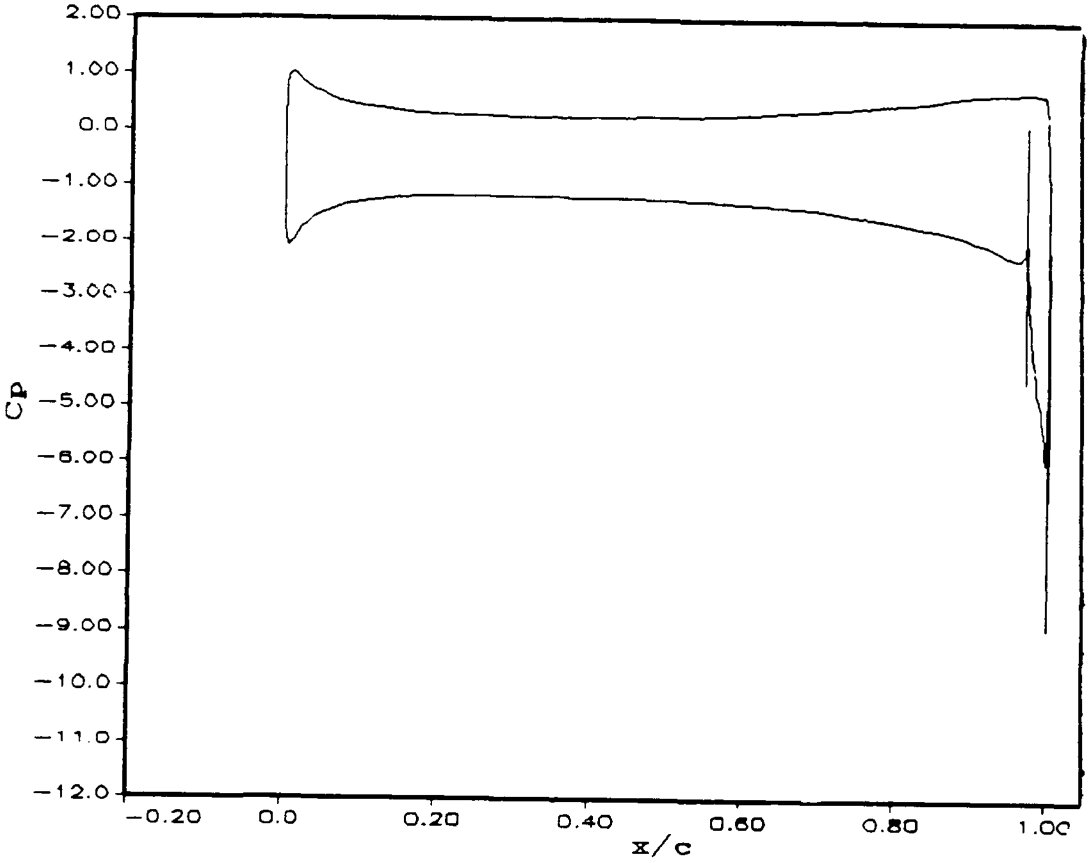

Figure 55. Case CC Pressure Coefficient (C_p) vs. x/c

C.4 Case CD Data

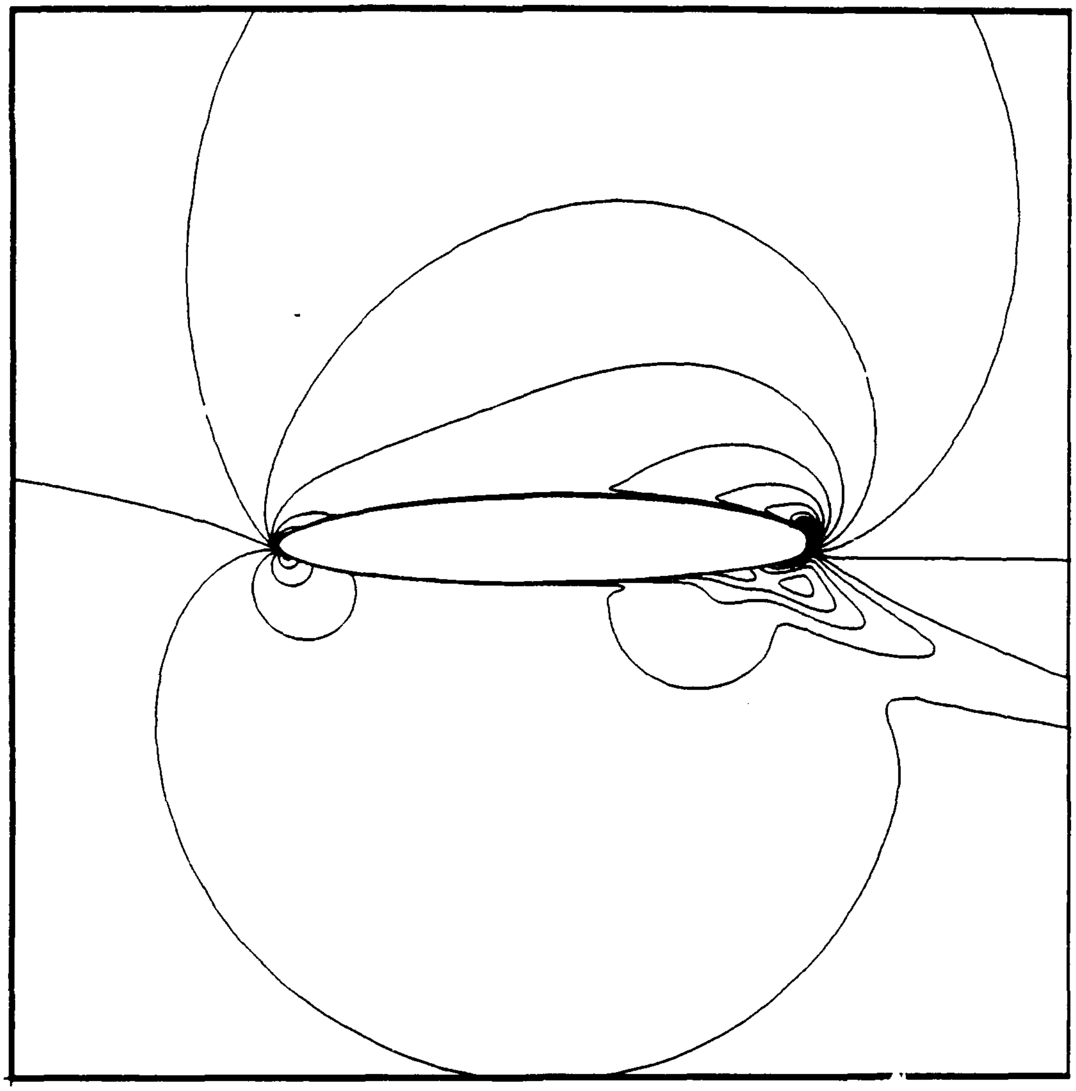

Figure 56. Case CD Mach Contour - Overview

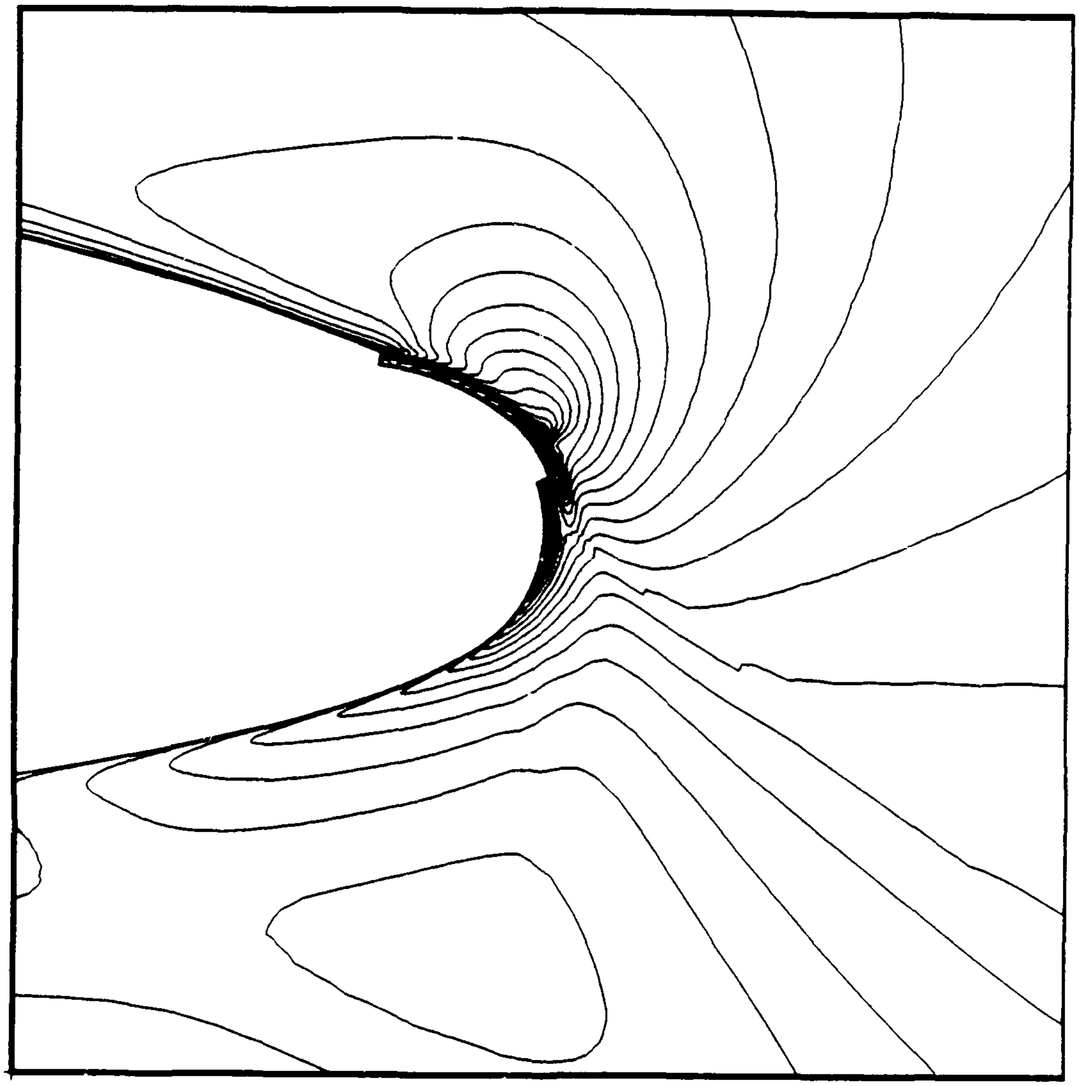

Figure 57. Case CD Mach Contour - Trailing Edge

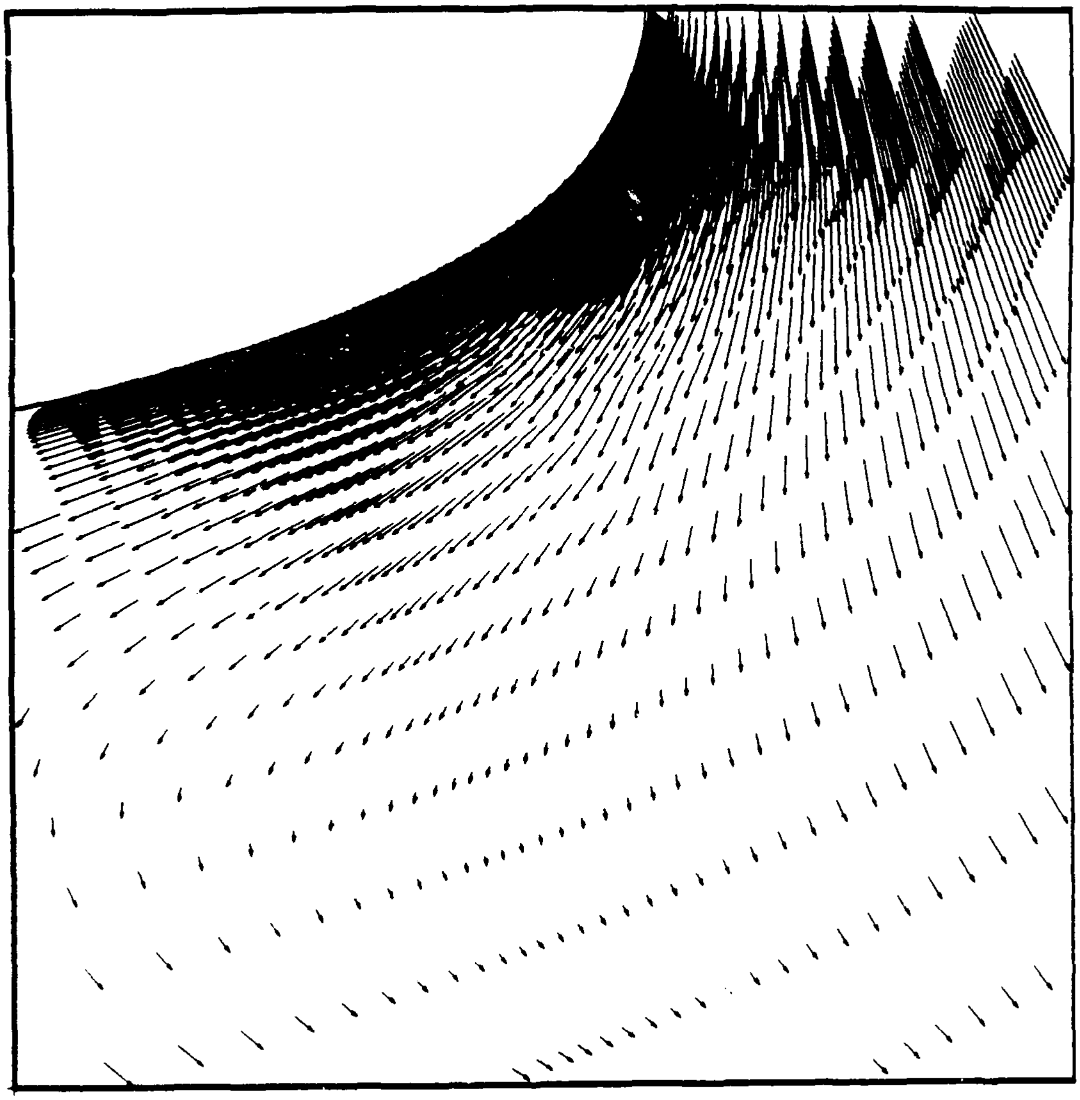

Figure 58. Case CD Trailing Edge Velocity Vector Field

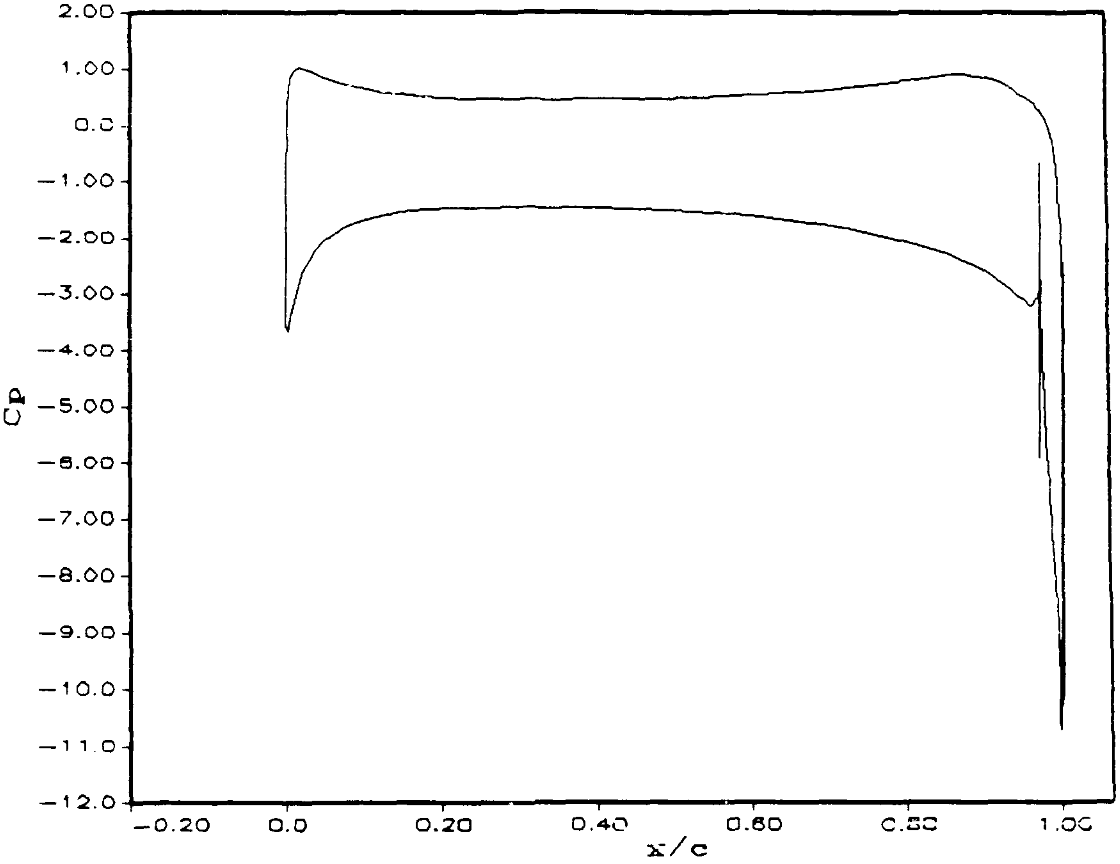

Figure 59. Case CD Pressure Coefficient (C_p) vs. x/c

Appendix D. *Cases with Slot 1 at Condition D*

D.1 Case DA Data

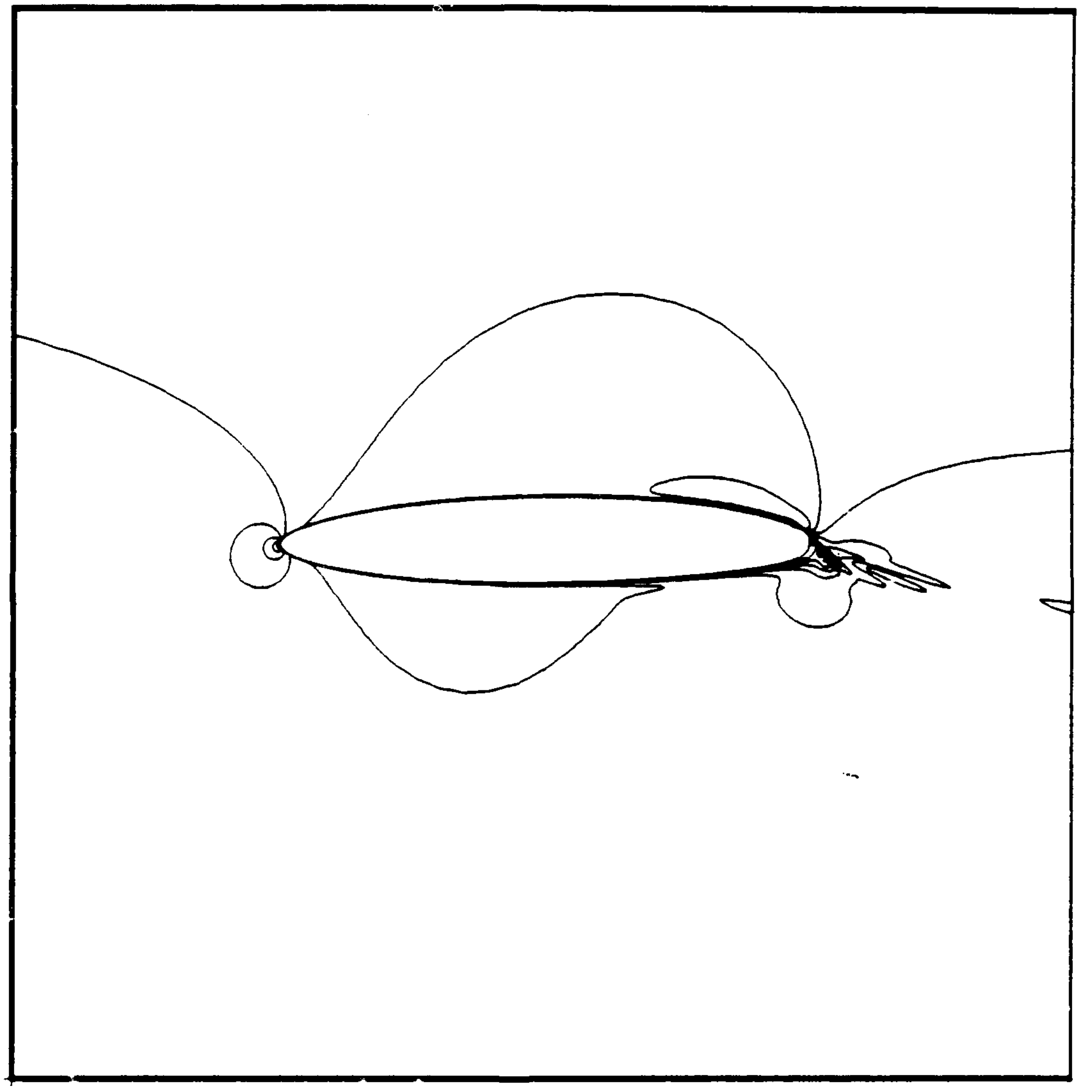

Figure 60. Case DA Mach Contour - Overview

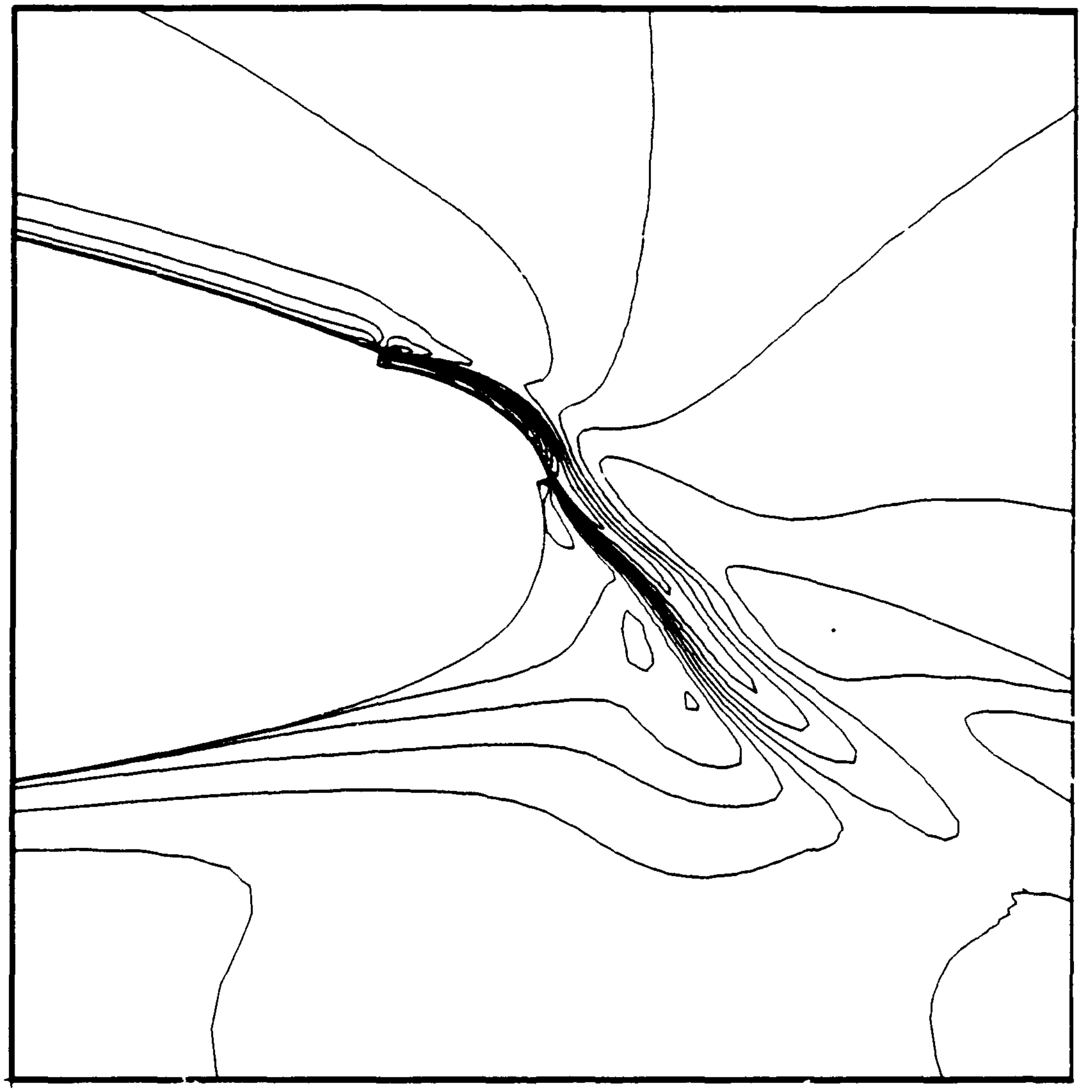

Figure 61. Case DA Mach Contour - Trailing Edge

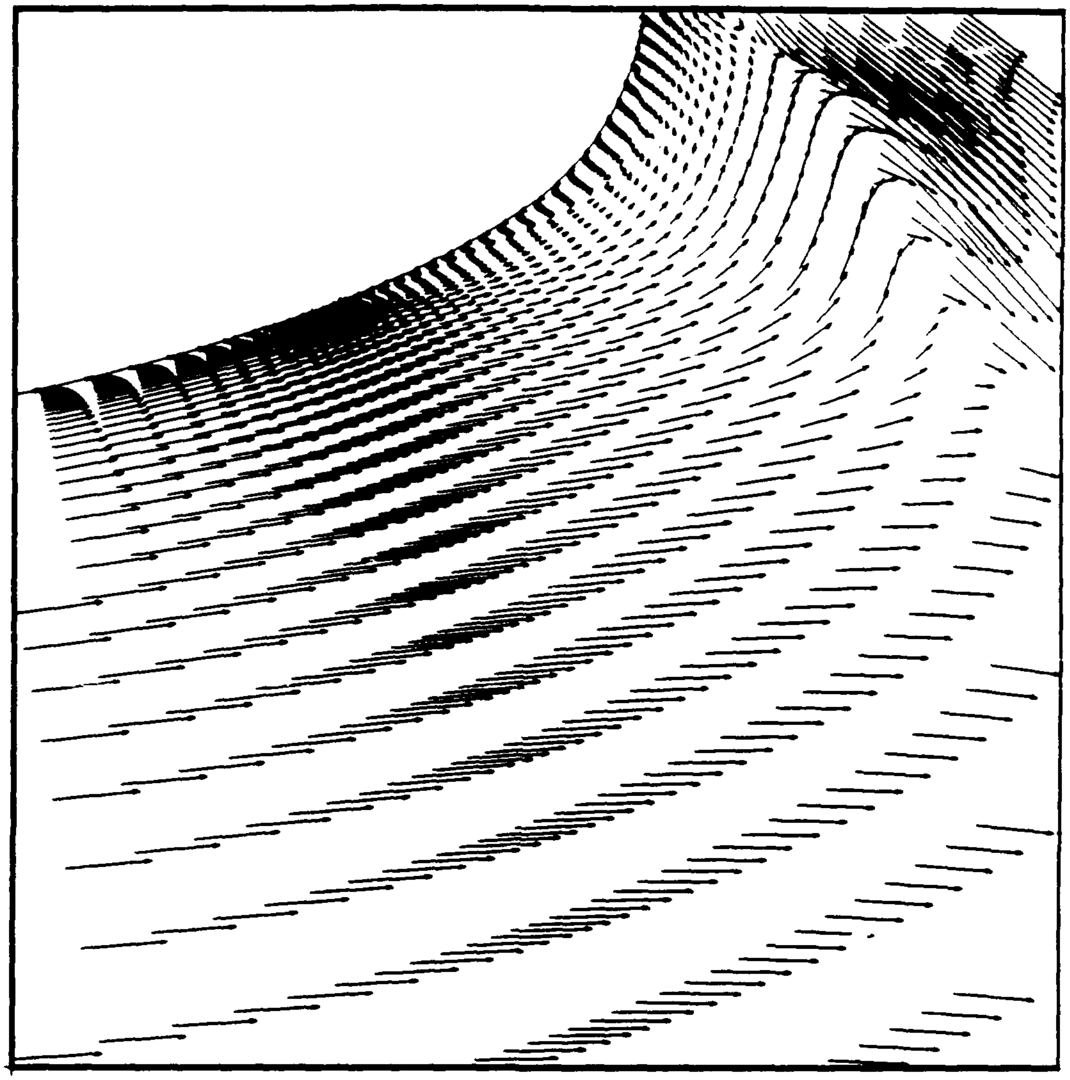

Figure 62. Case DA Trailing Edge Velocity Vector Field

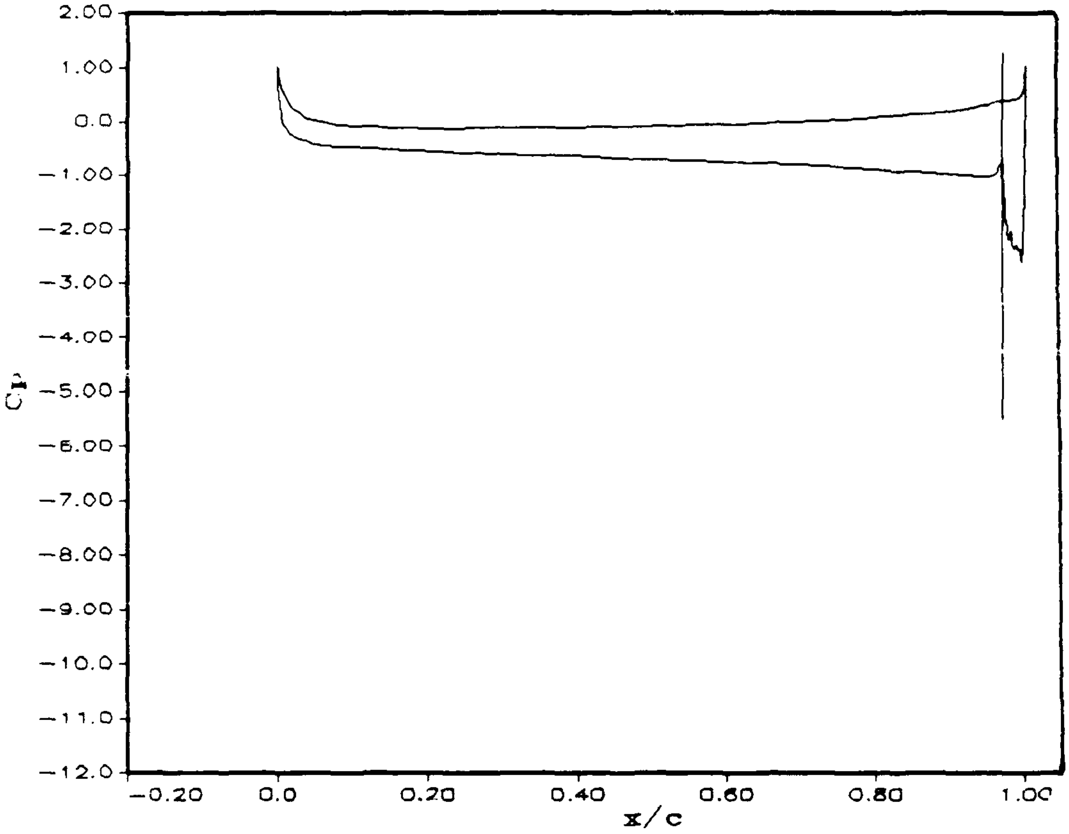

Figure 63. Case DA Pressure Coefficient (C_p) vs. x/c

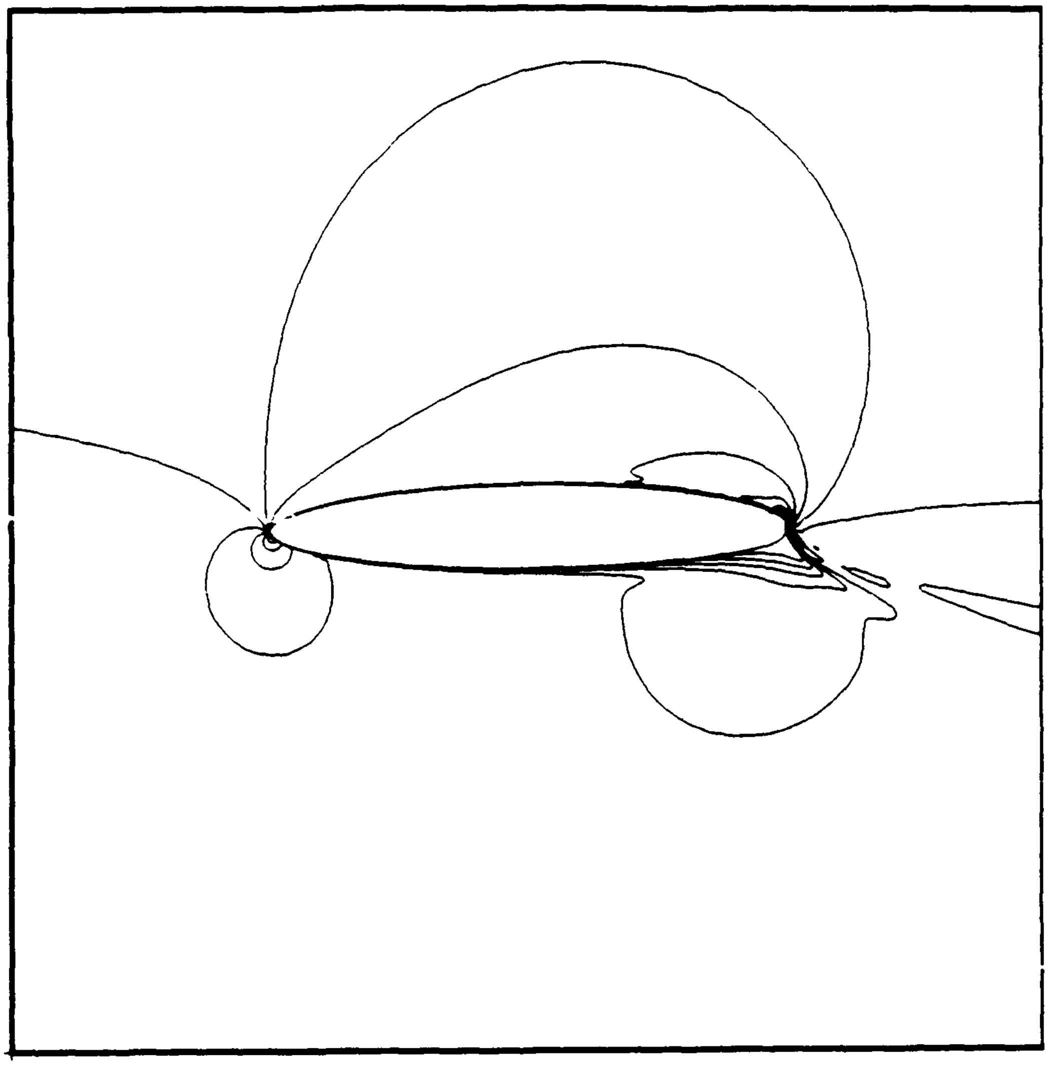

Figure 64. Case DB Mach Contour - Overview

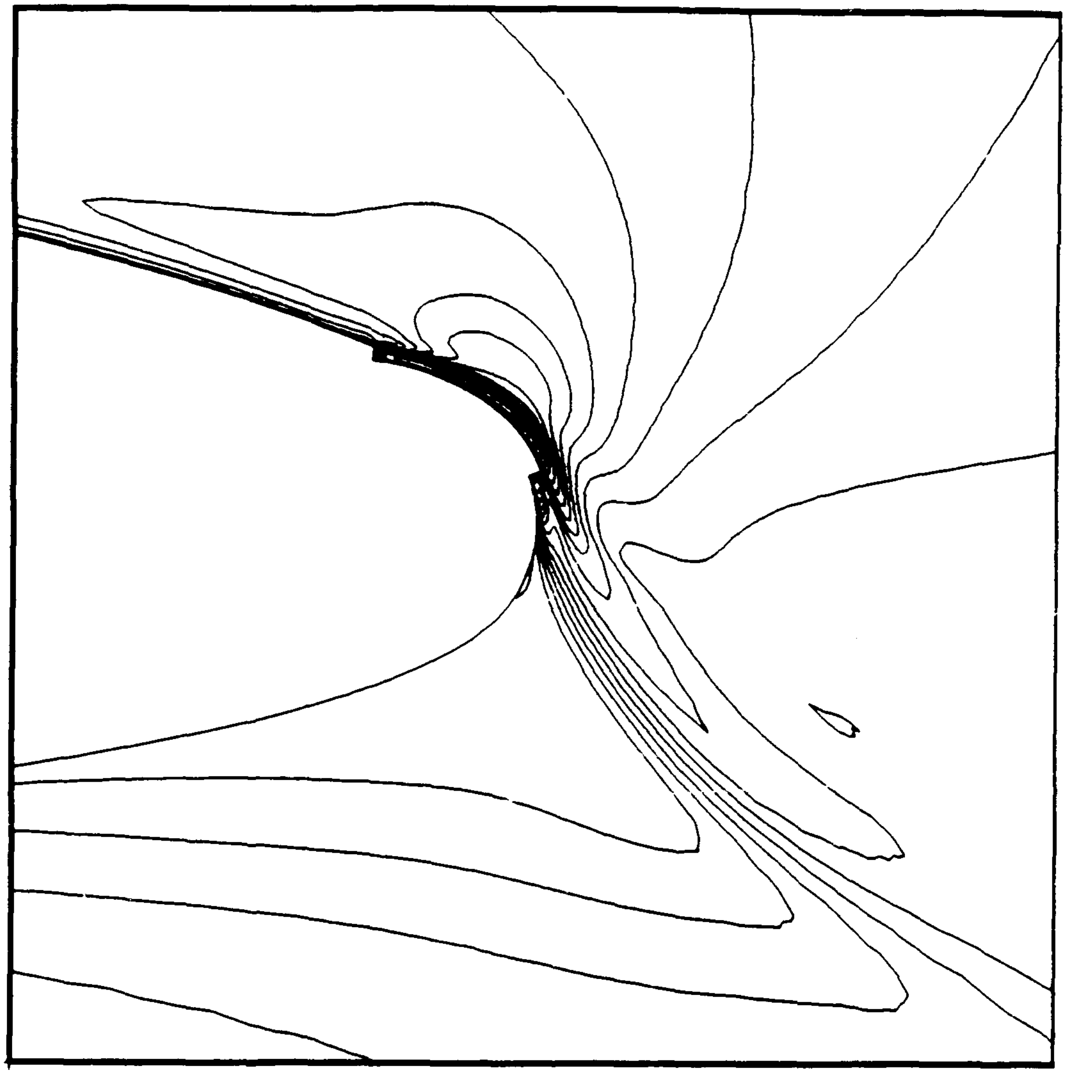

Figure 65. Case DB Mach Contour [illegible] Trailing Edge

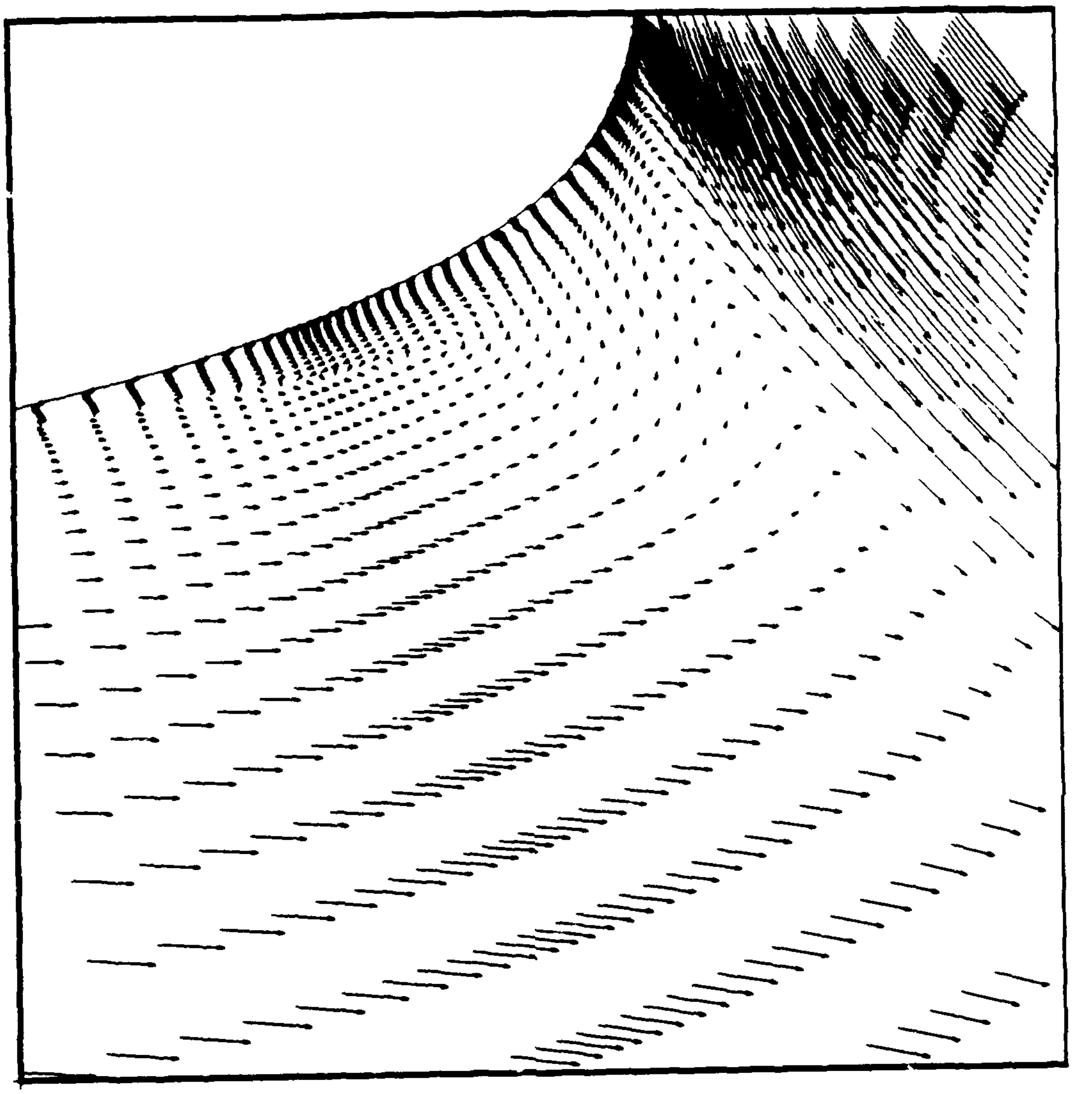

Figure 66. Case DB Trailing Edge Velocity Vector Field

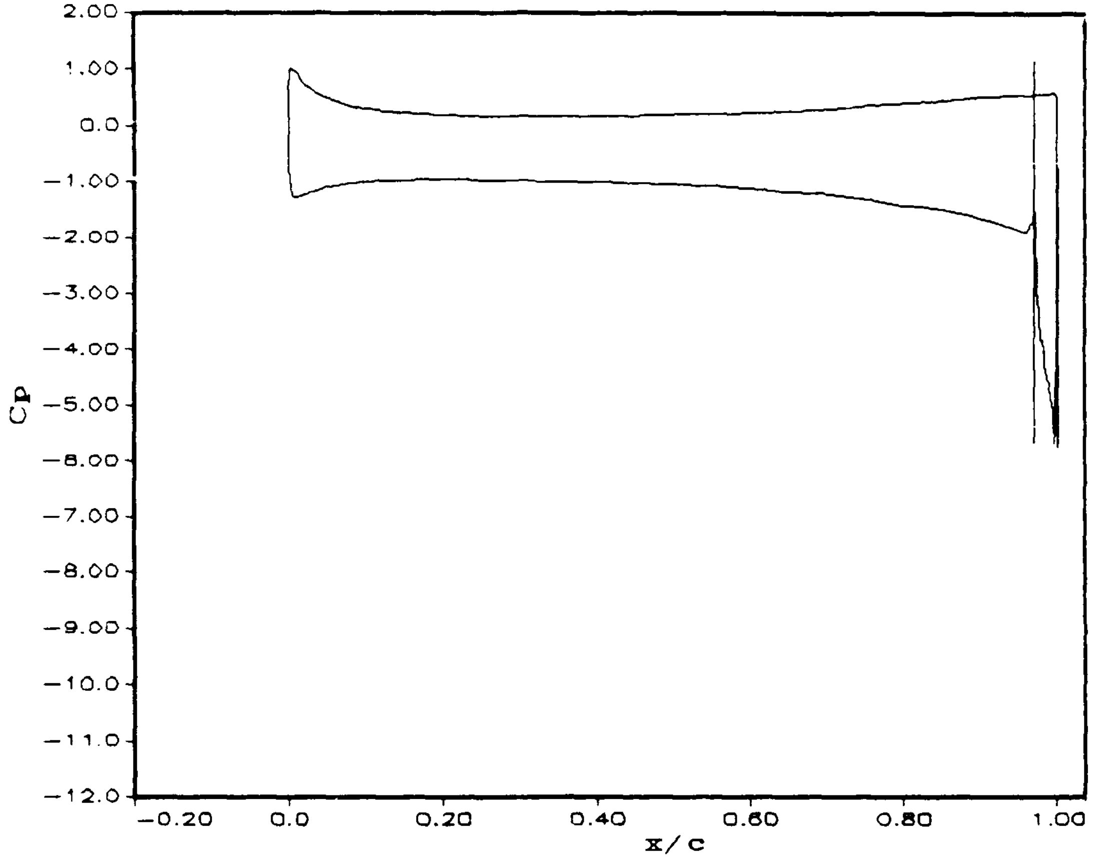

Figure 67. Case DB Pressure Coefficient (C_p) vs. x/c

D.3 Case DC Data

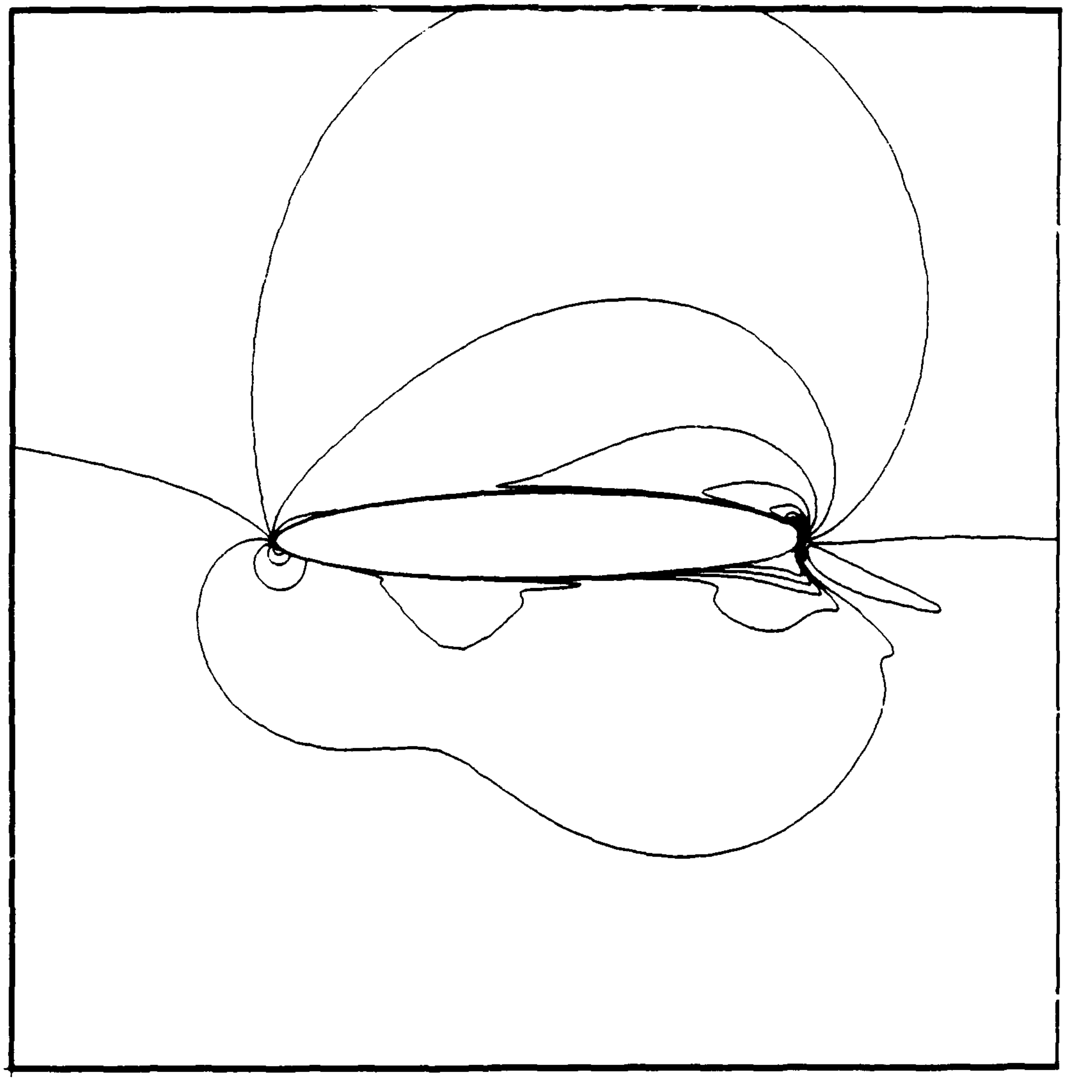

Figure 68. Case DC Mach Contour - Overview

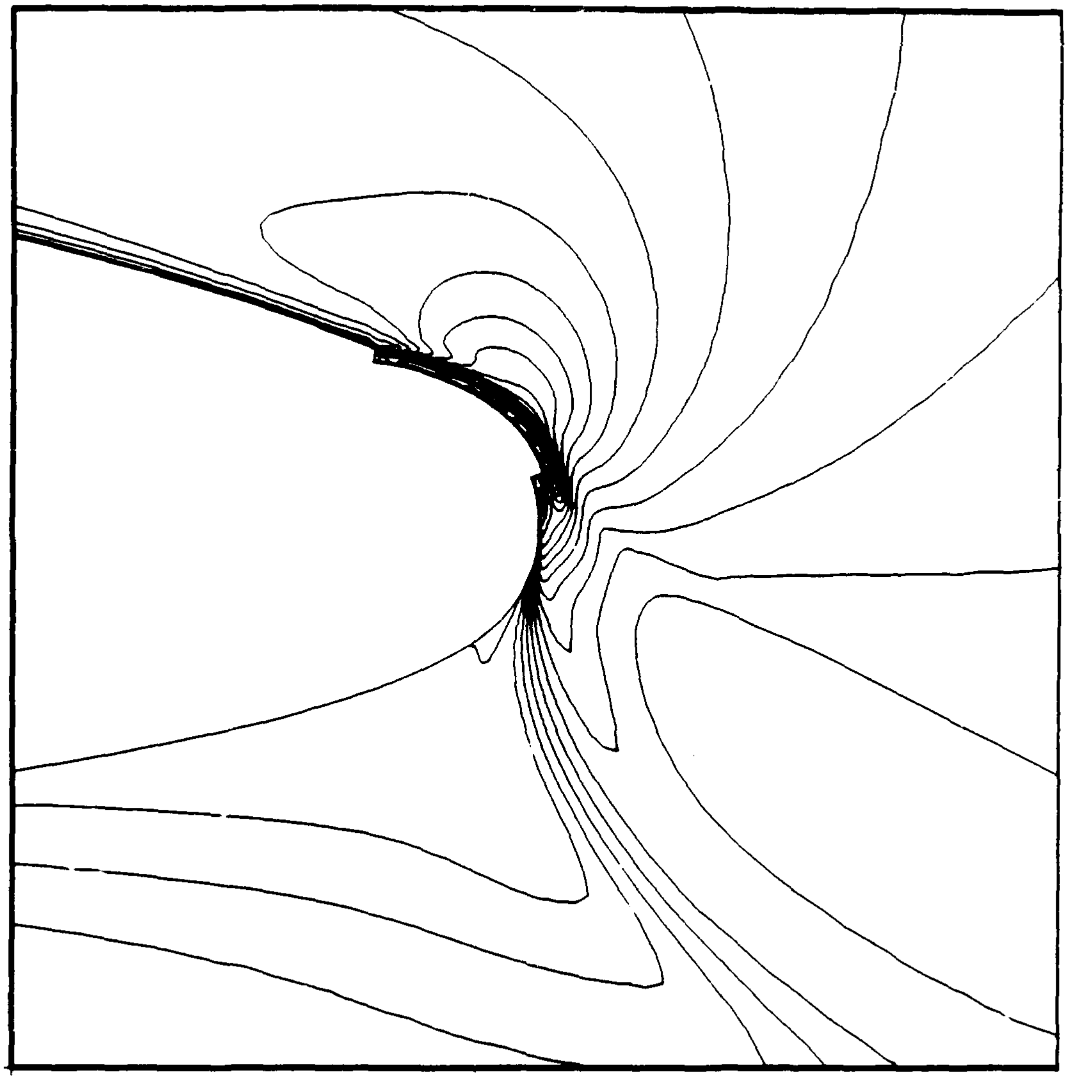

Figure 69. Case DC Mach Contour - Trailing Edge

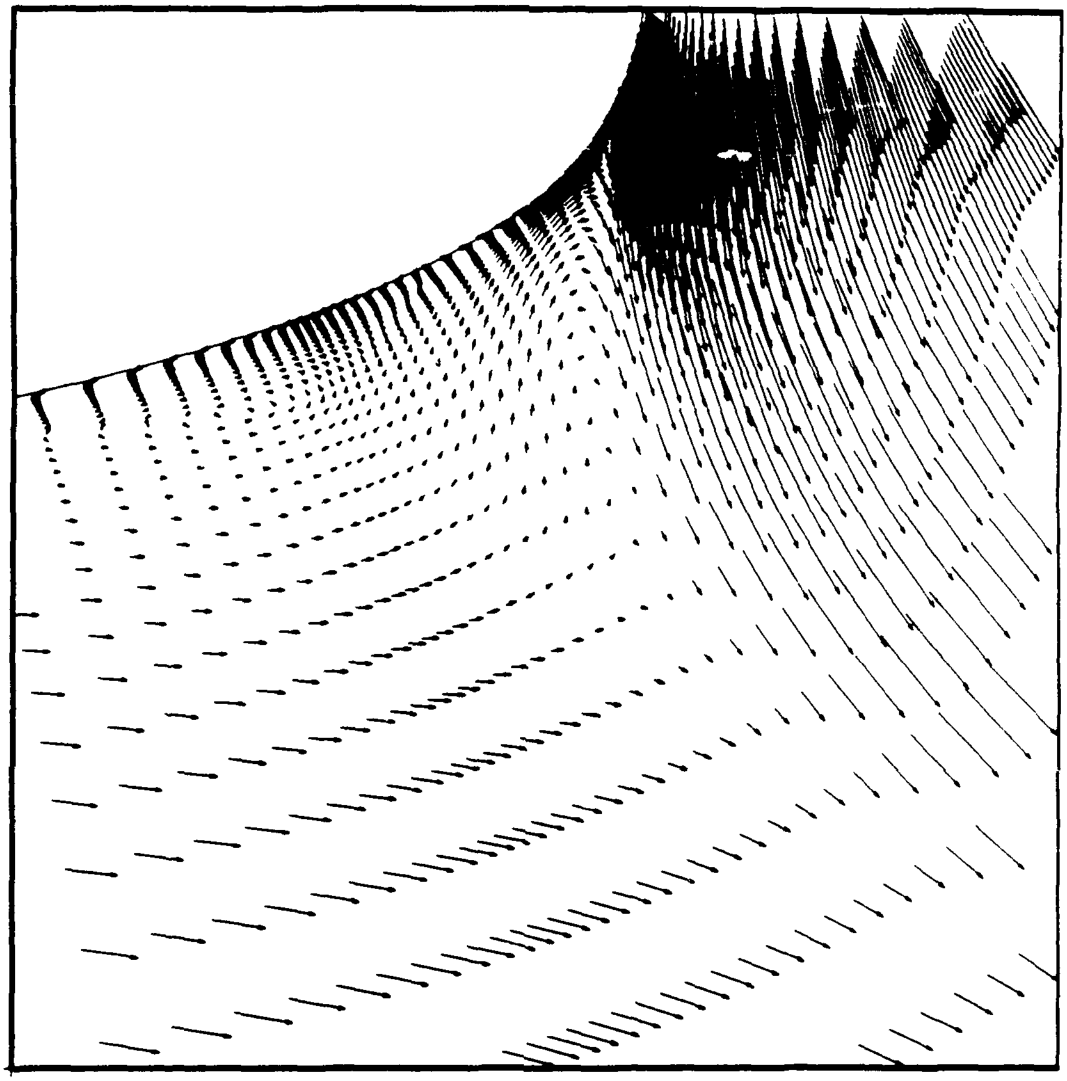

Figure 70. Case DC Trailing Edge Velocity Vector Field

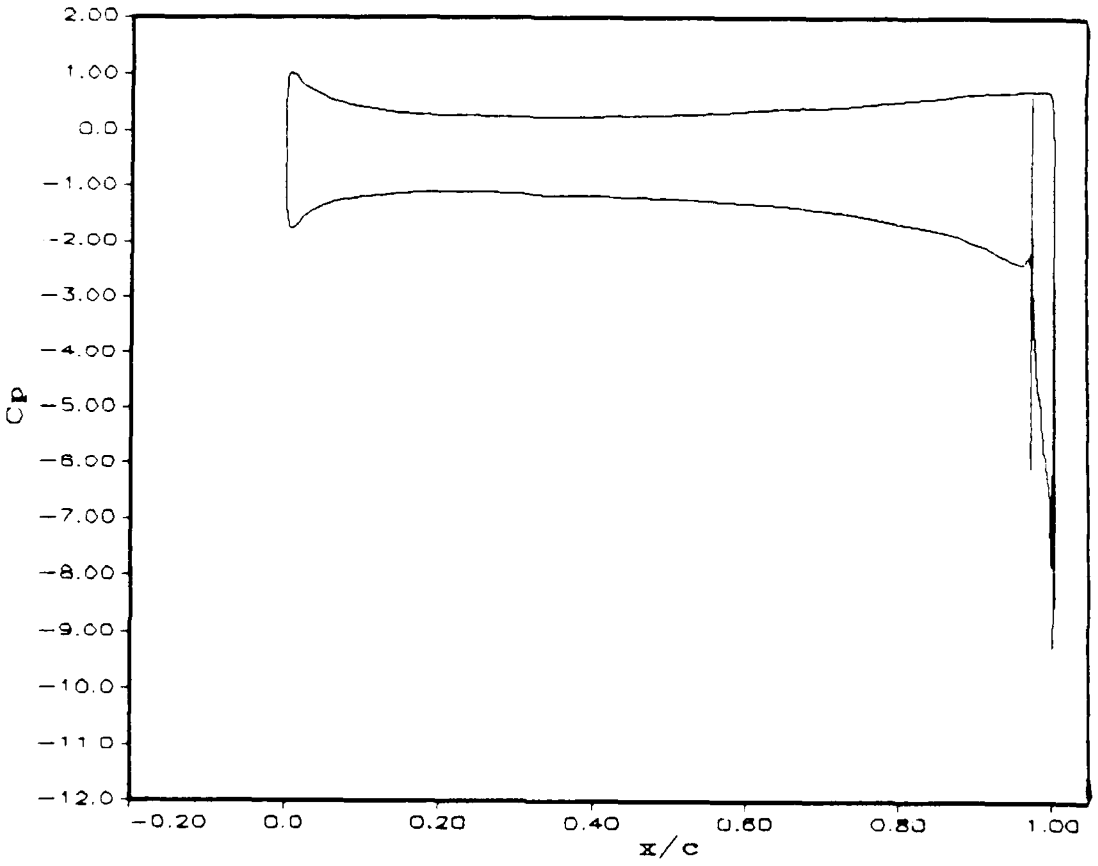

Figure 71. Case DC Pressure Coefficient (C_p) vs. x/c

D.4 Case DD Data

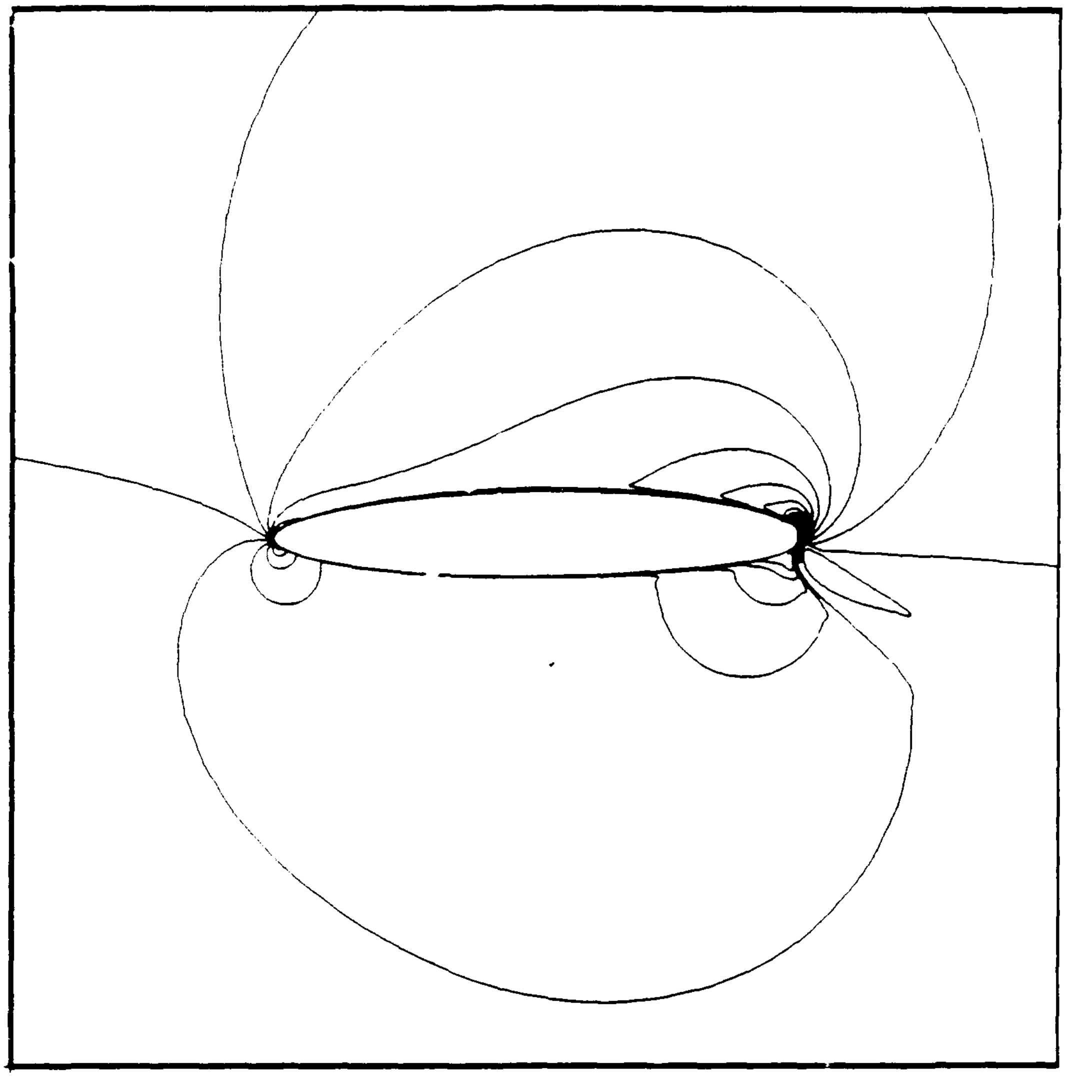

Figure 72. Case DD Mach Contour - Overview

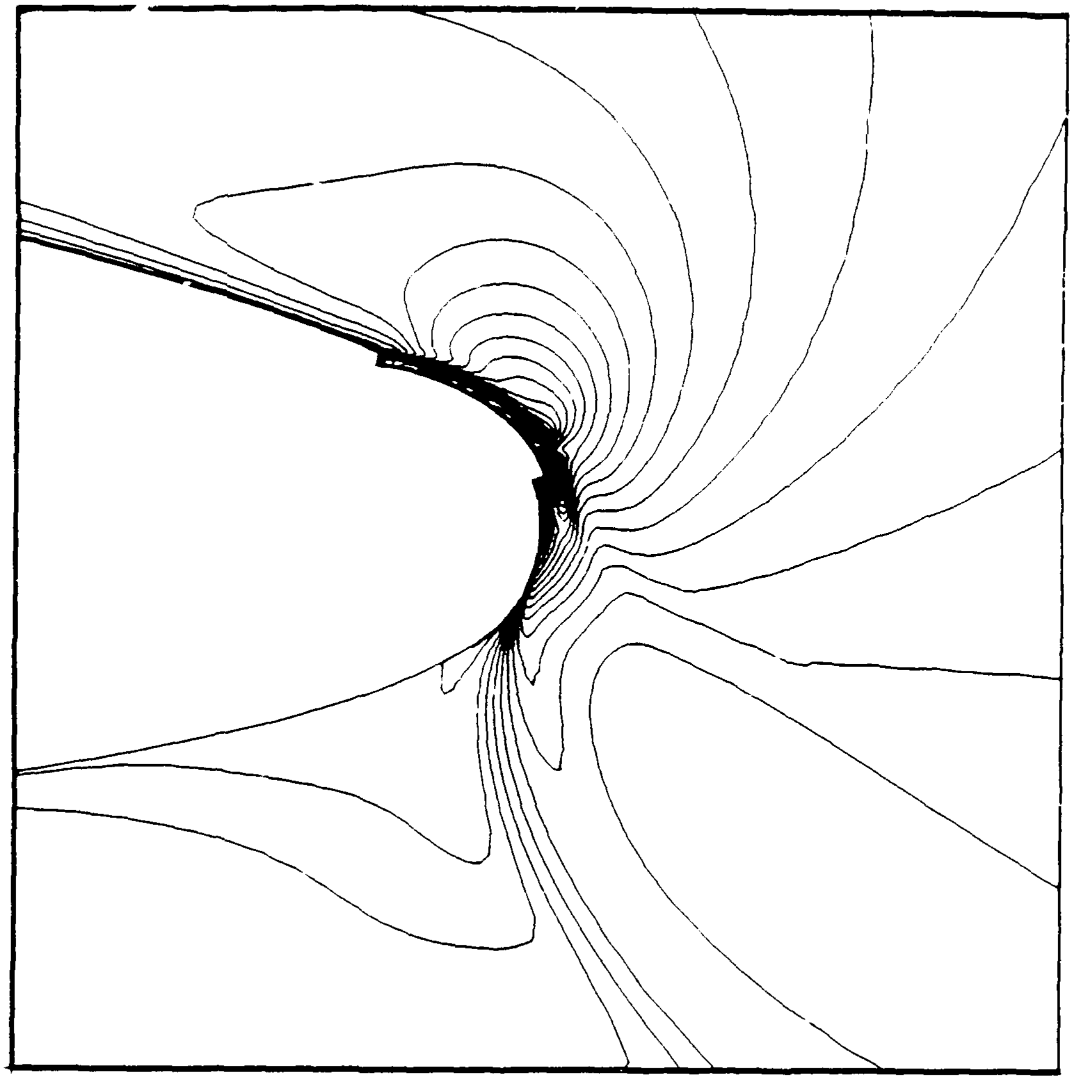

Figure 73. Case DD Mach Contour - Trailing Edge

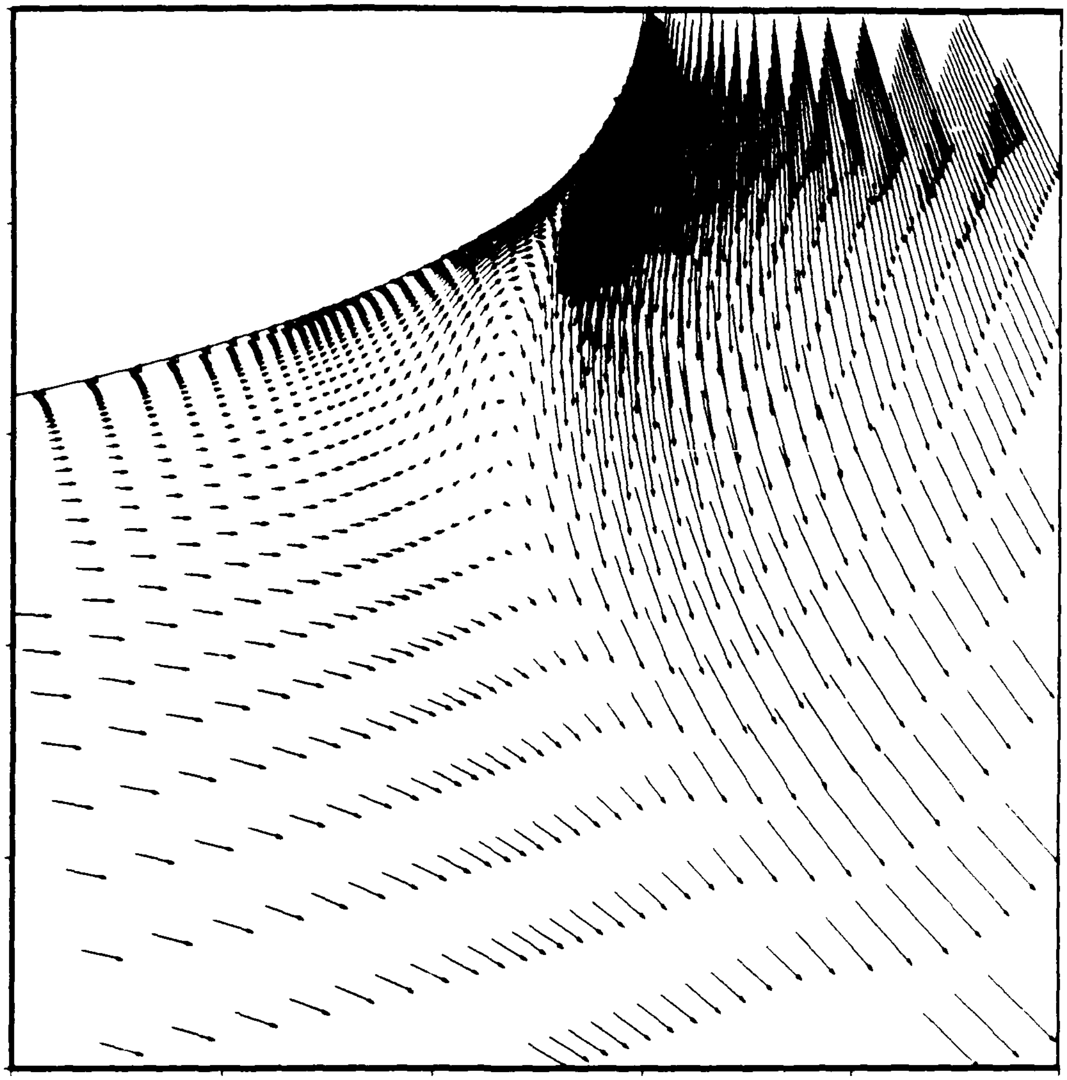

Figure 74. Case DD Trailing Edge Velocity Vector Field

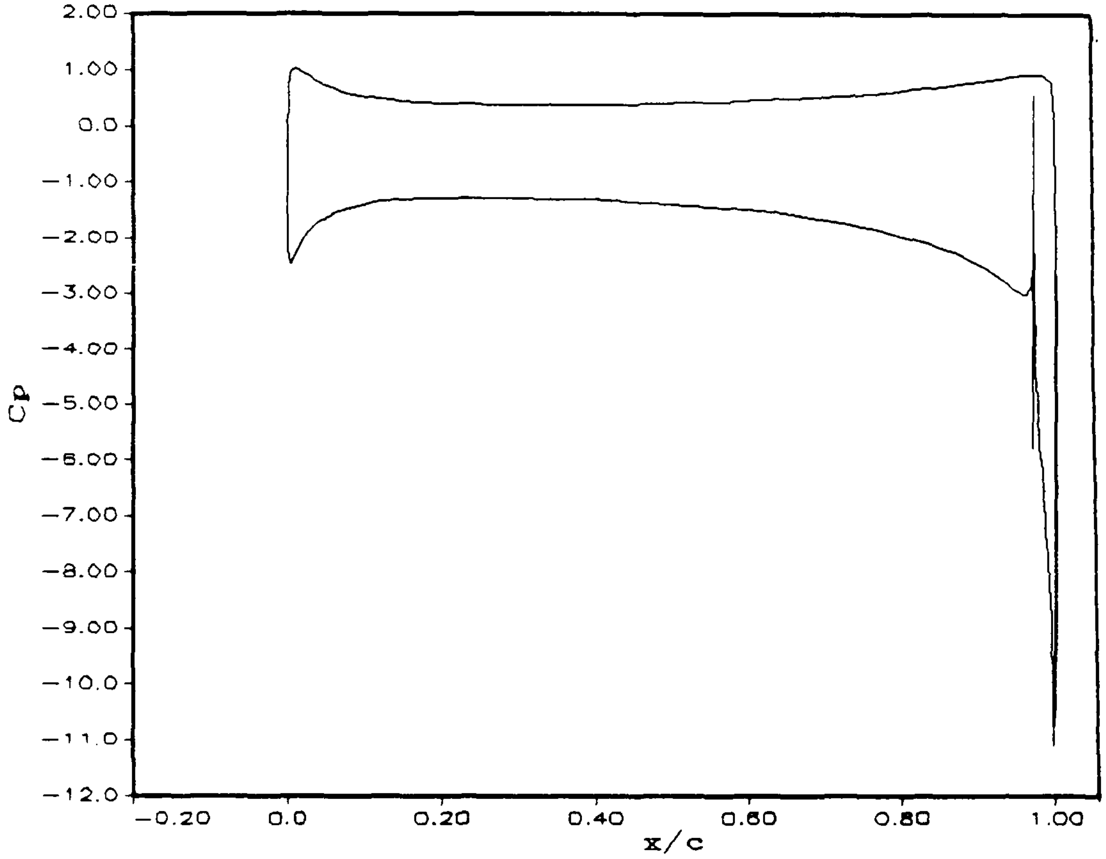

Figure 75. Case DD Pressure Coefficient (C_p) vs. x/c

Bibliography

1. Abramson,J. and E.O. Rogers. "High-Speed Characteristics of Circulation Control Airfoils", Paper No 83-0265. *AIAA 21st Aerospace Science Meeting.* Reno. NV, January 1983.

2. Anderson, D.A., J.C. Tannehill, and R.H. Pletcher. *Computational Fluid Mechanics and Heat Transfer.* New York: Hemisphere Publishing Corp., 1984.

3. Baldwin, B.S. and H. Lomax. "Thin Layer Approximation and Algebraic Model for Separated Turbulent Flows" , Paper No 78-257. *AIAA 16th Aerospace Sciences Meeting.* Huntsville, AL, January 1987.

4. Beam,Richard M., and R.F. Warming. "An Implicit Factored Scheme for the Compressible Navier-Stokes Equations", *AIAA Journal.* Vol. 16, No. 4, April 1978.

5. Bradshaw, P. "Effects of streamline Curvature on Turbulent Flow, " *AGARDograph No 169.* London: Technical Editing and Reproduction Ltd, August 1973.

6. Dorrell, E.W.,Jr.,and B.K. Soni. *INGRID: Interactive Two Dimensional Grid Generation.* AEDC-TR-86-49. Arnold Air Force Base, TN: AEDC/DOS, February 1987.

7. Dvorak, Frank A. and DO Hyng Choi. *The Development of an Analytic Method for Two-Dimensional Circulation-Control Airfoils in Transonic Flow.* Contract N00167-81-C-0041. Redmond WA: Analytical Methods, Inc., September 1981.

8. Harvell, Capt John K. *An Experimental/Analytical Investigation into the Performance of a 20-Percent Thick, 8.5-Percent Cambered, Circulation Control Airfoil.* MS Thesis, AFIT/GAE/AA/82D-13. School of Engineering, Air Force Institute of Technology (AU), Wright-Patterson AFB, OH, December 1982.

9. Harvell,J.K. and M.E. Franke,"Aerodynamic Characteristics of a Circulation Control Elliptical Airfoil with Two Blown Jets", *AIAA Journal,* Vol. 22, No. 9, September 1985.

10. Nielsen,Jack N. and James C. Biggers. " Recent Progress in Circulation Control Aerodynamics, " Paper 87-0001. *AIAA 25th Aerospace Science Meeting.* Reno. NV, January 1987.

11. Pulliam, Thomas H. et al. " Navier-Stokes Computations for Circulation Control Airfoils," *Proceedings of the Circulation-Control Workshop 1986.* NASA CP-2432:135-164. Washington: NASA, May 1987.

12. Schlichting, Hermann. ***Boundary-Layer Theory*** (Seventh Edition). NY: McGraw-Hill Book Company, 1979.

13. Shrewsbury, George D. " Analysis of Circulation Control Airfoils Using an Implicit Navier-Stokes Solver, " Paper 85-0171. *AIAA 23rd Aerospace Science Meeting.* Reno, NV, January 1985.

14. —–. " Numerical Evaluation of a Research Circulation Control Airfoil Performance Using Navier-Stokes Methods," Paper 86-0286. *AIAA 24th Aerospace-Sciences Meeting.* Reno, NV, January 1986.

15. —–. " Evaluation of a Research Circulation Control Airfoil Using Navier-Stokes Methods," Paper 87-0002. *AIAA 25th AerospaceSciences Meeting.* Reno, NV, January 1987.

16. Visbal, M.R. *Calculation of Viscous Transonic Flows About a Supercritical Airfoil.* AFWAL-TR-86-3013. Wright-Patterson AFB, OH, WRDC/FIMM, July 1986.

17. —-. " Evaluation of an Implicit Navier-Stokes Solver for Some Unsteady Separated Flows, " Paper 86-1053. *AIAA/ASME 4th Fluid Mechanics, Plasma Dynamics and Lasers Conference.* Atlanta, GA, May 1986.

18. —– and J.S. Shang. "Numerical Investigation of the Flow Structure around a Rapidly Pitching Airfoil," Paper 87-1424. *AIAA 19th Fluid Dynamics and Lasers Conference.* Honolulu, HI, June 1987.

19. Williams, Steven W. *Use of Navier-Stokes Methods to Predict Circulation Control Airfoil Performance.* MS Thesis, AFIT/GAE/AA/89M-4. School of Engineering, Air Force Institute of Technology (AU), Wright-Patterson AFB, OH, March 1989.

20. Wood, N. and J. Nielson. " Circulation Control Airfoils Past, Present and Future," Paper 85-0204. *AIAA 23rd Aerospace Sciences Meeting.* Reno, NV, January 1985.

Vita

Captain Donald J. Ferguson [redacted] He graduated co-valedictorian from high school in Carroll, Iowa in 1978, and attended Iowa State University. He graduated *Phi Kappa Phi* in May 1984, receiving the degree of Bachelor of Science in Aerospace Engineering. Upon graduation, he attended the Air Force Officer Training School, and received his commission in August 1984. He then was assigned to the Trajectory Division of the 544th Strategic Intelligence Wing at Offutt AFB, Nebraska, until entering the School of Engineering, Air Force Institute of Technology in June 1988.

[redacted]

[redacted]

UNCLASSIFIED
SECURITY CLASSIFICATION OF THIS PAGE

REPORT DOCUMENTATION PAGE

Form Approved
OMB No 0704-0188

1a REPORT SECURITY CLASSIFICATION UNCLASSIFIED	1b RESTRICTIVE MARKINGS
2a SECURITY CLASSIFICATION AUTHORITY	3 DISTRIBUTION/AVAILABILITY OF REPORT Approved for public release; distribution unlimited.
2b DECLASSIFICATION/DOWNGRADING SCHEDULE	
4 PERFORMING ORGANIZATION REPORT NUMBER(S) AFIT/GAE/ENY/89D-8	5 MONITORING ORGANIZATION REPORT NUMBER(S)
6a NAME OF PERFORMING ORGANIZATION School of Engineering	6b OFFICE SYMBOL (If applicable) AFIT/ENY
7a NAME OF MONITORING ORGANIZATION	
6c ADDRESS (City, State, and ZIP Code) Air Force Institute of Technology Wright-Patterson AFB, Ohio 45433-6583	7b ADDRESS (City, State, and ZIP Code)
8a NAME OF FUNDING/SPONSORING ORGANIZATION USAF	8b OFFICE SYMBOL (If applicable) WRDC/FIMM
9 PROCUREMENT INSTRUMENT IDENTIFICATION NUMBER	
8c ADDRESS (City, State, and ZIP Code) WPAFB, OH 45433-6583	10 SOURCE OF FUNDING NUMBERS

PROGRAM ELEMENT NO	PROJECT NO	TASK NO	WORK UNIT ACCESSION NO

11 TITLE (Include Security Classification)
COMPUTATIONAL ANALYSIS OF A TWO-SLOT CIRCULATION CONTROL AIRFOIL

12 PERSONAL AUTHOR(S)
Donald J. Ferguson, B.S.

13a TYPE OF REPORT	13b TIME COVERED	14 DATE OF REPORT (Year, Month, Day)	15 PAGE COUNT
MS Thesis	FROM ______ TO ______	1989 December	114

16 SUPPLEMENTARY NOTATION

17 COSATI CODES

FIELD	GROUP	SUB-GROUP
20	04	

18 SUBJECT TERMS (Continue on reverse if necessary and identify by block number)
Aerodynamics; Boundary-Layer Control; Circulation Control; High Lift; Navier-Stokes Equations

19 ABSTRACT (Continue on reverse if necessary and identify by block number)

Thesis Advisor: Milton E. Franke
Professor
Department of Aeronautics and Astronautics

20 DISTRIBUTION/AVAILABILITY OF ABSTRACT
☒ UNCLASSIFIED/UNLIMITED ☐ SAME AS RPT ☐ DTIC USERS

21 ABSTRACT SECURITY CLASSIFICATION
UNCLASSIFIED

22a NAME OF RESPONSIBLE INDIVIDUAL	22b TELEPHONE (Include Area Code)	22c OFFICE SYMBOL
Milton E. Franke, Professor	(513) 255-2362	AFIT/ENY

DD Form 1473, JUN 86 Previous editions are obsolete SECURITY CLASSIFICATION OF THIS PAGE

UNCLASSIFIED

A two-slot circulation control airfoil was analyzed using the two-dimensional, compressible, mass-averaged, Navier-Stokes equations. The implicit Beam-Warming approximate factorization technique was used to calculate airfoil characteristics for a flight Mach number of 0.3 and a Reynolds number near 3 million. The results were then compared to a previous one-slot solution.

An existing circulation control airfoil was modified to include a second slot. Different blowing rates were then applied to each slot in various combinations. The lift generated for a given total blowing momentum for the two-slot airfoil was nearly identical to that for a single-slot airfoil when the lowest blowing rate was applied to the first slot. Although the lift per unit blowing momentum did not increase over the single-slot case, the maximum lift coefficient was increased due to the increased momentum available from the additional slot. Separation angle increased when a small amount of blowing was applied to the first slot, and additional blowing applied to the second slot. The airfoil moment followed the same trend as the single slot, and was less dependent on which slot the flow was applied. Due to the lack of experimental data, and the difficulty in modeling drag for the circulation control airfoil, it is difficult to compare drag.